

**SHROOM3 AND PLANAR CELL POLARITY COUPLE APICAL CONSTRICTION
AND CONVERGENT EXTENSION DURING NEURAL TUBE MORPHOGENESIS**

by

Erica M. McGreevy

B.S. Biology, James Madison University, 2009

Submitted to the Graduate Faculty of the Kenneth P.
Dietrich School of Arts and Sciences in partial fulfillment
of the requirements for the degree of
Doctor of Philosophy

University of Pittsburgh

2014

UNIVERSITY OF PITTSBURGH
KENNETH P. DIETRICH SCHOOL OF ARTS AND SCIENCES

This dissertation was presented

by

Erica M. McGreevy

It was defended on

July 23, 2014

and approved by

Gerard Campbell, Ph.D., Associate Professor, Biological Sciences

Deborah Chapman, Ph.D., Associate Professor, Biological Sciences

Jonathan Minden, Ph.D., Professor, Carnegie Mellon University, Biological Sciences

Andrew VanDemark, Ph.D., Associate Professor, Biological Sciences

Dissertation Advisor: Jeffrey Hildebrand, Ph.D., Associate Professor, Biological Sciences

Copyright © by Erica M. McGreevy

2014

SHROOM3 AND PLANAR CELL POLARITY COUPLE APICAL CONSTRICTION AND CONVERGENT EXTENSION DURING NEURAL TUBE MORPHOGENESIS

Erica M. McGreevy, PhD

University of Pittsburgh, 2014

Neural tube closure is a critical developmental event that provides an extraordinary example of how coordinated cell behavior orchestrates the shaping of a complex tissue during vertebrate embryogenesis. Neural tube closure relies on actomyosin contractility to drive specific cellular behaviors such as apical constriction, tissue bending, and directional cell rearrangements. These complicated processes are facilitated by coordinating the activity of Rho-Kinase (Rock), to regulate cytoskeletal dynamics and actomyosin contractility, and the Planar Cell Polarity (PCP) pathway, which controls polarized cellular reorganization to mediate convergent extension of the tissue. Failure to properly coordinate these processes results in a class of highly prevalent, severely debilitating congenital malformations known as neural tube defects. The work described here investigates the role of Shroom3, a regulator of localized Rock activity, as a direct linker between planar cell polarity and actomyosin contractility to facilitate apical constriction, directional bending, cell topography, and subsequent neural tube morphogenesis.

In mice, simultaneous depletion of Shroom3 and the planar cell polarity components Vangl2 or Wnt5a results in convergent extension failure and an increased liability to neural tube defects. The Shroom3 and planar cell polarity pathways intersect at Dishevelled, as Dishevelled2 (Dvl2), Shroom3, and Rock co-distribute in cells. Dvl2 and Shroom3 form a physical complex mediated by discrete protein-protein domain interactions. Imaging of the neural plate of E8.5

embryos demonstrates that multiple components of the Shroom3 pathway are planar polarized along mediolateral cell junctions *in vivo* in a PCP-dependent manner. Finally, *Shroom3* mutant embryos exhibit defects in planar cell arrangement during neural tube closure, suggesting a role for Shroom3 activity in convergent extension. These findings support a model in which the Shroom3 and planar cell polarity pathways interact to control convergent extension and polarized bending of the neural plate. The results of this study lend insight into the intricate set of mechanisms that regulate neural tube closure and provide a clear illustration of the complex genetic basis of neural tube defects.

TABLE OF CONTENTS

PREFACE.....	XII
1.0 INTRODUCTION.....	1
1.1 EPITHELIAL MORPHOGENESIS.....	2
1.1.1 Adhesion and Polarity	2
1.1.2 Actomyosin Contractility	6
1.1.2.1 Actin	6
1.1.2.2 The Rho-Rock-Myosin II Pathway.....	7
1.1.3 Morphogenesis	11
1.1.3.1 Apical Constriction	11
1.1.3.2 Convergent Extension.....	14
1.2 EVENTS OF MAMMALIAN NEURAL TUBE MORPHOGENESIS	17
1.2.1 Neural Tube Defects	20
1.2.2 Forces That Close The Neural Tube	23
1.3 SHROOM3 DRIVES APICAL CONSTRICTION	24
1.3.1 Shroom Family Members: Shroom1, 2 and 4.....	31
1.3.2 <i>Drosophila</i> Shroom and the evolutionary conservation of Shroom-Rock Function	32
1.4 PLANAR CELL POLARITY.....	34

1.4.1	Mechanisms of Planar Cell Polarity in <i>Drosophila</i>	35
1.4.1.1	Wing Hair Orientation	35
1.4.1.2	Orientation of Ommatidia in the Compound Eye.....	40
1.4.2	Mechanisms of Planar Cell Polarity in Vertebrates.....	42
1.4.2.1	Orientation of Stereocilia in the Mammalian Inner Ear.....	44
1.4.2.2	Convergent Extension and Neural Tube Closure	47
1.5	SUMMARY AND DISSERTATION AIMS.....	51
2.0	SHROOM3 INTERACTS GENETICALLY WITH PLANAR CELL POLARITY	53
2.1	INTRODUCTION	53
2.2	RESULTS	55
2.2.1	Shroom3 Interacts Genetically With Vangl2	55
2.2.2	Shroom3 Interacts Genetically With Wnt5a.....	60
2.3	DISCUSSION.....	67
3.0	SHROOM3 PHYSICALLY INTERACTS WITH DISHEVELLED2.....	69
3.1	INTRODUCTION	69
3.2	RESULTS	73
3.2.1	Dvl2 Regulates the Distribution of Shroom3 and Rock.....	73
3.2.2	Dvl2 and Shroom3 Interact Through Specific Protein Domains	75
3.3	DISCUSSION.....	79
4.0	A PCP-SHROOM3 PATHWAY CONTROLS PLANAR CELL ARRANGEMENT	84
4.1	INTRODUCTION	84

4.2	RESULTS	85
4.2.1	Shroom3 Pathway Components Are Planarly Polarized	85
4.2.2	PCP is Upstream of the Shroom3 Pathway	88
4.2.3	Loss of Shroom3 Disrupts Planar Cell Arrangement	94
4.3	DISCUSSION.....	99
5.0	CONCLUSIONS AND FUTURE PROSPECTIVES.....	104
6.0	EXPERIMENTAL PROCEDURES	108
6.1	MICE AND EMBRYOS.....	108
6.2	GENOTYPING	108
6.3	AXIS LENGTH MEASUREMENTS	110
6.4	CELL CULTURE AND TRANSFECTION	110
6.5	IMMUNOHISTOCHEMISTRY	111
6.6	CO-IMMUNOPRECIPITATION.....	111
6.7	MOLECULAR BIOLOGY.....	112
6.8	GST PULL DOWN.....	112
6.9	MOUSE WHOLE MOUNT IMMUNOHISTOCHEMISTRY	113
6.10	PLANAR DISTRIBUTION ANALYSES.....	115
6.11	PLANAR CELL ARRANGEMENT ANALYSES	116
6.12	STATISTICAL ANALYSES	117
	BIBLIOGRAPHY	118

LIST OF TABLES

Table 1. Summary of core PCP genes in vertebrates.....	43
Table 2. The penetrance of the phenotypes upon depletion of Shroom3 and Vangl2.....	57
Table 3. PCR primers used for mouse genotyping of Wnt5a, Shroom3, and Vangl2 alleles.....	109

LIST OF FIGURES

Figure 1. Epithelial cells exhibit robust adhesion and polarity.....	4
Figure 2. The Rho-Rock-Myosin II pathway.....	10
Figure 3. Apical constriction drives tissue bending.....	12
Figure 4. Cellular mechanisms of convergent extension.....	16
Figure 5. The neural plate bends at hinge points to form the neural tube.....	19
Figure 6. Mouse models of neural tube defects.....	21
Figure 7. The Shroom-Rock pathway.....	26
Figure 8. Neural plate bending occurs along the mediolateral body axis.....	30
Figure 9. The planar cell polarity signaling module regulates fly wing hair orientation.....	37
Figure 10. Planar cell polarity functions during ommatidial differentiation and rotation.....	41
Figure 11. Vertebrate PCP controls inner ear hair patterning.....	46
Figure 12. Shroom3 interacts genetically with Vangl2.....	56
Figure 13. Quantification of spina bifida severity.....	58
Figure 14. Quantification of body axis length.....	59
Figure 15. Shroom3 interacts genetically with Wnt5a.....	63
Figure 16. <i>Wnt5a/Shroom3</i> embryos exhibit convergent extension and skeletal defects.....	64
Figure 17. <i>Wnt5a/Shroom3</i> double mutants die at or before E11.5.....	66
Figure 18. Summary of genetic interactions.....	69

Figure 19. Dvl2 domain structure	71
Figure 20. Dvl2 recruits Shroom3 and Rock into cytoplasmic puncta	74
Figure 21. The DEP domain of Dvl2 facilitates interaction with Shroom3.....	76
Figure 22. An uncharacterized region of Shroom3 mediates co-localization with Dvl2.....	79
Figure 23. Dvl DEP structure and binding interfaces	81
Figure 24. Shroom3 and F-actin are planarly polarized during neural plate bending	86
Figure 25. Dvl2, Rock1, and Myosin IIb are planarly polarized during neural plate bending	88
Figure 26. Planar polarity of Shroom3 and F-actin is lost in <i>Vangl2</i> mutants	89
Figure 27. Analysis of PCP pathway components in <i>Shroom3</i> mutant embryos	90
Figure 28. The apical F-actin network is disrupted in <i>Shroom3</i> mutants	92
Figure 29. Summary model of results.....	93
Figure 30. Wildtype neural epithelial cells are arranged in rosettes.....	95
Figure 31. <i>Shroom3</i> mutants exhibit defective planar cell arrangement	96
Figure 32. Model of Shroom3 and PCP pathway integration.....	99
Figure 33. Morphogenetic consequences of PCP-Shroom3 interactions.....	105
Figure 34. Whole mount immunohistochemistry methods.....	114
Figure 35. Fluorescence intensity measurements at cell-cell junctions	115
Figure 36. An automated rosette detector calculates cell overlap	116

PREFACE

The completion of this work would not have been possible without the support and encouragement of so many wonderful people. First, I must acknowledge my advisor, Dr. Jeffrey Hildebrand. Jeff, you told me in my first year that if I joined your lab, I would receive quality training in many different areas. I can confidently say that you held true to your word; in five years, I have learned numerous techniques in molecular biology, cell culture, mouse work, biochemistry, microscopy, image analysis, and the list goes on. Through your mentoring, I have learned how to write, design and execute experiments, analyze and interpret data, and most importantly, how to be a creative scientist. You provided me with countless opportunities, while remaining supportive of my interest to get involved in teaching, mentoring, outreach, GSO, and every other opportunity that came my way. Through all of these experiences, I have developed as a scientist and a professional and am very grateful for your patience and encouragement. Lastly, thank you for always keeping a box of kimwipes handy in your office and supporting me through my consistent emotional outbursts. I hope that I have in turn better prepared you for your daughters' tumultuous teenage years.

A huge thank you goes to everyone that has served on my committee: Dr. Deborah Chapman, Dr. Beth Roman, Dr. Andrew VanDemark, Dr. Jonathan Minden, and Dr. Gerard Campbell. I am grateful for your guidance and critical discussions over the years. You each brought a unique perspective to my committee and challenged me to think about my project from

every standpoint. A very special thank you goes to Debbie for being my cheerleader and constantly feeding my self-confidence with positive feedback and my sweet tooth with delicious baked goods. Your advice and encouragement over the years has been invaluable.

I'd also like to acknowledge the labs and people that have contributed materials and assistance along the course of this work. Dr. Lance Davidson and members of his lab generously provided automated systems to help with image analysis and quantification. Lance, Deepthi, and Holley, your advice, assistance, and patience with data analysis were integral to this project. Dr. Roman and Liz Rochon, thank you for maintaining Lucille the Leica in working condition and helping me with my imaging experiments. To the Chapman, Roman, Rebeiz, Campbell, and Boyle labs, thank you for your insightful comments at lab meetings and for the use of shared equipment and the occasional borrowed reagent.

The experiences that I have had through the teaching minor and various TA assignments have molded the teacher and mentor that I am today. I must thank every person that I have taught with: Dr. Tony Bledsoe, Dr. Valerie Oke, Dr. Nancy Kaufmann, Dr. Sara Ernst, Dr. Alison Slinsky Legg, Dr. Gerard Campbell, and Dr. Tia-Lynn Ashman. You each have unique teaching and mentoring styles that I have learned from and adapted to develop my own style. Alison, your guidance has been instrumental in my success. Teaching bio prep with you drastically improved my confidence in the classroom and allowed me the freedom to practice with various teaching techniques. I also can't thank you enough for helping me with my teaching minor project. It was an incredible opportunity and a fun challenge and I enjoyed every step of developing the module, revising it, and sharing it. On top of all of the help with teaching, you were always available to talk, whether it professional or personal. I value your advice and I appreciate your friendship and support over the years. Nancy, your enthusiasm for undergraduate

education is unsurpassed. I have never met someone who cared so much about the improvement and success of her students. You have truly been an inspiration and role model. I look forward to working with you this fall! Thank you also to Valerie, for coordinating the teaching minor, serving as a wonderful teaching mentor, and providing loads of career advice.

To past and present Hildebrand lab members, thank you for making this a great place to work. Matt, I will always remember our morning discussions and I will never forget the cicada bombs. I hope we will continue to stay in touch as friends and colleagues. Dee, we've certainly had some fun times in the lab and I will miss you! Hilary, we only got to share a bay for a short time, but it was enjoyable nonetheless. You chose a great lab and I am sure you will be successful in your endeavors. And to all the undergraduates: Dan, Oyin, Theo, Ruth, Anna, Jad, and Serena, ya'll are great! You gave the lab a buzz of positive, youthful energy that I've always appreciated. Good luck with your future plans, wherever they may take you.

Finally, I'd like to thank my friends and family. To all of my departmental friends over the years, thank you for being a support group and for joining me at countless happy hours to commiserate the pains and celebrate the joys of graduate school. I don't think I would've survived this journey without ya'll! Becca and Amy, your love and friendship have provided comfort and support for the past five years, despite the 200-mile separation. I am very lucky to have you both as best friends. To my wonderful roommates, Claire and Natalie, thank you for being a haven away from science and for listening to me cry after a bad day, when discussing my future, or before my seminar (every single year); you are both invaluable friends. And last, but certainly not least, to my parents, you have been my sounding board throughout this whole process and have had faith in me even when I thought I was sure to fail. I would not be where I am today without your unwavering support and for that I am eternally grateful.

1.0 INTRODUCTION

One of the most fundamental questions in biology is how multicellular organisms, with organs of complex and varied form and function, arise from a single cell: the fertilized egg. Organs such as the lungs, kidneys, vasculature, brain, and intestines are composed of elaborate epithelial structures that form during embryogenesis through the folding, bending, stretching, and sculpting of epithelial sheets [1]. Shaping of epithelial tissues is accompanied by cell proliferation and death, differentiation of cells into distinct cell types, and patterning of these populations into distinct compartments. The correct formation of these organs is essential to the health and viability of the organism. Proper epithelial morphogenesis requires that cells are perfectly coordinated in time and space to achieve the dramatic shape changes and tissue rearrangements that form adult tissues with such diverse and elaborate architecture. How cell shape and behavior is controlled on a cell and molecular level to achieve proper tissue morphogenesis is a critical question in developmental biology and an area of intense investigation. Research using animal models has demonstrated that cells in the developing embryo utilize the coordinated efforts of transcriptional programs, signaling pathways, and cytoskeletal networks to elicit changes in cell morphology and behavior. Our laboratory studies the role of the Shroom family of proteins in epithelial morphogenesis as a model for understanding the molecular regulation of cell shape and behavior during animal development. The Shroom family member, Shroom3, regulates cell shape and behavior during vertebrate neural tube closure, a developmental event that provides a remarkable example of how coordinated cell behavior orchestrates the shaping of a complex tissue.

1.1 EPITHELIAL MORPHOGENESIS

Epithelia are sheet-like layers of tightly linked cells that line body cavities and comprise essential functional components of major organs. They provide protective barriers between compartments that serve different physiological functions and also perform a wide array of functions including secretion, absorption, and sensory reception. Epithelial sheets are characterized by several distinct features: close cell-cell contact mediated by specialized intercellular junctions, connections with a supportive underlying extracellular matrix known as the basal lamina, and robust polarization that specifies different cellular domains. Establishing polarity allows cells to organize into tissues and perform various functions (reviewed in [2]). Polarity of cells in an epithelial sheet can exist in the x-, y-, and z- planes. Polarity along the z- axis is a characteristic feature of all epithelia and separates the cell membrane into upper and lower compartments, termed apical and basal (Figure 1A). The apical surface faces a lumen, whereas the basal surface contacts the basal lamina. The molecular details of epithelial adhesion and apical-basal polarity will be discussed in the following sections.

1.1.1 Adhesion and Polarity

Epithelial cells possess a specialized apical junctional complex (AJC) comprised of adhesive structures that connect cells to their neighbors (reviewed in [3-5]). Two types of adhesive structures make up the AJC: tight junctions and adherens junctions (Figure 1A). Tight junctions form a selective permeability barrier to regulate the movement of water, ions, and other solutes and serve as molecular barriers that divide the apical and basolateral domains into distinct compartments [6]. Adherens junctions provide strong adhesive contacts between cells [7].

Components of the AJC anchor and organize the cytoskeleton and interact with transcription factors and signaling molecules, thereby functioning as a relay center for signal transduction events (reviewed in [8]). Thus, the AJC is fundamentally important for the function of epithelial tissues; it allows cells to adhere to each other, provides a platform for receiving and transmitting extracellular and intracellular signals, and can transmit those signals directly to the cytoskeletal network of the entire tissue.

The molecular organization of the junctions that make up the AJC comprises three main types of molecules: 1) membrane-bound cell-adhesion molecules that interact in the extracellular space between cells, 2) adapter proteins that interact with the cytoplasmic domains of the membrane bound adhesion molecules, and 3) cytoskeletal filaments that connect to the adapter proteins. Tight junctions are composed of the four-pass transmembrane proteins occludin, claudin, and junctional adhesion molecule (JAM) [9-11]. The cytoplasmic domains of these proteins interact with PDZ (PSD/SAP90, Discs large, ZO1) domain-containing proteins such as those of the zonula-occludens family (ZO-1, ZO-2, ZO-3) [12-14]. The PDZ proteins form complexes with claudin, occludin, and several cytoskeleton-related proteins, thereby providing a scaffold to link the membrane bound proteins to the actin cytoskeleton [15-19].

These complexes are not only required for the assembly of the AJC, but also play an important role in establishing apical-basal polarity (Figure 1B). There are several polarity complexes associated with tight junctions that function to establish and maintain apical-basal polarity and determine the relative sizes of the apical and basal domains. The Crumbs3/PALS1/PATJ complex is found in the apical-most region, enriched at the boundary between the apical and lateral sides of the cell. Interactions between PATJ with ZO3 and claudins dock the Crumbs/PALS/PATJ complex at the tight junction [20]. Mutations in any

component of this complex disrupt the formation of an apical domain and lead to a loss of polarity [21, 22]. The Crumbs/PALS/PATJ complex also functions to restrict the recruitment of a second polarity complex, PAR3/aPKC/PAR6, such that it can only be localized laterally to the Crumbs/PALS/PATJ complex [23]. Its localization along the apical-lateral membrane is mediated by interactions between PAR3 and the tight junction component JAM-1 [24]. The basolateral Scribble/Dlg/Lgl complex antagonizes the PAR3/aPKC/PAR-6 complex, thus restricting its formation to the apical domain [25]. Because of mutual exclusion between polarity complexes and the fact that interactions between polarity complexes and the tight junction are required for tight junction assembly, tight junctions can only assemble in the correct domain.

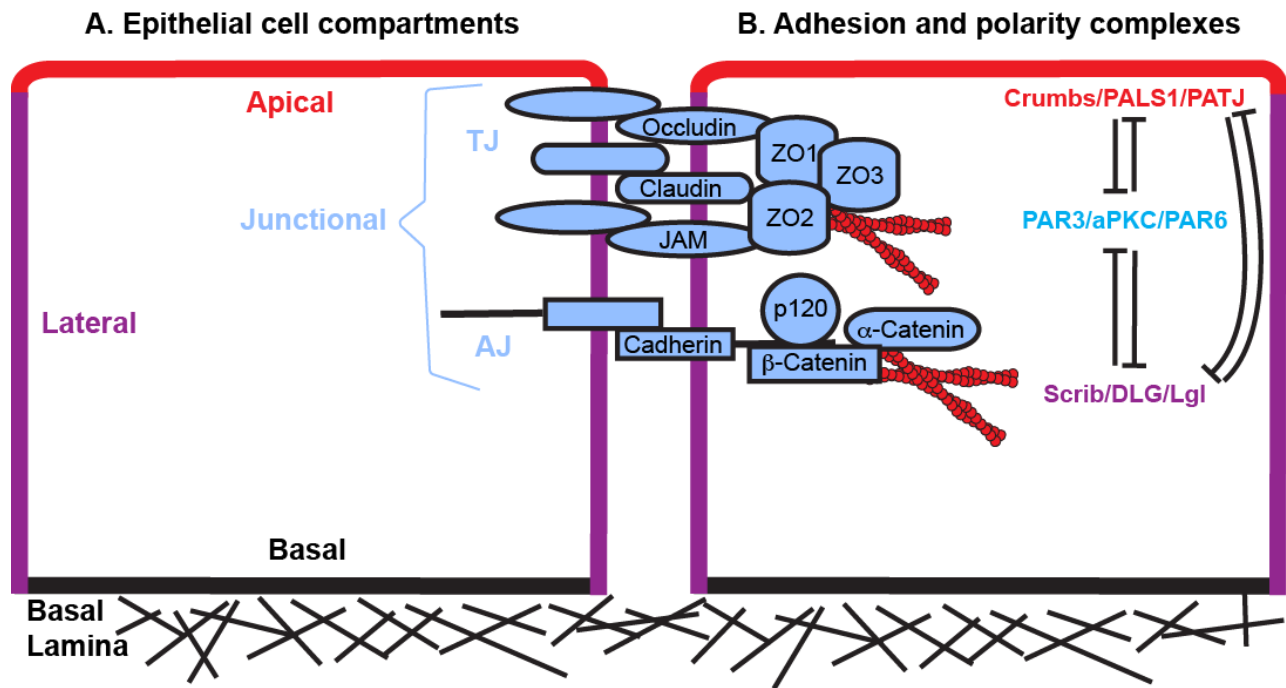


Figure 1. Epithelial cells exhibit robust adhesion and polarity

A. Epithelial cells are divided into apical, lateral, basal, and junctional compartments, each of which is fundamentally important for epithelial tissue structure and function. **B.** The apical-junctional complex is composed of tight junctions (TJ) and adherens junctions (AJ). TJs are composed of the transmembrane components Occludin,

Claudin, and JAM, which are restricted to the apical-most domain by the polarity complexes Crumbs/PALS1/PATJ, PAR3/aPKC/PAR6, and Scrib/DLG/Lgl. Intracellular interactions with ZO proteins connect the TJ to the actin cytoskeleton. AJs are composed of transmembrane Cadherins that bind p120-catenin, β -catenin, and α -catenin intracellularly to link to the cytoskeleton. Polarity complexes mutually exclude each other from different subcellular compartments and are required for junction assembly such that junctions can only form in the correct position.

Adherens junctions are composed of transmembrane adhesion molecules called cadherins, of which there are over twenty varieties that are expressed in specific tissues [26]. Calcium ions bind to the cadherin extracellular domains resulting in a conformational change that makes them capable of interacting with cadherins on neighboring cells. This provides a mechanism for regulating their adhesive capacity [27, 28]. The cytoplasmic domains of cadherin molecules interact with the scaffolding proteins p120catenin and β -catenin. β -catenin binds α -catenin, an actin-binding protein, which connects the cadherin-catenin complex to the cytoskeleton [29]. Additional molecules reinforce these interactions to generate robust adhesive contacts between cells. During development, epithelial tissues experience intense mechanical stresses as they are shaped into various structures. Thus, cell-cell adhesions are strong to maintain the integrity of the tissue and resist and respond to stress. Concurrently, the junctions are also highly dynamic during morphogenesis to enable tissue remodeling. If junctions were not flexible in this way, cells would be fixed within tissues and unable to rearrange, change shape, proliferate, migrate, or differentiate. Endocytosis and recycling of AJC components plays a key role in promoting junction turnover, allowing junctions to be assembled and disassembled when necessary (reviewed in [30]).

1.1.2 Actomyosin Contractility

Developmental processes that require changes in cell shape depend on the cell's ability to modulate the behavior of its actin cytoskeleton: a network of actin filaments and Myosin motors (referred to as actomyosin) that contract to provide tension and force (reviewed in [31-33]). Actomyosin contractility plays a key role in tissue morphogenesis by defining cyto-architecture, cell shape, cell adhesion, cell motility, and tissue stiffness [34-37]. The activity of actomyosin requires the correct actin architecture and the activity of type II Myosin motors.

1.1.2.1 Actin

Actin is composed of a single monomer of globular actin (G-actin), which reversibly polymerizes into two-stranded helices termed filamentous actin (F-actin) [38]. The structure of G-actin provides inherent polarity, thus when assembled into F-actin, individual fibers are polarized and additional monomers can only be added in one direction [39]. F-actin can be organized into various types of structures. Cells contain a distinct network of F-actin, known as the cell cortex that extends through the cell just below the plasma membrane, providing strength and structural integrity [40]. In epithelial cells, F-actin is tightly associated with the AJC and thus forms a contractile band around each cell, referred to as the adherens belt [41, 42]. Myosin-dependent contractions of the cell cortex and/or adherens belt can have profound effects on cell shape and motility. Long cables of linearly aligned F-actin bundles can be utilized to build finger-like cell surface projections known as filopodia, whereas branched two-dimensional networks can be used to build large, flat, protrusions called lamellipodia (reviewed in [43]). Actin assembly and disassembly into these structures can occur very rapidly, thereby altering cell shape, adhesion and motility whenever necessary. F-actin architecture is controlled by various

factors that regulate actin polymerization, bundling, branching, and ultimately filament length and organization (reviewed in [44]).

Some actin regulatory proteins positively affect the assembly and stability of F-actin networks. Examples include Arp2/3 (actin-related protein), which facilitates nucleation of new filaments from the side of existing filaments, thereby promoting the formation of branched networks [45]. Filamin can crosslink existing F-actin at right angles to each other, also forming branched networks [46]. Growth and assembly into branched networks occurs at the site of lamellipodial formation to drive cell migration (reviewed in [47]). Members of the Ena/VASP or Formin protein families facilitate G-actin addition to the growing end of an actin fiber, thereby promoting long filament assembly [48, 49]. Proteins such as α -Actinin can crosslink these long filaments into parallel arrays to generate tight bundles, such as those that make up filopodial extensions [50]. Proteins such as Tropomyosin bind along the filament length and stabilize the filament, preventing depolymerization [51]. Conversely, a wide array of molecules function to either block F-actin network assembly or actively disassemble F-actin networks. Capping proteins can bind to existing filaments and prevent the addition of new G-actin monomers, thereby limiting actin filament length [52]. Some proteins, such as Cofilin, actively remove G-actin subunits, while others, such as Gelsolin, can physically sever existing filaments to break down F-actin networks [53, 54]. Thus, cells have a comprehensive toolkit at their disposal for rapidly building and demolishing unique F-actin structures to drive morphogenesis.

1.1.2.2 The Rho-Rock-Myosin II Pathway

Myosins are actin-based molecular motors, of which there are at least 35 different classes (reviewed in [55, 56]). The largest class is the type II Myosins, which include muscle and non-muscle varieties. Non-muscle Myosin II (Myosin II) is commonly found in epithelial tissues and

drives most Myosin-dependent processes in non-muscle cells (reviewed in [57]) (Figure 2E). The structure of Myosin II is a hetero-hexamer of three different peptides: two myosin heavy chains (MHC), two regulatory light chains (MRLC), and two essential light chains (MELC) (Figure 2D). The MHC is the major structural component and contains two globular head regions that provide actin binding capacity and an ATPase motor. These features allow Myosin II to reversibly bind to F-actin, hydrolyze ATP in an actin-binding dependent manner, and convert the chemical energy into mechanical force to exert tension onto actin filaments (reviewed in [58]). The MHC also contains a neck region and a long coiled-coil region. The coiled-coil is essential for the self-association of Myosin molecules into bipolar filaments, an arrangement that facilitates contractile functions [59, 60]. The flexible neck regions allow for conformational changes during contraction. They also bind the two MRLCs, which serve to regulate Myosin motor activity. Myosin II activity is enhanced by phosphorylation of the MRLC at two specific sites, serine-19 and threonine-18 (pMRLC), which results in a conformational change that allows Myosin II to form filaments and increases its actin-dependent ATPase activity, thus promoting actin filament contraction [61-63]. A Myosin phosphatase (MP) can remove these phosphates, thereby returning Myosin II to its closed, inactive state (reviewed in [64]). The ability to regulate Myosin II activity in this manner allows cells to rapidly respond to environmental signals. In mammals, there are three MHC genes, producing three distinct Myosin II isoforms. These isoforms include Myosin IIA, IIB, and IIC, which differ slightly in their kinetic properties, making IIB more suitable for prolonged contractions, and IIA and IIC more suitable for rapid bursts of contraction [65-67].

Spatial and temporal control of actomyosin contractile force is achieved by regulating the activity of protein kinases that phosphorylate and activate Myosin II. Although a large number of

kinases have been implicated in the regulation of Myosin II, Rho-kinase (Rock, dRok in *Drosophila*) is the primary regulator of Myosin II activity in epithelial tissues and is a critical determinant of where and when actomyosin networks are utilized within the cell (reviewed in [68]). Rock proteins (Rock1 and Rock2) are serine/threonine kinases that function to phosphorylate a wide array of targets including both MRLC and MP. Phosphorylation of MRLC activates Myosin function. Phosphorylation of MP blocks its phosphatase activity, thereby preventing the dephosphorylation of Myosin. Thus, Rock acts both directly and indirectly to upregulate Myosin activity [69]. Rock proteins are characterized by a conserved set of protein domains including an N-terminal kinase domain, a central coiled-coil domain, and a C-terminal pleckstrin-homology (PH) domain that binds lipids [70-73] (Figure 2C). The C-terminus functions to negatively regulate the kinase domain by directly binding to the kinase, thereby maintaining Rock in a closed, inactive conformation. This autoinhibition can be relieved by the binding of proteins or lipids to the C-terminus, which release the intramolecular interaction to activate kinase catalytic activity [74, 75].

One such protein is Rho, which binds to a specific Rho binding domain (RBD) within the coiled-coil domain of Rock [75]. Rho is a member of the family of p21 small GTPases which regulate the activity of a variety of cellular proteins including many actin-binding and cytoskeletal regulatory proteins (reviewed in [76, 77]). GTPases are molecular switches that are turned “on” when bound to GTP and “off” when bound to GDP (Figure 2B). Hydrolysis of GTP is enhanced by interactions with GTPase activating proteins (GAPs) and exchange of GDP for GTP is activated by guanine-nucleotide exchange factors (GEFs) [78, 79]. Signaling pathways regulate the activity of Rho through GAPs and GEFs to regulate the activity of Rock (Figure 2A). Other mechanisms exist to regulate the activity of Rock including proteolytic cleavage to

release the kinase domain or binding of additional factors that function to inhibit kinase activity [80-83]. Thus, signaling pathways can be utilized in multiple ways to regulate the activity of Rock in order to control the activity of Myosin II.

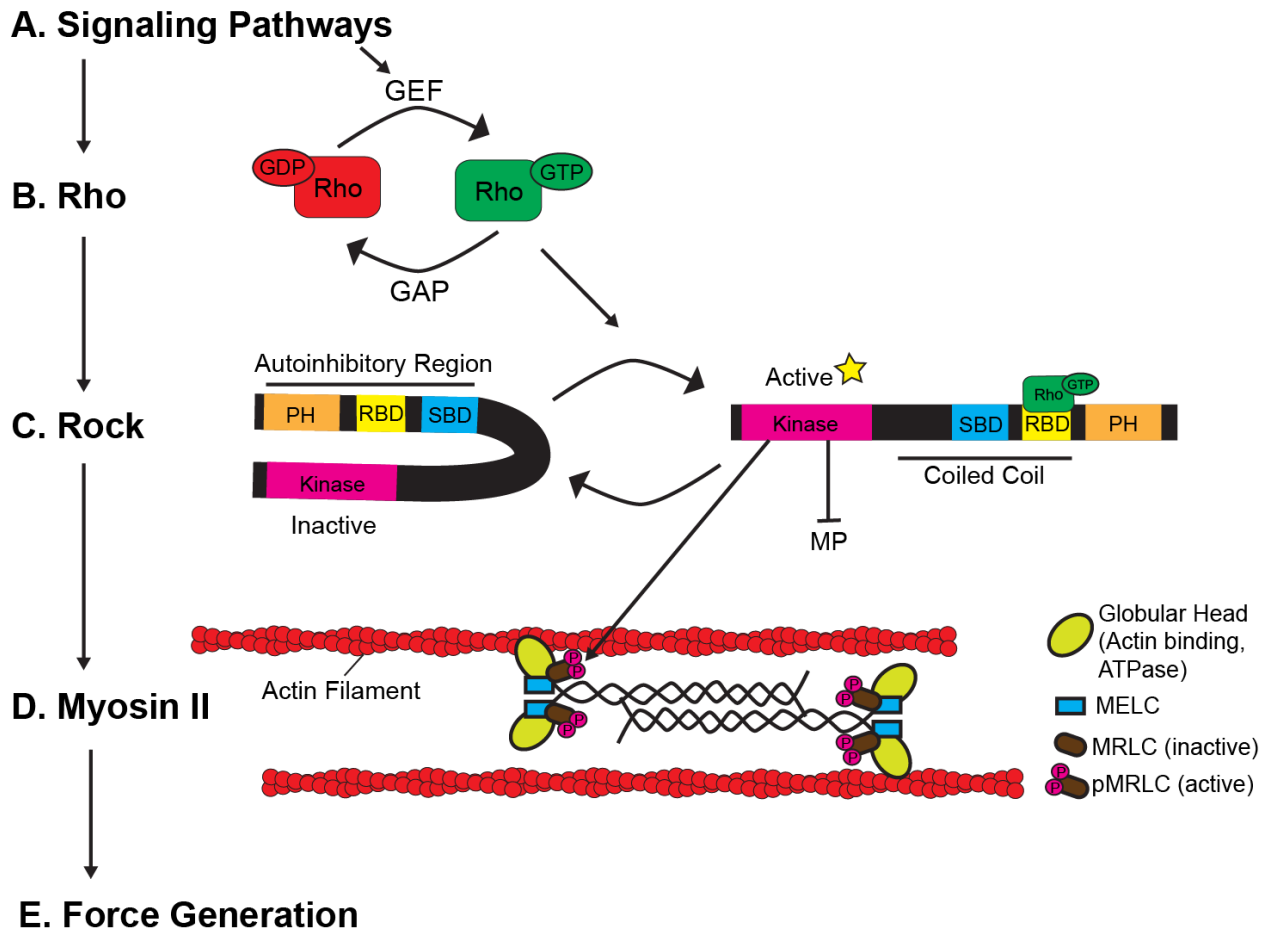


Figure 2. The Rho-Rock-Myosin II pathway.

A-E. Signaling pathways promote actomyosin contractility through the activation of the Rho-Rock-Myosin II pathway. External signals such as morphogens or mechanical force activate signaling pathways (A), which recruit and activate guanine exchange factors (GEFs) to aid in the conversion of inactive Rho-GDP to active Rho-GTP (B). Rho-GTP binds the Rho-binding domain (RBD) of Rho-kinase (Rock) to relieve intramolecular autoinhibition and activate kinase activity (C). Active Rock phosphorylates the Myosin regulatory light chain (MRLC) at two sites to activate the actin-binding and ATPase activity of Myosin II (D). Rock also phosphorylates Myosin phosphatase (MP) to block dephosphorylation of Myosin II. Active Myosin II exerts tension on actin filaments to produce

contractile force that can be used to drive cellular processes such as motility, division, and shape change (**E**). GAP: GTPase-activating protein, PH: pleckstrin homology, SBD: Shroom binding domain, MELC: Myosin essential light chain.

1.1.3 Morphogenesis

Spatially and temporally controlled epithelial morphogenesis defines animal development and is controlled by a series of cellular inputs that instruct and permit changes in cyto-architecture. Actomyosin contractility is universally used to control cell shape and behavior in response to environmental stimuli [84-90]. Morphogenetic programs are often specified by specific transcription factor profiles, which build signaling pathways that are primed for receiving signals that initiate morphogenetic behaviors (reviewed in [91]). Altering the network of signaling pathway components can drastically change the ability of a cell to execute morphogenesis. Extracellular signals such as morphogens or physical forces induce signal transduction pathways in specific cells (reviewed in [31]). Cells that are capable of receiving such signals transduce the message across the tissue through cellular adhesion structures and intracellularly through cytoplasmic effector molecules. Cells then translate the signal transduction into a morphological output by altering cyto-architecture to facilitate changes in adhesive properties, cell shape, and motility. Not only is the study of how epithelial tissues take shape important for understanding animal development and congenital disease, but also has implications for tissue regeneration and engineering.

1.1.3.1 Apical Constriction

Tissue bending is used throughout development to drive tissue invagination, to create tissue

layers, and to transform flat epithelial sheets into three-dimensional structures such as tubes. The majority of epithelial folding that underlies morphogenesis involves the concerted constriction of the apical pole of a group of cells within an epithelial sheet (reviewed in [92]). To elicit apical constriction, forces generated by actomyosin contractility at the apical adherens belt are exerted on the cell circumference and transmitted between cells through adherens junctions. These forces cause the cell apex to shrink, perhaps analogous to drawing a purse-string [93, 94] (Figure 3). Apical constriction of a single cell converts that cell from a columnar shape to a wedge-shape. When a group of cells in an epithelial sheet simultaneously undergo apical constriction, the epithelium is forced to bend, which can dictate amazing large-scale changes in tissue morphology (5) [95].

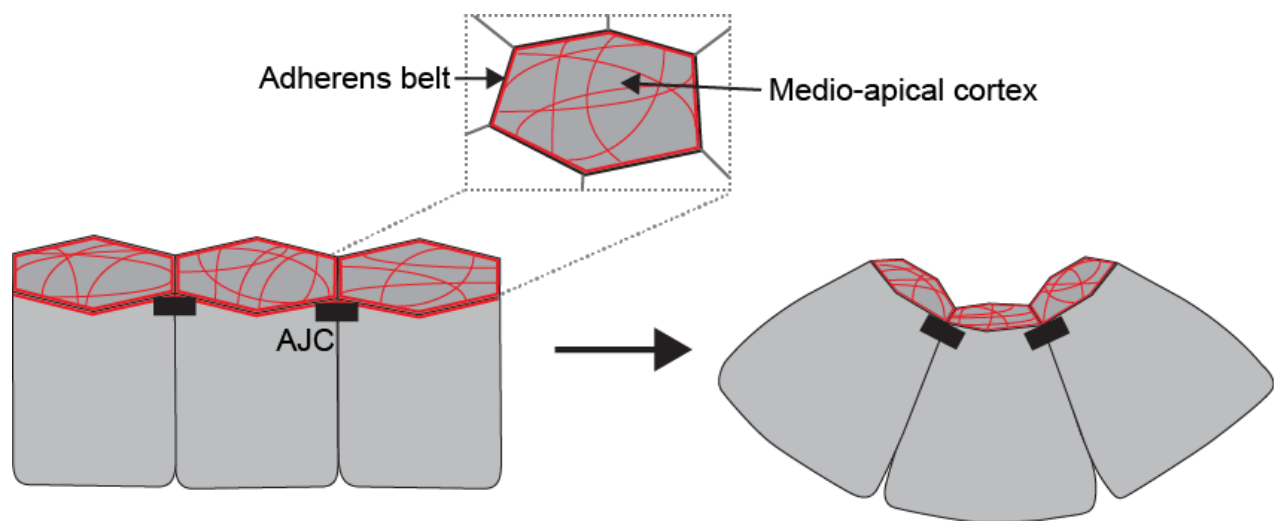


Figure 3. Apical constriction drives tissue bending

Apical constriction of cells in an epithelial sheet drives tissue bending. Epithelial cells are typically columnar and exhibit distinct populations of F-actin in the apical domain. The adherens belt forms from a circumferential population of F-actin that is associated with the apical junctional complex (AJC). F-actin fibers also form a meshwork at the apical membrane, known as the medioapical cortex. Ratchet-like constriction of these F-actin networks by Myosin II causes shrinkage of the apical surface and subsequent bending of the tissue.

The upstream signals that target and upregulate Myosin activity in cells undergoing apical constriction vary in different contexts but often require the small GTPase Rho [96-99]. A widely studied example of apical constriction is the *Drosophila* presumptive mesoderm, which apically constricts during gastrulation to form a ventral furrow that invaginates to form the primary germ layers [100, 101]. This example provides a comprehensive illustration of how transcriptional programs, signaling pathways, and cytoskeletal dynamics are utilized to drive morphogenesis. Apical constriction in this context is regulated by the transcription factors Snail and Twist, which cooperatively activate expression of signal pathway components that enhance the localization and activation of RhoGEF2 at the apical cell cortex [102]. RhoGEF2 activates Rho, which can activate the formin-family protein Diaphanous (Dia) to facilitate the polymerization of unbranched actin filaments [103]. Rho also activates Myosin II by stimulating Rock activity, thus regulating apical constriction through coordinated F-actin assembly and Myosin activation [96, 97, 102-106].

The purse-string analogy of apical constriction has recently been refuted based on multiple lines of evidence (reviewed in [107]). First, live imaging studies of *Drosophila* mesoderm have suggested that apical constriction does not occur through a single sustained contraction, but rather occurs through a ratcheting mechanism in which a series of repeated pulsed contractions serve to incrementally reduce the apical area [88]. Secondly, although Rho and Dia are localized to circumferential actin belts at the AJC, they are more apparently enriched at the medioapical cell cortex (Figure 3). Rock is excluded from the AJC and found concentrated at the center of the medioapical cell cortex. These spatial domains are important for apical constriction, suggesting that contractility of the entire cell apex is required for apical constriction

in this context [88, 89]. Importantly, contraction of the cortex must be coupled to the adherens belt, otherwise medioapical F-actin and Myosin II would contract into a ball, without the ability to translate that contraction into a change in cell shape [31]. Thus, the adherens belt is functionally important for transmitting actomyosin contraction at the cell apex through cell-cell contacts to drive tissue deformation.

Other examples of apical constriction that utilize unique mechanisms have been described. Even though apical constriction is an inherently similar cell shape change no matter the context, cells can differentially position their actomyosin contractile networks and regulate the dynamics of those networks to bring about different forms of apical constriction to drive different morphogenetic processes [92].

1.1.3.2 Convergent Extension

Morphogenesis of a population of cells often occurs through cell rearrangements. Many tissues during development undergo a process known as convergent extension, in which cells rearrange directionally to narrow the tissue along one axis, while consequently extending it along another [108]. Convergent extension is driven by directed cellular intercalation and can occur in both epithelial and non-epithelial tissues. The most widely appreciated example of convergent extension is during gastrulation in which the nascent germ layers narrow significantly along the mediolateral axis and extend along the anterior-posterior axis to form the elongated body shape characteristic of metazoans. Descriptions of convergent extension during gastrulation have been well documented in the dorsal mesoderm and ectoderm of frogs, fish, mice, sea urchins, flies, and worms [85, 109-122]. Later in development, organogenesis of tissues that require an extended morphology also relies on convergent extension. Examples include formation of the *Drosophila* hindgut and tracheal system, vertebrate neural tube morphogenesis, and mammalian

kidney tubule morphogenesis [123-128]. In some of these cases, such as neural tube formation, convergent extension occurs in an epithelial sheet, while in other cases, such as mammalian kidney tubule morphogenesis, convergent extension occurs in a preformed epithelial tube and thus results in the extension of the tube with concomitant reduction in tube diameter.

Two distinct cellular mechanisms for convergent extension have been proposed. The first is 'cell crawling' in which cells form actin-rich protrusions, called lamellipodia, oriented towards the direction of movement (Figure 4A) [110, 116]. Cells use these protrusions to form stable attachments to nearby cells and generate tractile forces to crawl across other cells and/or the extracellular matrix (reviewed in [129]). This type of convergent extension is apparent in mesenchymal cell populations such as the dorsal mesoderm in frogs, fish, and mice, which undergoes convergent extension during gastrulation to achieve axial elongation [112, 113, 116, 120, 121, 129]. Examples of cell crawling have also been described for epithelial tissues. These include the neural plates of *Xenopus*, and mouse, the neural keel of zebrafish, and the notochord of zebrafish [110, 112, 115, 117, 124, 125]. In these cases, basolateral lamellipodial projections are utilized to guide the direction of intercalation.

The second cellular mechanism is polarized remodeling of cell-cell contacts, in which cells change position while remaining connected by junctions that maintain the continuity of the sheet (Figure 4B). This type of intercalation has been most extensively studied in the cells in the *Drosophila* germband, the part of the embryo that gives rise to the segmented body of the adult. During germband extension, the tissue doubles in length along the anterior-posterior axis, while subsequently narrowing along the dorsoventral axis in the absence of cell division [114].

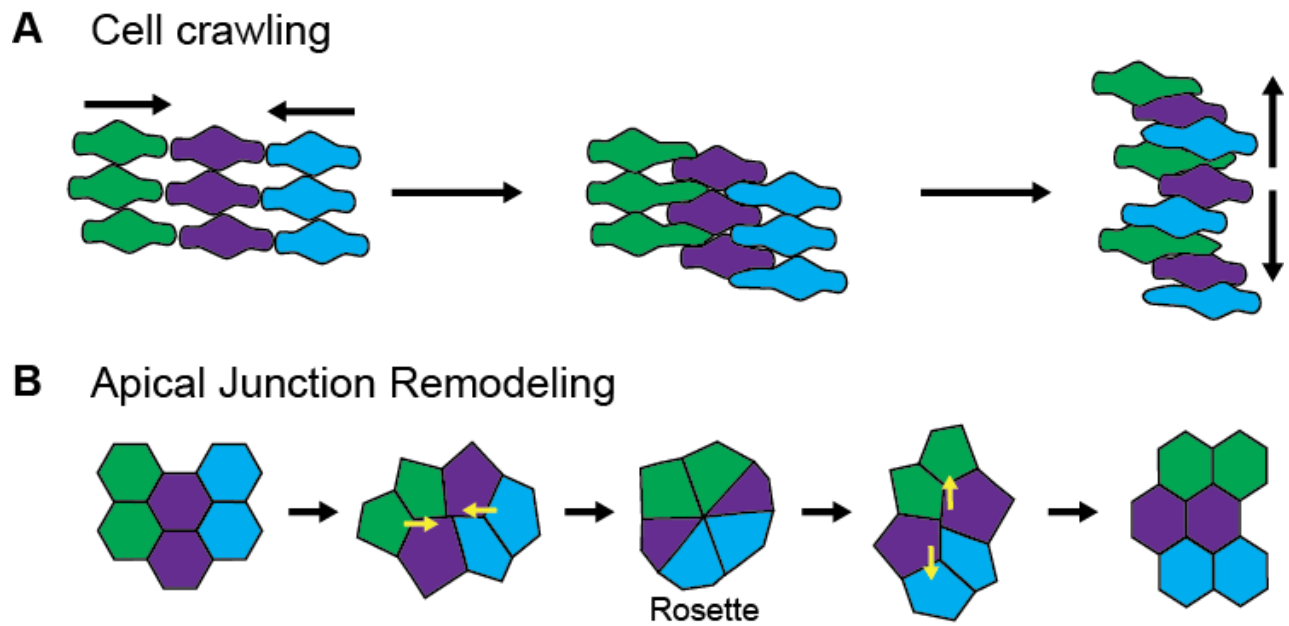


Figure 4. Cellular mechanisms of convergent extension

A and B. Convergent extension is the process through which tissues narrow and elongate along perpendicular axes. There are two main cellular mechanisms that drive convergent extension. Cell crawling (**A**) and apical junction remodeling (**B**). Cell crawling typically occurs in mesenchymal populations. Cells undergo mediolateral intercalation by extending lamellipodial protrusions in the direction of movement to generate tractile forces to pull themselves towards the midline. Epithelial tissues, which maintain robust cell-cell adhesion, undergo mediolateral intercalation through polarized junction remodeling. Junctions oriented along one axis shrink, while those oriented along the opposite axis enlarge, thereby bringing groups of cells together to form multicellular rosettes. Rosettes resolve perpendicular to the axis of formation to drive convergent extension of the tissue.

Germband extension is driven by directional cell intercalation, which is achieved molecularly through the coordination of actomyosin contractility and cell-cell adhesion [130-132]. F-actin, Myosin II, and Rock become polarized along junctions parallel to the dorsoventral axis, whereas adherens junction-associated proteins such as E-cadherin, β -catenin, and PAR-3 become enriched at junctions parallel to the anterior-posterior axis [85, 122, 130]. Actomyosin contractility along dorsoventral interfaces causes those cell junctions to shrink. Junction

shrinkage is enhanced by a positive feedback system in which the force generated by Myosin II leads to the recruitment of more Myosin II to these junctions [86]. As the dorsoventral junctions shrink, the junctions oriented along the opposing axis expand. The enrichment of junctional components at these interfaces helps to stabilize the junctions as they lengthen. Disassembly of dorsoventral adherens junctions occurs through endocytosis and recycling of junctional components such as E-cadherin [133]. As a result of shrinking and stretching, junctions are remodeled such that linearly aligned groups of cells simultaneously constrict and disassemble their dorsoventral interfaces to bring anywhere from 4-10 cells into a cluster that are all connected at a single vertex. These multicellular clusters, termed rosettes, form along the dorsoventral axis and resolve along the anterior-posterior axis, thus groups of cells exchange neighbors in a directional fashion to achieve a net extension of the germband [109].

Examples of convergent extension by polarized formation and resolution of rosettes have recently been described in other systems including the neural plates of chick and mice, and in developing mouse kidney tubules which form cellular rosettes around the circumference of the tubules [98, 128, 134, 135]. Thus, the coordinated activity of actomyosin contractility and adhesion underlies epithelial intercalation in a wide array of contexts.

1.2 EVENTS OF MAMMALIAN NEURAL TUBE MORPHOGENESIS

An extraordinary example of epithelial morphogenesis is neural tube closure, a dramatic series of morphogenetic events that initiate the development of the vertebrate central nervous system. The neural tube is an epithelial embryonic structure that extends the entire length of the body axis and provides a platform for forming the brain and spinal cord; the anterior region

develops into the brain and the posterior region develops into the spinal cord. Much of what we know about the events of neural tube closure in humans comes from studies done in mice, in which the process is very similar (reviewed in [136-139]). Neural tube closure begins with the formation of the neural plate, a flat, thickened epithelial sheet derived from neural ectoderm on the dorsal surface of the early embryo (Figure 5A). The neural plate is initially short and wide and must narrow and elongate to extend along the anterior-posterior axis of the embryo. This is accomplished through convergent extension, whereby cells from the lateral edges of the neural plate intercalate towards the midline. Convergent extension of the neural plate occurs through a combination of cellular mechanisms including apical junctional remodeling and the projection of mediolaterally directed basolateral protrusions [134]. During this elongation, the neural plate is transformed into a key-hole shaped structure, with a wide cranial region and narrow spinal region. Concomitantly, the neural plate bends at a single medial and paired dorsolateral hinge points parallel to the anterior-posterior axis to initiate elevation of the lateral edges of the neural plate (Figure 5B) [140]. Neural plate bending is driven by apical constriction of cells within these hinge points. As bending proceeds, the lateral edges of the plate fold towards each other and eventually fuse at the dorsal midline, thereby converting the flat sheet of cells into a hollow tube (Figure 5C).

Neural tube closure initiates sequentially along the anterior-posterior axis during a well-defined timeframe (Figure 6A). In mice, closure begins at embryonic day 8.5 (E8.5) initiating at the base of the future hindbrain and proceeding bidirectionally from that point. This initial closure point is referred to as 'Closure 1'. At E9.0, two additional closure points form rostral to Closure 1 to initiate closure of the neural tube in the future brain [141]. Progression of closure continues from these three initiation points in a zipper-like fashion and the tube is completely

sealed by E10. In humans, there are only two initiation sites and closure is typically complete 28 days post conception (reviewed in [142, 143]). As development proceeds, the neural tube proliferates and differentiates to build the brain and spinal cord.

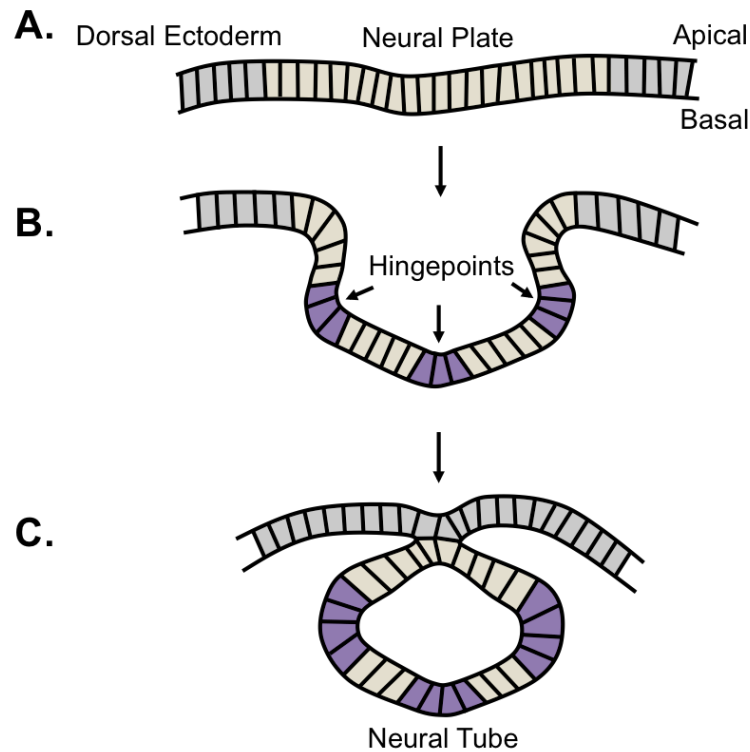


Figure 5. The neural plate bends at hinge points to form the neural tube

A. The neural plate is a thickened epithelial sheet derived from the neural ectoderm on the dorsal surface of vertebrate embryos. B. Neural tube formation is initiated by the formation of hinge points that bend the neural plate, causing the neural folds to elevate towards the midline. Hinge point formation involves apical constriction of neural plate cells. C. Once the neural folds have converged on the midline, they fuse along the entire anterior-posterior axis to form a tube ventral to the dorsal ectoderm.

As noted, the process of neurulation is highly conserved in mice and humans. Studies in other animal model systems such as frog, chick, and zebrafish, have been extremely valuable in delineating the series of events of neural tube closure and their cell and molecular regulation.

The usefulness of these models in identifying the molecules and pathways at play during neural tube formation cannot be overstated. However, there are some differences in the process of neural tube morphogenesis in non-mammalian models. For example, neurulation in chick occurs through a different sequence of closure events along the body axis [144, 145]. In contrast to the pseudostratified neural plate of mice and humans, the frog neural plate consists of two distinct cell layers and closure occurs almost simultaneously at all levels along the anterior-posterior axis [146]. Lastly, zebrafish form a neural tube by an entirely different morphogenetic process that does not involve bending and fusion of a flat epithelial plate (reviewed in [147]). Instead, the zebrafish neural tube initially forms as a solid cord that subsequently hollows through precisely timed apoptosis. Therefore, although many aspects of neural tube formation are conserved across animal models, there are key differences in the morphogenetic programs that are likely to be reflected in the molecular machinery that drives neural tube formation in each animal. Thus, the use of mouse as a model system is essential for understanding mammalian neural tube morphogenesis.

1.2.1 Neural Tube Defects

Neural tube closure is highly sensitive to alterations in the precise coordination of cell behavior. Errors in neural tube closure result in neural tube defects, the second most prevalent class of human congenital malformations behind congenital heart disease [148]. These debilitating or fatal birth defects occur in approximately 1 in 1000 human pregnancies worldwide and arise when the neural tube fails to close, leaving a connection between the lumen and the outside environment (reviewed in [149]). Neural tube defects are characterized by the region of the embryonic axis affected (Figure 6A).

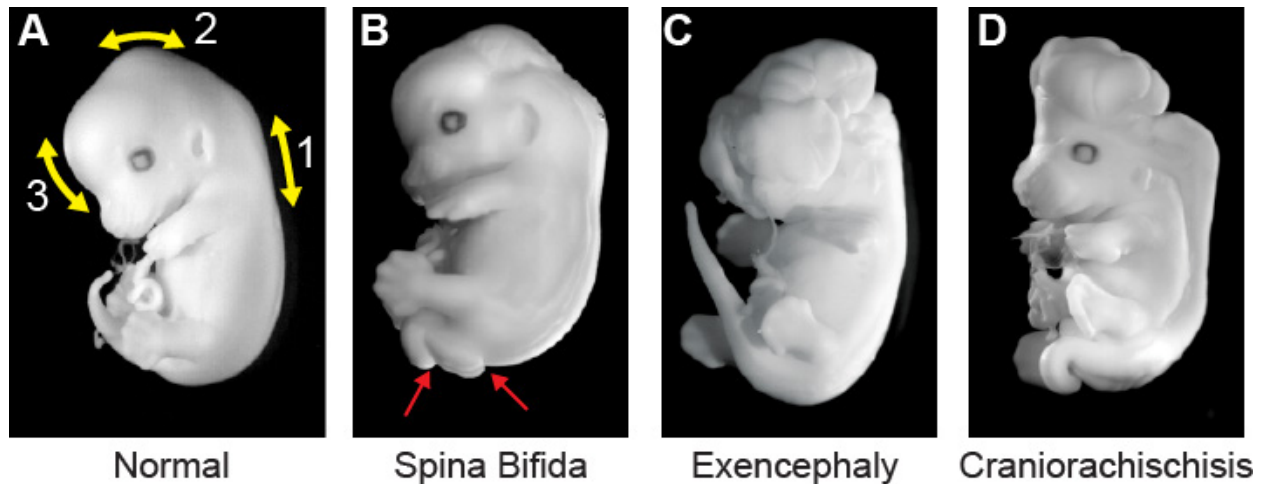


Figure 6. Mouse models of neural tube defects

A-D. Mouse embryos with genetic lesions linked to neural tube defect development were isolated at embryonic day 13 (E13), fixed, and photographed. **A.** Wildtype embryo with a properly formed central nervous system. Yellow arrows show locations of closure points 1-3 along the anterior-posterior axis. **B.** Spina bifida is characterized by an open spinal cord in the caudal region (between red arrows). **C.** Incomplete closure of the cranial neural tube causes exencephaly. **D.** The most severe neural tube defect results from failure to initiate closure at closure point 1 and is termed craniorachischisis. The neural tube in this case remains open along the entire body axis.

Failure to complete closure caudally from closure point 1 results in a defect known as spina bifida (Figure 6B). This condition is characterized by an open posterior neural tube and can vary in severity depending on how much of the neural tube remains open. Infants with spina bifida can survive with extensive surgical intervention, however they face lifelong handicaps associated with neurological impairment [150]. Failure to close the anterior region of the neural tube results in exencephaly, whereby the developing forebrain remains in contact with the amniotic fluid and degenerates as embryogenesis proceeds (Figure 6C). Failure to initiate closure point 1 causes craniorachischisis, a condition in which the neural tube remains open along the entire anterior-posterior axis (Figure 6D). All infants with exencephaly or craniorachischisis are stillborn [151].

The mechanisms underlying neural tube defect development are complex and poorly understood. The majority of cases arise sporadically without a family history [138]. Many non-genetic factors have been attributed to neural tube defect development including parental age, race, socioeconomic status, hyperthermia during pregnancy, maternal diabetes, obesity, nutrition, and/or drug use, and exposure to chemical agents [152-161]. Although there are no mutations in single genes that are known to predispose a person to a neural tube defect, there is evidence for a genetic basis of inheritance of neural tube defects such as high recurrence rates after an affected pregnancy, high concordance rates among twins, and association with known chromosomal abnormalities, genetic syndromes, and gene variants found among cohorts of neural tube defect patients [162-167]. Furthermore, susceptibility to environmental risk factors may be modified by genetic predisposition (reviewed in [149]). Thus, the etiology of neural tube defects is thought to be multifactorial, resulting from a combination of environmental factors and risk alleles. Little is known about the identity of specific risk alleles in humans, how many risk alleles are typically present in an affected individual, what combinations of risk alleles produce a neural tube defect, or even if risk alleles are the same between different populations of people. Studies using mice have generated over 250 mutant lines that give rise to neural tube defects (reviewed in [168, 169]). These mutants provide candidate risk alleles for human neural tube defect development and include genes that regulate a wide array of cellular functions such as apoptosis, migration, proliferation, differentiation, actomyosin contractility, neuroepithelial polarity, folate metabolism, and epigenetic modification. The genetic complexity of neural tube defects is recapitulated in the mouse, in which heterozygosity for multiple risk alleles is often sufficient to cause neural tube defects. Genetic approaches in mice lend the opportunity to combine multiple risk alleles simultaneously to model how neural tube defects develop in human populations

(reviewed in [170]). The discovery of how neural tube defect risk alleles interact in mice is imperative to eventually forming a complete genetic understanding of their development in humans.

1.2.2 Forces That Close The Neural Tube

The major morphogenetic processes required for neural tube closure are apical constriction, which drives hinge point formation, and convergent extension, which drives tissue elongation. There are several extrinsic forces known to promote these morphogenetic events. These mainly include pressure on the neural folds from adjacent tissues such as the dorsolateral surface ectoderm and the expanding head mesenchyme that surrounds the cranial neural plate. Evidence for such a role for extrinsic force comes from phenotypes associated with mutations in genes that either increase or decrease head mesenchyme expansion (e.g., *Twist*, *Cart1*, *Alx3*, *Hect*) [171-174]. Neural tube closure fails upon genetic manipulation of these genes, indicating a role for external forces in aiding neural fold elevation. However, *Xenopus* and mouse neural plates can form hinge points and converge and extend in the absence of surrounding tissues, suggesting that these processes are also highly active and rely on intrinsic forces generated within neural epithelial cells [126, 141]. These forces are attributed to actomyosin contractility; disruptions of the F-actin network through pharmacological or genetic perturbation inhibit hinge point formation in multiple animal models [175-177]. Additionally, neural tube defect mouse models often have mutations in actin-binding proteins such as n-Cofilin, Mena, and Profilin I [178, 179]. Myosin II and Rock are both required for apical constriction and convergent extension, as exposing embryos to small molecule inhibitors of Myosin II (Blebbistatin) or Rock (Y267632) causes neural tube defects due to failure of both

morphogenetic processes [180]. Neural tube defects are also seen upon genetic manipulation of either component in multiple animal models [146]. Thus, understanding the molecular regulators of actomyosin contractility during neural tube morphogenesis is critical for understanding how the neural tube is shaped.

1.3 SHROOM3 DRIVES APICAL CONSTRICTION

Since its discovery nearly fifteen years ago, the cytoskeleton-associated protein Shroom3 has emerged as a major player in the developmental control of epithelial cell shape in a number of different tissues across diverse animal phyla [99, 131, 181-188]. Shroom3 was originally identified in a gene-trap mutagenesis screen in mice, which spliced a lacZ reporter gene into the *Shroom3* locus, thereby disrupting its function and providing a system to track endogenous *Shroom3* expression by X-Gal staining [182]. Mice homozygous for the gene-trap *Shroom3* allele, *Shroom3^{gt}(rosa53)sor* (*Shroom3^{gt/gt}*), display the cranial neural tube defect exencephaly with a penetrance of 100%. The spinal region of the neural tube closes, however histological analysis shows apparent defects along the entire anterior-posterior axis including a loss of rigidity and collapsed lumen. *Shroom3* mutant neural tubes and surrounding tissues do not exhibit defects in cell proliferation, differentiation, or apoptosis. Additional less-penetrant phenotypes associated with Shroom3 depletion include facial clefting (87%), spina bifida (23%), and ventral closure defects leading to herniation of internal organs (12%) [182]. When orthologs of mouse *Shroom3* are disrupted in *Xenopus* or chick, similar phenotypes are observed [135, 181]. In wildtype embryos, prior to initiation of neural tube closure, Shroom3 is expressed along the entire length of the neural plate and localized to the AJC. Shroom3 functions as a scaffold

and is required for the apical accumulation of F-actin, Myosin IIB, Rock1, and pMRLC [135, 181, 182, 189]. Despite its scaffolding functions, Shroom3 is not required for establishing apical-basal polarity, as its depletion does not affect the localization of apical junction markers such as ZO1 or β -Catenin [135, 182, 189, 190]. When Shroom3 is ectopically expressed in Madin Darby Canine Kidney (MDCK) cells, or *Xenopus* blastomeres, it induces apical accumulation of F-actin, Rock, and pMRLC and subsequent apical constriction [181, 189]. Thus, the defects in *Shroom3* mutant embryos are attributed to a role in driving apical constriction through the regulation of actomyosin contractility.

Shroom3 is expressed in a myriad of developing epithelial tissues including the optic pit, hindgut, foregut, kidneys, lungs, and somites [182]. Since the discovery of Shroom3 as a major regulator of neural tube morphogenesis, it has been shown to regulate apical constriction in several developing epithelial tissues including the *Xenopus* and mouse gut, zebrafish lateral line, and the lens vesicle of chick and *Xenopus* [99, 184-187]. The transcriptional regulation of Shroom3 is not well understood. Pax6 and Pitx1 have been shown to regulate Shroom3 expression in the lens placode and the gut, respectively [184, 186]. However, a potential role for Pax6 in the neural plate has not been investigated and Pitx1 is not present in the neural plate at the right time to be a candidate for regulating Shroom3 expression during neural tube morphogenesis.

The Shroom3 protein is characterized by a specific array of domains: an N-terminal PDZ domain followed by a serine proline rich region (SPR), a centrally located Shroom-Domain 1 (SD1), and a C-terminal Shroom-domain 2 (SD2) (Figure 7) [182]. The SD1 and SD2 are unique motifs found only among Shroom family members.

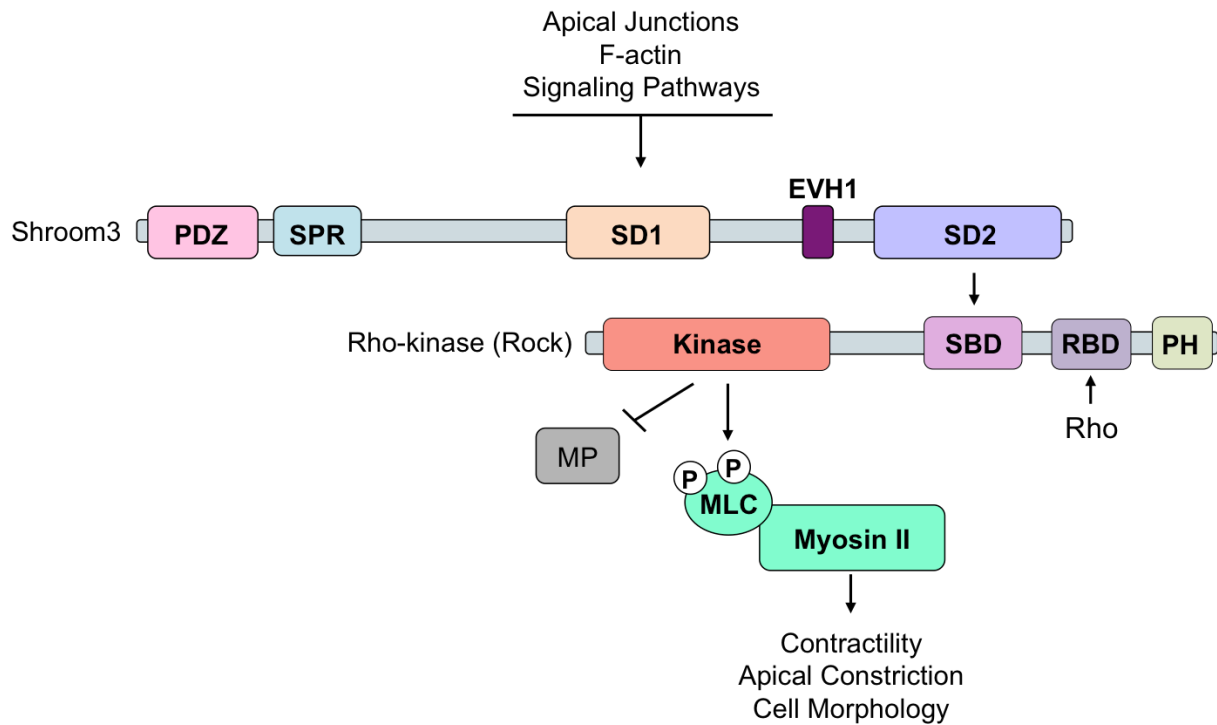


Figure 7. The Shroom-Rock pathway

Shroom3 determines cyto-architecture through the regulation of actomyosin contractility. Shroom3 is recruited to the AJC through direct binding of F-Actin to the centrally located SD1 domain. Additional junctional components and signaling pathways are likely to participate in targeting Shroom3 to the AJC. Rock binds to Shroom3 through a direct interaction between the SD2 of Shroom3 and the SBD of Rock. Shroom-Rock binding facilitates recruitment and potentially activation of Rock to the AJC, where it activates Myosin II directly through phosphorylation of the MRLC and indirectly through phosphorylation of Myosin phosphatase (MP).

Shroom3 also contains a putative EVH1 (Ena/VASP homology domain) binding site and a PDZ binding motif. An isoform of Shroom3 that lacks the PDZ domain exists endogenously and can induce apical constriction when ectopically expressed in MDCK cells or *Xenopus* blastomeres, indicating the PDZ domain is dispensable for Shroom3 function [189]. Shroom3-induced apical constriction requires the SD1, SD2, and EVH1 binding site. Shroom3 directly binds F-actin through an actin-binding motif in the SD1, facilitating junctional recruitment [181,

182, 189, 191]. The EVH1 binding site binds to the actin-regulatory protein Ena/VASP, an interaction that likely facilitates remodeling of the apical actin network [186]. Shroom3 binds Rock through a direct interaction between the SD2 domain of Shroom3 and a specific Shroom binding domain (SBD) of Rock [73, 192]. In every tissue in which Shroom3 function has been studied, Shroom3-induced apical constriction is contingent upon its proper subcellular localization and its ability to bind Rock.

Structural studies of the Shroom SD2 and Rock SBD have provided insight into the importance of Shroom-Rock binding in regulating cyto-architecture [73, 192]. The crystal structures of each domain reveal that they are both composed of coiled-coil dimers. The SD2 is a unique antiparallel coiled-coil dimer divided into three segments, a long central body segment flanked by two arm segments [192]. The SBD of Rock is a parallel coiled-coil [73]. Mutations that disrupt dimerization prevent SD2-SBD binding, indicating that dimerization is important for building Shroom-Rock complexes, consistent with the fact that both proteins exist as dimers in solution and interact with a stoichiometry of 1:1 [73, 192]. Through site-directed mutagenesis, a series of mutations were generated to map the specific amino acids on each domain that are required for interaction. Patches of conserved residues on the surface of the main body segment of SD2 were identified as the Rock-binding interface; alanine substitutions at these residues do not disrupt dimerization but dramatically reduce Rock binding [192]. Two highly conserved surface patches on the SBD dimer constitute the Shroom-binding interface [73]. Importantly, substitutions that interfere with either binding interface block Shroom-induced apical constriction in MDCK cells, emphasizing the importance of the Shroom-Rock interaction in Shroom function [73, 192]. Additionally, ENU-induced alleles of Shroom3 that contain mutations in the Rock-binding interface cause exencephaly, thus even when properly targeted *in*

in vivo, failure to bind Rock abrogates Shroom3 function (Das and Hildebrand, unpublished data). Based on the known function of Rho binding in relieving Rock autoinhibitory interaction and the fact that the RBD and SBD are only separated by fifty amino acids, it is an intriguing possibility that Shroom3 binding can also relieve Rock autoinhibition, thereby activating kinase function.

It is currently unclear whether Shroom3 plays an instructive role in activating Rock or is simply required for its localization. It is possible that Shroom3 recruits a previously activated population of Rock, recruits inactive Rock that is subsequently activated by another molecule, such as Rho, or is sufficient to activate Rock by binding and relieving autoinhibition. Despite the close molecular proximity of the RBD and SBD, both Rho and SD2 can simultaneously bind Rock *in vitro* [186]. As the main upstream activator of Rock in many contexts, it has long been hypothesized that Rho activates Rock during Shroom3-induced apical constriction. Rho is localized to the AJC of the neural epithelium and loss of Rho function through the use of small molecule inhibitors causes a loss of activated Myosin regulatory light chain (pMRLC), failure of hingepoint formation, and neural tube defects [180]. In MDCK cells, apically targeted Rho induces apical constriction in a Rock-Myosin II-dependent manner [99]. Moreover, mice that harbor mutations in the Rho inhibitor p190RhoGAP inhibit neural tube closure and mimic defects seen upon Rho depletion, indicating that a precise level of Rho activity is required for proper neural plate morphology and hingepoint formation [180, 193].

Several lines of evidence suggest that Rho is not required for Shroom3-induced apical constriction. Firstly, dominant negative Rho does not interfere with ectopic Shroom3-mediated apical constriction in MDCK cells or *Xenopus* blastomeres, [181, 189]. Secondly, co-expression of Shroom3 and a Rock construct that lacks the RBD in MDCK cells does not interfere with Shroom3-induced apical constriction [73]. Taken together, this suggests that Shroom3 is capable

of mediating Rho-independent Rock activity, but input from Rho may be required to generate a precise level of Rock activation. Additional experiments are required to parse the relationships between Rho, Shroom3, and Rock.

In addition to Rock binding and activation, Shroom3 function relies on its proper targeting to adherens junctions. Whether Shroom3 is recruited through F-actin binding alone or via additional upstream factors that regulate its subcellular distribution is largely unknown. In recent years, a potential upstream regulator of Shroom3 has been identified. Lulu is member of the FERM (Four-point-one, Ezrin, Radixin, Moesin) protein family, a collection of cytoskeletal regulators that link F-actin to the cell membrane. Lulu depletion in mice causes early lethality (E8.5) due to severe gastrulation defects [194]. The neural plate in these embryos is properly specified, however it is extremely broad, severely deformed, and lacks hinge points. Despite the deformation, the neural plate maintains adherens junction architecture and apical-basal polarity. F-actin and Myosin IIb are diffusely distributed throughout the cytoplasm, suggesting a role for Lulu in regulating apical actomyosin networks [194]. Morpholino knockdown of *Xenopus* Lulu recapitulates these phenotypes [195]. Ectopically expressed Lulu in MDCK cells or *Xenopus* blastomeres induces apical accumulation of F-actin and pMRLC, and apical constriction, phenotypes that mimic ectopic expression of Shroom3. These phenotypes can be reverted with small molecule inhibition of Myosin (Blebbistatin) or Rock (Y26732). In the absence of Lulu, endogenous Shroom3 fails to accumulate at apical junctions and ectopic expression of Shroom3 fails to induce apical F-actin accumulation and apical constriction [195, 196]. Taken together, these results suggest that Lulu drives Myosin-dependent apical constriction by regulating the subcellular distribution of Shroom3. Whether Lulu directly binds to Shroom3 is yet to be determined. Interestingly, the Shroom family member, Shroom2, was shown to directly bind to

the FERM domain of MyosinVIIa through a region of Shroom2 N-terminal to the SD1 [197]. Thus, a binding interface for FERM domains exists in other Shroom family members and may be conserved in Shroom3. Besides Lulu, Rho is a suggested candidate for regulating Shroom3 localization. In MDCK cells, basolaterally targeted Rho recruits both ZO1 and Shroom3 to the basal end of the cell and induces basal constriction, indicating that Rho may play a role in Shroom3 junctional localization [99].

Our current understanding of Shroom3-Rock pathway function is not sufficient to explain neural plate bending. Presumably, if every cell in the neural plate were to simultaneously undergo uniform apical constriction, the plate would roll up into a sphere instead of forming an elongated tube. Instead, the neural plate only bends along the mediolateral axis so that the neural folds converge on the midline (Figure 8). Thus, further studies are necessary to understand how apical constriction is regulated to bend the neural plate in a polarized fashion.

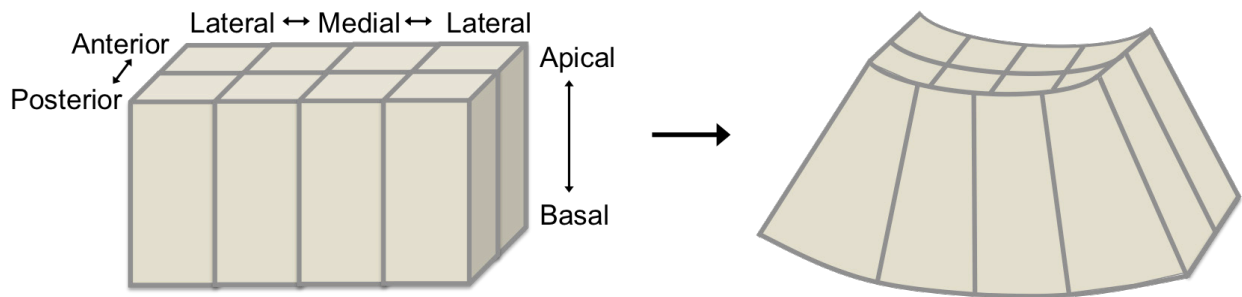


Figure 8. Neural plate bending occurs along the mediolateral body axis

Neural epithelial cells undergo apical constriction along the mediolateral body axis to form a hollow tube. How polarized neural plate bending is regulated remains to be determined.

1.3.1 Shroom Family Members: Shroom1, 2 and 4

Shroom3 is the most extensively characterized member of the Shroom protein family. However, other vertebrate Shroom family members, Shroom1, 2 and 4, are likely involved in a wide range of biological processes in adults and embryos. Shroom2 is required for melanosome function, retinal morphogenesis, and endothelial branching [198-200]. Specific functions for Shroom1 and Shroom4 have not been determined, however they are both expressed in an assortment of epithelial tissues and have been shown to influence cyto-architecture [201-203]. Additionally, loss of Shroom protein function contributes to human disease conditions. For example, mutations in hShroom4 have been associated with X-linked mental retardation and mutations in hShroom2 are associated with Ocular albinism type 1 [204, 205]. We predict that Shroom proteins are utilized in various morphogenetic processes to influence cell shape and behavior through the regulation of actomyosin contractility.

The ability to broadly employ Shroom proteins in various morphogenetic processes is reflected in their varying domain structures. Shroom2 and Shroom4 contain N-terminal PDZ domains. As is the case for Shroom3, elimination of the PDZ does not impact Shroom4 localization. Conversely, loss of the PDZ domain marginally affects Shroom2 localization [189, 191, 199]. All Shroom proteins can bind F-actin, however Shroom4 does not contain an SD1 domain [191, 203]. All family members have SD2 domains that share significant homology. Shroom2 and Shroom4 have been shown to physically interact with Rock via the SD2 [199, 203]. Although Shroom1 has not been tested, the high degree of conservation within the SD2 suggests Shroom1 is also capable of binding Rock. The presence of highly conserved SD2 domains in all family members provides further evidence for the importance of Shroom-Rock interactions in facilitating Shroom function.

Despite the fact that all Shroom family proteins contain SD2 domains and can bind Rock, Shroom3 is the only member that induces apical constriction of MDCK cells [191]. Interestingly, apical constriction is induced by chimeric versions of Shroom3 that contain the SD2 of any other family member, indicating that all family members are capable of inducing apical constriction when properly targeted [191]. The inability of Shroom1, 2, and 4 to induce apical constriction is likely because of a difference in the subcellular localization of each protein. The localization of these proteins is determined by differential actin-binding capacity and unique binding partners that target them to different subcellular locales [189, 191, 197, 199, 201, 203, 206]. Thus, the varying N-terminal regions of Shroom proteins control their subcellular localization, while the C-terminus provides the functional capacity to alter actomyosin contractility through the modulation of Rock activity [189, 191].

1.3.2 *Drosophila* Shroom and the evolutionary conservation of Shroom-Rock Function

Drosophila has a Shroom ortholog that codes for at least two protein isoforms, the functions of which have been addressed by two studies [131, 183]. Early characterizations of dShroom isoforms dShroomA and dShroomB determined that these proteins contain C-terminal SD2 domains but lack N-terminal PDZ and central SD1 domains [183]. The dShroomA isoform is more abundantly expressed than dShroomB and localizes to cortical F-actin at the adherens junctions of several epithelial tissues undergoing morphogenesis including the extending dorsal ectoderm and the invaginating gut [183]. Despite lacking an SD1, dShroomA is capable of binding actin through an actin-binding motif that shares little sequence conservation with vertebrate Shroom proteins [183]. Ectopic expression of dShroomA in the dorsal ectoderm causes apical constriction and disorganization of cells at their apical surface. These phenotypes

are absent when a truncated version of dShroomA that lacks the SD2 is overexpressed, indicating that like Shroom3, dShroomA elicits apical constriction through dRok. *In vitro* binding assays confirmed a direct interaction between the SD2 of dShroomA and the SBD of dRok. Furthermore, simultaneous overexpression of dShroomA and either dominant negative dRok or dominant negative Myosin II specifically blocks dShroomA-induced apical constriction [183].

A study published this year by Simoes et al. identified dShroomA as a major regulator of dRok localization and activity during germband extension [131]. It had previously been shown that dRok is required for polarized junction remodeling during convergent extension of the germband through multiple means. First, dRok is planar polarized along the dorsoventral axis, where it recruits and activates Myosin II to allow for directional junction shrinkage. Second, dRok phosphorylates Par3, thereby antagonizing its localization at dorsoventral junctions and promoting adherens junction disassembly in shrinking junctions [130]. The mechanisms that regulate the planar polarized distribution of dRok, however, remained elusive. Both dShroomA and Rho were likely candidates based on their localization to adherens junctions prior to germband extension and capacity to bind and recruit dRok. Indeed, both dShroomA and Rho localize primarily to shrinking junctions and depletion of either disrupts the planar polarized distribution of dRok. dShroomA likely functions downstream of Rho, as loss of Rho causes a loss of dShroomA planar polarity, whereas loss of dShroomA has no effect on Rho localization. dShroomA does not contain a canonical Rho binding site, thus the recruitment of dShroomA by Rho either occurs through a non-canonical binding site or an indirect interaction that is mediated by another molecule. F-actin is planar polarized in a Rho-dependent fashion, and a dShroomA construct that lacks the actin-binding motif fails to polarize, suggesting that Rho localizes dShroomA through its regulation of the F-actin network. Finally, dShroomA is required for

maintaining planar polarity of Myosin II and generating force at shrinking junctions, thus, dShroomA depletion causes failure of multicellular rosette formation and subsequent convergent extension of the tissue. This study suggests a role for the Shroom-Rock-Myosin pathway in regulating convergent extension.

Taken together, these studies identified dShroomA as an invertebrate Shroom protein that is functionally similar to Shroom3, indicating evolutionary conservation of the Shroom-Rock-Myosin pathway in epithelial morphogenesis [183]. The Shroom-Rock-Myosin pathway is likely conserved among diverse animal phyla, as potential orthologs of the SD2 have been identified in the cnidarian *Hydra magnipapillata*, the ascidian *Ciona intestinalis*, and the echinoderm *Strongylocentrotus purpuratus* [191]. Yeast and *Arabidopsis thaliana* genomes do not contain *Shroom* orthologs, indicating that Shroom is an animal-specific protein. However, *Shroom* orthologs have not been identified in all animals, for example the nematode worm *Caenorhabditis elegans* and the flatworm *Schmidtea mediterranea* do not contain clear *Shroom* orthologs [191].

1.4 PLANAR CELL POLARITY

Planar cell polarity (PCP) refers to the polarization of an epithelial sheet along the x-y axis, perpendicular to the apical-basal axis [207]. Formation of proper apical-basal polarity is generally a prerequisite for the formation of planar cell polarity. Planar cell polarity is an intrinsic property of many epithelial tissues including all adult *Drosophila* cuticular epithelia and mammalian tissues such as the skin and inner ear (reviewed in [208]). In its most basic form, manifestations of planar polarity are seen throughout the animal kingdom; the feathers on a bird,

the alignment of scales on a fish, or the hair covering mammalian skin are just a few examples. Disruption of planar cell polarity results in disorganized epithelial structures. For example, planar cell polarity disruptions in mammalian epidermis disrupt hair follicle orientation and thus hairs are arranged in random directions [209-211]. Planar cell polarity is established and maintained in a field of cells by a highly conserved core signaling module referred to as 'PCP signaling'. This signaling module is employed in a wide array of tissues across species to generate asymmetric structures and to promote directional cell behavior.

1.4.1 Mechanisms of Planar Cell Polarity in *Drosophila*

The PCP signaling module is encoded by a deeply conserved set of PCP genes. The initial identification of so-called 'PCP genes' arose from genetic studies of *Drosophila* mutants that display misorientation of normally highly ordered structures. Thus, our mechanistic understanding of how the PCP signaling module establishes and maintains polarity and subsequently translates that polarity into morphological asymmetry is rooted in intensive genetic investigations in *Drosophila*. The two best-studied systems are the pupal wing and the compound eye, which will be discussed in the following sections.

1.4.1.1 Wing Hair Orientation

The *Drosophila* wing is a simple single-layered epithelium that develops from the wing imaginal disc. In early pupal stages, the wing imaginal disc undergoes a complex series of cell rearrangements, shape changes, divisions, and expansions to form the wing blade [212]. Later in development, each cell of the wing develops a single actin-rich protrusion called a trichome or wing hair. Hairs exhibit obvious planar polarization along the proximal-distal axis of the wing; a

hair initiates at the apical surface of the distal side of each cell and points distally (Figure 9A) [213]. Hair development begins with the localization of actin and microtubules at the apical-distal membrane, which polymerize to form structures that extend from the tissue [214-216]. By the onset of hair formation, cellular proliferation, differentiation, and movement within the wing blade are mostly completed [217, 218].

Planar cell polarity is established mechanistically through a set of protein components that form membrane-bound complexes that become asymmetrically localized across adherens junctions to establish molecular asymmetry within and between cells (reviewed in [219]). A set of six proteins comprises the ‘core PCP signaling pathway’, and includes the seven-pass transmembrane protein Frizzled (Fz), the four-pass transmembrane protein Van Gogh (Vang, also called Strabismus), the seven-pass transmembrane cadherin Flamingo (Fmi, also known as Starry Night), and the cytosolic proteins Dishevelled (Dsh), Diego (Dgo), and Prickle (Pk) [220-227]. Complete loss of any of these core components causes a loss of planar polarity and phenotypes in which hairs initiate at the center of each cell and point in random directions (Figure 9B) [220, 225, 227].

The core planar cell polarity pathway is often referred to as non-canonical Wnt signaling, as many of the required components overlap with the canonical Wnt- β -catenin pathway. The canonical pathway is essential for the control of embryonic segmentation in flies and for specifying the dorsoventral axis in early vertebrate embryos. The pathway initiates through the binding of a Wnt ligand to a Fz receptor, leading to Dsh activation and subsequent stabilization of β -catenin, which can enter the nucleus and regulate gene transcription [228]. Dsh is a multidomain protein and the domains required to transduce canonical and non-canonical signals are distinct (reviewed in [229]).

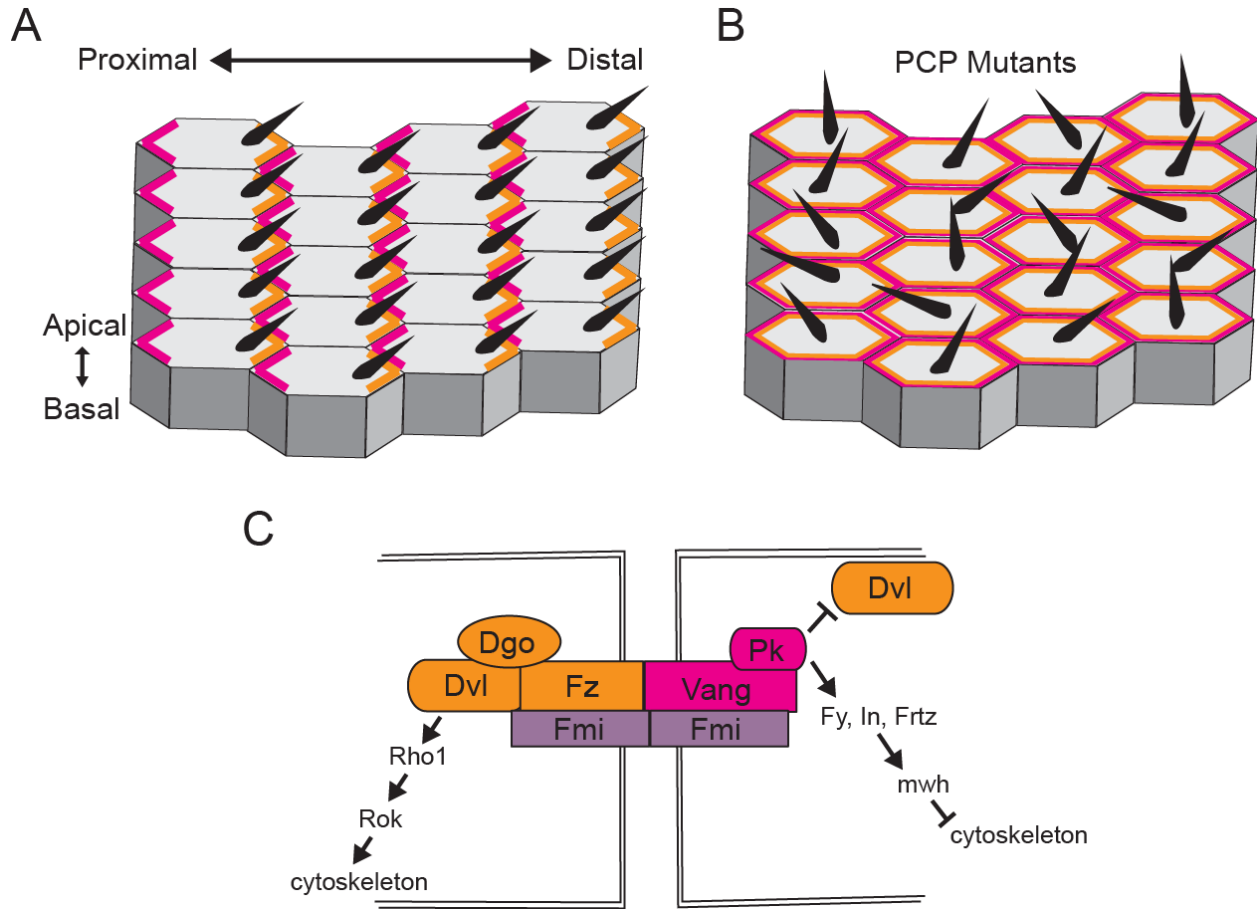


Figure 9. The planar cell polarity signaling module regulates fly wing hair orientation

A. *Drosophila* wings exhibit planarly polarized hairs that form at the distal end of each cell and point distally. The asymmetric formation of hairs is established by planar cell polarity signaling components, which become asymmetrically localized across adherens junctions to restrict hair formation to one pole of each cell. Pink = proximal complex. Orange = distal complex. **B.** Mutations in PCP components lead to aberrant hair positioning, whereby hairs form in the middle of each cell and point in various directions. Additionally, loss of any one PCP component causes a loss in apical enrichment and molecular asymmetry of the remaining components. **C.** The proximal complex comprises Vang and Pk. The distal complex comprises Fz, Dvl, and Dgo. Fmi cadherins stabilize the complexes on both sides of the adherens junction. Intracellular and intercellular interactions between core components facilitate formation of protein complexes restricted to mutually exclusive domains. Signaling downstream of Fz/Dvl leads to activation of the cytoskeleton in the distal domain, whereas signaling downstream of Vang/Pk blocks cytoskeletal rearrangements in the proximal domain.

Asymmetric localization of core PCP proteins is essential to establish polarity in a tissue [219]. The core proteins are initially recruited to the apical cortex and are then segregated to opposite sides of the cell prior to and during hair formation (Figure 9C). Fz, Dsh, and Dgo form complexes that are confined to cell junctions at the apical-distal side of the cell, whereas Vang, and Pk form complexes that are confined to the apical-proximal side [230-234]. Fmi is localized to both proximal and distal adherens junctions [224, 235, 236]. Asymmetric distribution of core components requires that all six components are present and intact, suggesting a tight feedback mechanism that maintains molecular asymmetry.

Asymmetric protein localization is initiated, stabilized, and maintained through several mechanisms. Live confocal imaging of wing blades prior to hair formation confirmed that one mechanism is directional trafficking of nascent proteins. Fz, Dsh, and Fmi preferentially traffic on non-centrosomal microtubules oriented along the proximal-distal axis, leading to a slight bias in localization of these components at the apical-distal membrane [216, 237]. A second mechanism is a global cue that reinforces the initial bias. The cells at the wing margin express the Fz ligands Wingless (Wg) and dWnt4, which diffuse from the margin in a graded fashion with highest Wg/dWnt4 distally [238-242]. Mosaic clones of cells that overexpress Wg and dWnt4 induce neighboring wildtype cells to reorient Fz receptors towards the source of Wg/dWnt4. These experiments implicate Wg/Wnt4 as an initial directional cue that biases Fz to the distal side of cells near the wing margin [239]. A third mechanism involves intercellular interactions between core PCP components that serve to reinforce and stabilize the directionality of polarization across the entire tissue. Fmi forms homodimeric bridges across cell membranes in both proximal and distal domains and binds to both Fz and Vang to bring them into close molecular proximity. Not only is Fmi a scaffold for Fz and Vang, but it also differentially

recruits Fz and Vang to opposite cell borders, thereby playing a direct role in biasing localization [224, 235, 236, 243]. The extracellular domains of Fz and Vang interact specifically to form stable complexes [234]. Wg and dWnt4 can directly modulate the capacity of Fz to bind Vang, thus providing a mechanism for the initial establishment of direction by Wg and dWnt4 ligands [239]. Lastly, intracellular interactions further restrict the polarity of Vang/Pk and Fz/Dsh complexes into mutually exclusive regions at opposite poles of the cell. Vang recruits Pk to the membrane and Fz recruits Dsh and Dgo [230, 244-247]. Binding of these cytoplasmic factors further stabilizes the complexes [231, 233, 245]. There is an antagonistic relationship between Vang/Pk complexes and Fz/Dsh/Dgo complexes, such that Pk physically binds to Dsh to antagonize its Fz-mediated membrane recruitment [233, 245, 246]. The Dsh-Pk interaction is strongly inhibited by the presence of Dgo, which blocks the antagonistic effects of Pk at the proximal side of the cell [248]. Together, these layers of regulation create robust polarity across the entire tissue. The proposed intercellular interactions and intracellular feedback mechanisms are sufficient to explain why loss of *Fz* or *Vang* disrupts PCP component asymmetry in a non-cell autonomous fashion, whereas loss of *Dsh*, *Dgo*, or *Pk* disrupts PCP component asymmetry in a cell autonomous fashion [249].

Once the asymmetric distribution of PCP components is established and elaborated, tissue-specific downstream effectors translate the molecular subcellular asymmetry into morphological asymmetry. A wide array of molecules have been implicated as downstream effectors of PCP across diverse tissues, reflecting the assortment of potential morphological readouts that can be achieved once PCP has been established. In the wing, mutations in core components often lead to a loss in hair polarity, whereas mutations in downstream effectors may or may not disrupt hair polarity because the core module is still intact. Instead, disruption of

downstream effectors leads to loss of hair formation or the formation of multiple hairs. Additionally, mutations in the core components disrupt the asymmetric distribution of downstream effectors, however, mutations in downstream effectors do not influence the asymmetrical distribution of core components [250]. In the wing, the genes for Inturned (In), Fuzzy (Fy), Fritz (Frtz), and Multiple wing hairs (Mwh) have been implicated as downstream effectors [250-252]. In, Fy and Frtz bind Vang/Pk complexes and are thus enriched in the apical-proximal domain [250]. These effectors recruit and activate Mwh, a protein that prevents actin polymerization, thereby blocking hair formation at the proximal edge (Figure 9C) [253-255]. Mutations in these components result in the formation of ectopic hairs at the proximal side of the cell. Distally, Dsh signals to Rho, which binds and activates dRok, which upon activation can phosphorylate and activate Myosin II [256, 257]. Activation of Myosin II promotes actin polymerization at a single initiation site (Figure 9C).

1.4.1.2 Orientation of Ommatidia in the Compound Eye

The mechanisms of PCP signaling have been extensively studied in other *Drosophila* tissues that exhibit ordered epithelial structures. One such tissue is the eye, which serves as an example of how the core PCP module is conserved across tissues, yet utilized in a unique way to generate specific morphological manifestations of polarity. The eye is composed of clusters of photoreceptors organized into ommatidia that exhibit mirror-image asymmetry across the dorsoventral midline (Figure 10A). The PCP pathway controls two aspects of ommatidial orientation. Within each ommatidium, two R3/R4 photoreceptor precursor cells are initially aligned perpendicular to the dorsoventral midline. These precursors are equipotent, having the ability to differentiate into either R3 or R4. Core PCP components are asymmetrically oriented along the junctions connecting R3/R4 photoreceptor precursors [231, 258-260]. Downstream of

PCP in this context is the inhibition of Notch signaling, which biases the R3/R4 fate decision between the two cells, thereby specifying their fates based on their position relative to the dorsoventral midline (Figure 10B) [260-263].

After R3/R4 fates have been decided, the ommatidia above the dorsoventral midline rotate 90° clockwise, whereas the ommatidia below the midline rotate 90° counterclockwise, producing mirror-image asymmetry across the dorsoventral midline (Figure 10C).

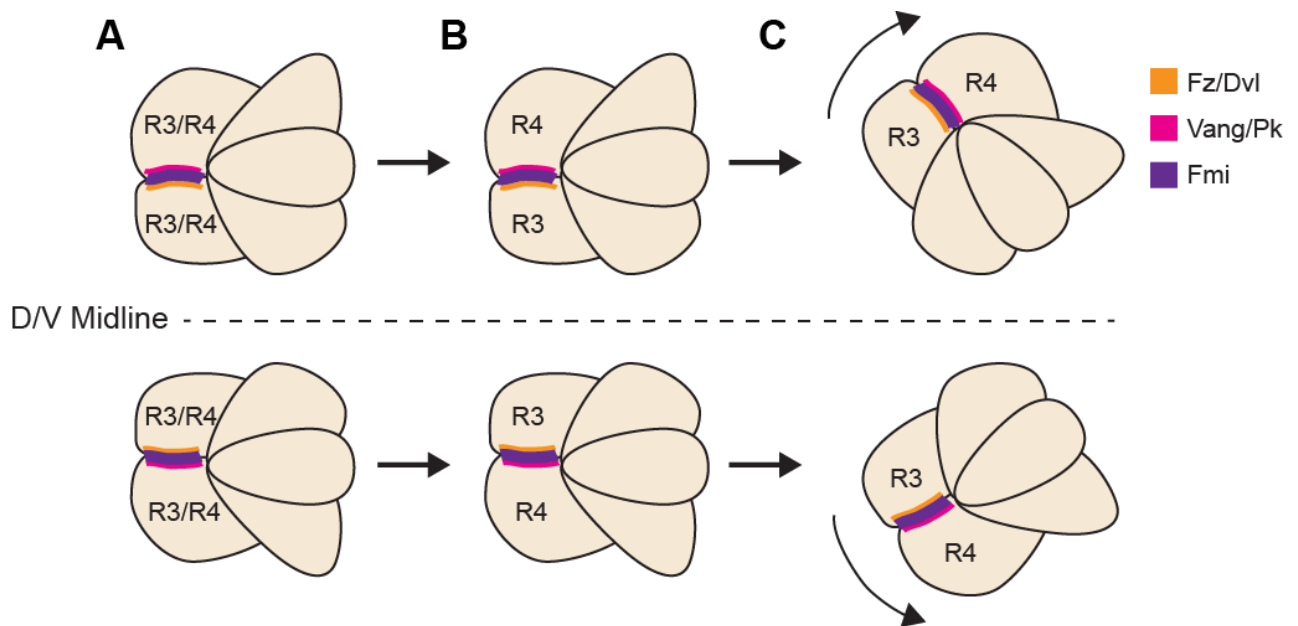


Figure 10. Planar cell polarity functions during ommatidial differentiation and rotation

A-B. In the developing fly eye, R3/R4 photoreceptors are specified in an asymmetric fashion such that the cells closest to the dorsoventral midline become R3, while those farthest away become R4. The fate decision is controlled by PCP proteins, which become asymmetrically localized across R3/R4 junctions. Signaling downstream of Fz/Dvl induces differentiation to the R3 fate. **C.** PCP also controls ommatidial rotation such that ommatidia dorsal to the midline rotate clockwise, whereas ommatidia ventral to the midline rotate counterclockwise. Together, these processes produce a mirror-image arrangement of photoreceptors, which is essential for the functionality of the compound eye. Figure adapted from [264]

Downstream of Dsh during ommatidial rotation is Rho and dRok, which regulate the cytoskeleton to promote rotation. Suppression of Rho function gives rise to ommatidial rotation defects, but also suppresses overexpression phenotypes of Fz or Dsh [257, 260]. A direct molecular link between Dsh and Rho remains to be determined.

Several important points can be made about the PCP pathway by comparing the wing and the eye. First, not only can the core pathway employ different downstream effectors in different tissues, it can also utilize different effectors within the same tissue to elicit distinct morphological responses. Additionally, a potential unifying theme for PCP function is downstream modulation of the cytoskeleton, which occurs in both the wing and the eye, along with many other tissues that have not been discussed here. The ease of genetic manipulation in the fly has made for intense progress in understanding the mechanisms of PCP signaling in various contexts. Many PCP components are difficult to purify and express as recombinant proteins, therefore, their interactions have not been extensively studied from a biophysical standpoint. With the advent of sophisticated techniques for elucidating protein structures and interaction interfaces, it is likely that studies of PCP in the future will elucidate exactly how PCP components physically interact with each other to transmit PCP signals.

1.4.2 Mechanisms of Planar Cell Polarity in Vertebrates

Morphological examples of planar polarity in vertebrates have long been recognized and in recent years a conserved PCP pathway has emerged as a global regulator of planar polarized cell behavior in diverse tissues. The vertebrate orthologs of each *Drosophila* core PCP gene are summarized in Table 1. Disruptions of these genes are linked to a wide array of defects

associated with hair follicle orientation, inner ear patterning and function, orientation of motile cilia and left-right (L-R) asymmetry, kidney and lung morphogenesis, ciliogenesis, axial elongation, and neural tube closure (reviewed in [265-267]).

Table 1. Summary of core PCP genes in vertebrates

<i>Drosophila</i> PCP Genes	Vertebrate Orthologs
<i>van gogh (vang)</i>	Van Gogh-like: <i>Vangl1, Vangl2</i>
<i>frizzled (fz)</i>	Frizzled:* <i>Fzd1, Fzd2, Fzd3, Fzd6, Fzd7, Fzd8</i>
<i>flamingo (fmi)</i>	Cadherin EGF LAG seven pass G-type receptors: <i>Celsr1, Celsr2, Celsr3</i>
<i>dishevelled (dsh)</i>	Dishevelled: <i>Dvl1, Dvl2, Dvl3</i>
<i>prickle (pk)</i>	Prickle-like: <i>Pk1, Pk2</i>
<i>diego (dgo)</i>	Inversin (<i>inv</i>)** Diversin (<i>div</i>)**
N/A***	Protein Kinase 7: <i>Ptk7</i>

* The number of frizzled genes varies widely between vertebrate species and the Frizzled proteins implicated in PCP vary across tissues and species.

** It is not clear whether *inv* and *div* are core PCP components or downstream effectors in certain contexts.

*** Flies have a *Ptk7* ortholog, however it does not cause PCP phenotypes when depleted and is not considered part of the PCP signaling module in flies.

In addition to the conserved PCP components, protein tyrosine kinase 7 (*Ptk7*) has been identified as a novel PCP regulator in vertebrates. *Ptk7* is a receptor-tyrosine kinase, however it is predicted to lack endogenous kinase activity because an invariant motif essential for correct positioning of ATP is not conserved [268]. In vertebrates, mutations in *Ptk7* lead to the same array of defects as mutations in other core PCP component [120, 269-271]. Despite having a *Ptk7* ortholog, mutations in *Drosophila Ptk7* do not cause PCP phenotypes, indicating that its

role in PCP evolved in vertebrates.

A substantial amount of work has been done in many different vertebrate systems to understand how the PCP genes are involved in such a wide array of morphogenetic processes. Our understanding of the mechanisms of PCP in vertebrates is largely derived from making analogies to the fly system. There are many features that are analogous in certain contexts; however, there is also a plethora of data suggesting that novel aspects of PCP signaling have evolved in vertebrates and that the core PCP signaling cascade is utilized in different ways. Understanding PCP mechanisms in vertebrates is complicated by the existence of multiple orthologs of each *Drosophila* gene, making genetic manipulation and interpretation of phenotypes more challenging. Despite these challenges, the relevance of PCP to a wide array of human diseases has encouraged continued exploration into the conserved and novel mechanisms of PCP function in vertebrate tissues.

1.4.2.1 Orientation of Stereocilia in the Mammalian Inner Ear

The inner ear is one of the most thoroughly studied examples of vertebrate PCP. The cochlear epithelium is a mosaic of hair cells that form four rows interdigitated by supporting cells (reviewed in [272, 273]). Each hair cell projects a V-shaped bundle of actin-based structures called stereocilia. At the vertex of the bundle sits a single microtubule-based structure called a kinocilium. The kinocilium is anchored at the lateral pole of the cell, thus hair bundles display planar polarization across the tissue (Figure 11A). Mutations in *Vangl2*, *Fzd3* and *Fzd6*, at least two *Dvl* homologs, *Ptk7*, and *Celsr1* cause a loss in planar polarity of hair bundles [270, 271, 274-278].

The arrangement of hair bundles is intuitively equivalent to *Drosophila* wing hairs except that hair cells in this case are surrounded by cells that do not form hairs. Despite this difference,

it was initially hypothesized that inner ear cells would exhibit planar polarized membrane complexes analogous to the fly wing such that Vangl and Pk would accumulate on the medial pole (opposite to where the bundle sits) and Fzd and Dvl would accumulate at the lateral pole [279]. In support of such a model, Vangl2 and Pk2 have been shown to accumulate on the lateral pole and Dvl2 on the medial pole [280-283]. However, both Fzd3 and Fzd6 co-localize with Vangl2 and Pk2 on the lateral pole [277, 278, 284]. Loss of Vangl2 causes a loss of asymmetric localization of Dvl2, Fzd3 and Fzd6, consistent with the interdependence of core components in the *Drosophila* system [278, 281]. Thus, many aspects of the model are conserved, however the Fzd localization is opposite to what would be predicted. It is possible that inner ear polarization occurs through a divergent mechanism compared to the *Drosophila* wing, or that Dvl2 is recruited to the membrane by another molecule.

Exactly how PCP signaling influences hair bundle position remains elusive, however recent studies suggest that it involves a strong interplay between PCP components with several downstream or parallel signaling pathways that regulate cytoskeletal dynamics (Figure 11B). The novel vertebrate PCP component, Ptk7, appears to play a pivotal role in linking PCP to these pathways. Loss of Ptk7 causes misoriented hair cells and loss of planarly polarized Fzd3 and Fzd6 [271, 285]. Ptk7 is required for the accumulation of Myosin IIb, Rock2 and activated Src Kinase to medial cell interfaces. Src kinase activates Rock2 at these sites, thereby increasing actomyosin contractility at medial cell interfaces [286]. Additionally, mosaic analysis indicates that Ptk7 is required in support cells to regulate hair cell PCP such that lack of Ptk7 in support cells can misorient hair bundles in neighboring wildtype hair cells. Taken together, Ptk7 is important for orienting PCP components and for mediating the assembly of actomyosin networks at medial cell interfaces and in neighboring support cells. PCP components are still

asymmetrically localized in Src mutants indicating that Src-Rock-Myosin activity may be downstream of PCP, however additional experiments are needed to parse the relationship between PCP and Src signaling.

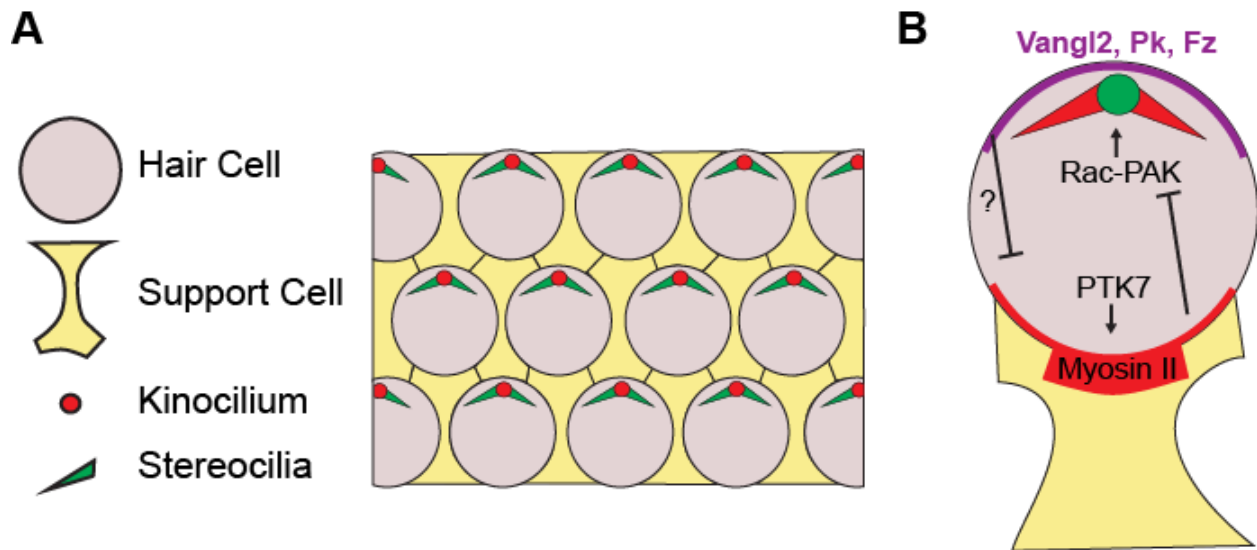


Figure 11. Vertebrate PCP controls inner ear hair patterning

A. The mammalian inner ear epithelium is a mosaic of hair cells and support cells. Hair cells project planar polarized V-shaped bundles of stereocilia with a single kinocilium located at the vertex. **B.** Molecularly, PCP, Rac-PAK and Ptk7-Src signaling regulate cytoskeletal dynamics to position the hair bundle. Figure adapted from [286]

How does contractile tension at medial cell interfaces orient hair bundles? It was shown recently that kinocilia docking requires signaling through a separate pathway comprising the small GTPase Rac1 and p21-activated kinase (PAK) [287-289]. *In vitro* studies suggest that tension can block Rac activity [290]. Thus it has been proposed that contractile tension at medial interfaces and from neighboring support cells prevents Rac activity at the medial pole. Consistent with this idea, activated PAK is present only at lateral-cell interfaces [285]. Whether Vang-Pk and Fzd3/Fzd6 influence Rac-PAK signaling at the lateral cell interfaces or Ptk7-Src signaling at

medial interfaces remains to be determined, however it is clear that PCP, Src, and Rac-PAK signaling cooperate to coordinate hair bundle placement.

1.4.2.2 Convergent Extension and Neural Tube Closure

The planar polarity of the inner ear is conceptually similar to the planar polarity of *Drosophila* tissues. There are additional novel PCP phenotypes in vertebrates, however, that do not correlate with classic *Drosophila* PCP phenotypes. These include shortened body axes and neural tube defects. Both of these phenotypes are a hallmark of impaired PCP in vertebrates and have been attributed to a role for PCP signaling in regulating convergent extension. PCP function during convergent extension is rather different than *Drosophila* examples of PCP because it occurs in a tissue where persistent cell contacts are either non-existent or highly dynamic.

Convergent extension occurs during vertebrate gastrulation through cellular intercalation, whereby cells of the dorsal mesoderm project lamellipodia in a specific direction and employ cell crawling to move past each other. The first clue that this polarized cell behavior is driven by directional cues from the PCP pathway came from mutational studies in *Xenopus*, which clearly illustrated a role for both Dvl2 and Fzd7 in controlling convergent extension and axial elongation [291, 292]. Point mutations in Dvl that had been shown to specifically block PCP signaling in *Drosophila* were sufficient to elicit convergent extension defects, excitingly showing that Dvl2 and Fzd7 were functioning through PCP, not canonical Wnt pathways [293]. Subsequent genetic manipulation and live-embryo imaging of *Xenopus* and zebrafish demonstrated that modulation of any core PCP signaling component negatively impacts the directional cell behaviors of intercalating mesoderm. Defects associated with loss of PCP include both disruptions in the polarity and stability of directed lamellipodial protrusions and subsequent failure of polarized cell intercalations and convergent extension [113, 293-295].

The first hypotheses for how PCP functions during gastrulation were based on analogies to the fly system. Several lines of evidence show that PCP components are localized to the membrane during convergent extension, however data supporting asymmetric localization are limited. In fact, several studies have clearly demonstrated that PCP components are not asymmetrically localized, but exhibit uniform membrane localization [296, 297]. The transient nature of cell-cell contacts in this type of cell population likely prevents the accumulation of asymmetric protein complexes. So how do PCP proteins regulate convergent extension during gastrulation? On a cellular level, PCP signals stabilize and orient lamellipodia and promote waves of actomyosin contractility at the cell cortex that help propel cells in the direction of convergence [298]. The regulators downstream of PCP that promote directed cell migration include the cytoskeletal regulatory components Rho, Rock, and Myosin II. An additional factor, DAAM1 (Dvl associated activator of morphogenesis 1), is required to link Dvl to Rho [299]. DAAM1 is a formin-homology adaptor protein that normally exists in the cytoplasm in an autoinhibited state that is relieved upon direct binding of Dvl2 [300]. DAAM1 also binds to a Rho activating GEF to form a Dvl-DAAM1-RhoGEF complex that locally activates Rho to induce cytoskeletal contraction and remodeling [301]. Interestingly, despite the connections between Dvl and DAAM1 in vertebrates, mutations in the *Drosophila* DAAM ortholog show no PCP-related phenotypes [302]. The upstream global cues that orient the direction of convergent extension may be Wnt ligands. Loss of Wnt11 in *Xenopus* or zebrafish causes convergent extension defects that can be rescued by ectopic expression of Dvl, implicating Wnt11 as an upstream regulator of PCP in this context. Whether Wnt ligands are responsible for determining the direction of convergent extension relative to the body axes remains to be determined.

PCP-driven convergent extension also underlies the neural tube defects commonly seen among PCP mutants. The *looptail* mouse mutant exhibits craniorachischisis and represents a classical model of severe neural tube defects that has been studied since the 1940s [303]. A role for PCP signaling in neural tube closure was made apparent in 2001, when the *looptail* gene was identified as *Vangl2* [304, 305]. Subsequently, depletion of *Dvls*, *Celsrs*, and *Frizzleds* were also found to cause craniorachischisis in both mice and *Xenopus* [274, 277, 278, 294, 306, 307]. Given the role of PCP in convergent extension during gastrulation and the observation that the neural plate elongates during closure, it was hypothesized that PCP signaling regulates convergent extension of the neural plate. Sure enough, studies have demonstrated that manipulation of PCP genes results in convergent extension failure, leading to a neural plate that is too wide to permit apposition of the lateral edges onto the midline [277, 307, 308].

The question of how PCP-dependent convergent extension is linked to closure of the neural tube has been addressed by several studies over the past few years. In zebrafish, oriented cell divisions driven by PCP signaling are partially responsible for convergent extension during neurulation [309, 310]. PCP has also been shown to orient the axis of cell division in sensory organ precursors in *Drosophila*, indicating this is an evolutionarily conserved function of PCP [311, 312]. The mouse neural plate is highly proliferative during closure [313], therefore, one could imagine that oriented cell divisions contribute to the extension of the mouse neural plate. However, it was recently shown that cell divisions are not coordinated along a specific axis but occur in random directions [134]. Therefore, extension of the neural plate is due to cell intercalation alone.

Cell intercalation during neurulation occurs primarily through rosette-based apical junctional remodeling, a mechanism resembling that of the *Drosophila* germband [98, 134].

Germband elongation, however, occurs independently of input from PCP signaling components, thus the use of PCP to drive this type of cellular rearrangement may have evolved in vertebrates [122]. PCP components are also required for rosette-based intercalation during morphogenesis of mammalian kidney tubules and the cochlear epithelium, suggesting that PCP signaling regulates this type of epithelial morphogenesis in multiple contexts in mammals [128, 314].

A recent study by Nishimura et al. addressed the question of how PCP regulates rosette-based intercalation of cells in the chick neural plate [135]. They found that both actin and pMRLC are localized in a cable-like array across adherens junctions of linearly aligned groups of cells. The cables are most often oriented along the mediolateral axis of the embryo, reminiscent of the planar bias of Myosin II in the *Drosophila* germband. Additionally, live imaging revealed rosette behaviors that are driven by contraction of planar polarized pMRLC cables. Recruitment of pMRLC cables, rosette formation, and convergent extension failed when embryos were treated with a small molecule Rock inhibitor, indicating that rosette-based convergent extension of the neural plate is dependent on Rock activity. The PCP components Celsr1 and Dvl2 were found to co-localize with F-actin and pMRLC, and knockdown of either resulted in a loss of planar polarity of these components, defective convergent extension, and an increased apical cell area, indicative of defective apical constriction. Downstream of Dvl2 is DAAM1 and PDZRhoGEF, which both specifically bind to Dvl2, are recruited to mediolateral cell junctions in a Celsr1-dependent manner, and are required for neural tube closure. These interactions are required for planar polarized activation of Rock1, which increases contractility along the mediolateral axis to drive both polarized bending of the neural plate and directional rosette formation. How Dvl2-DAAM1-PDZRhoGEF recruits and activates Rock1 was not determined, however it was hypothesized that Rho provides the link. These data support a model in which

actomyosin contraction is preferentially localized along the mediolateral axis in a PCP-dependent manner to promote rosette formation.

The relevance of vertebrate PCP genes to human neural tube closure is evident; case-control association studies have demonstrated that PCP genes contribute to the etiology of human neural tube defects. Rare variants in human VANGL1, VANGL2, FZD6, CELSR1, DVL2, and PK1 have been identified in cohorts of neural tube defect patients [166, 167, 315-323]. Characterization of the molecular consequences of the specific variants have found that most are single amino acid substitutions that either block membrane recruitment in cell culture or prevent binding to other PCP components *in vitro* [167, 319, 321]. Thus, a collection of evidence has accumulated to support the involvement of PCP genes in the pathogenesis of human neural tube defects. It is clear from these studies that neural tube closure requires functional core PCP proteins that can traffic to the cell membrane and interact with each other once localized, two features of PCP signaling that appear to be deeply conserved throughout animal evolution.

1.5 SUMMARY AND DISSERTATION AIMS

Despite the high prevalence and devastating outcome of neural tube defects in humans, their causes are poorly understood. To achieve the morphological changes required during neural tube morphogenesis, apical constriction and convergent extension must be coordinated in time and space. How these seemingly independent cell behaviors are coordinated at the molecular level is the major biological question addressed in this work. Using a mouse model to mimic human neural tube defect development, this project aims to understand how the functions of molecular pathways required for apical constriction and convergent extension are interconnected and

ultimately lead to the complex tissue changes required to form the neural tube. Based on the current literature, I hypothesized that Shroom3 and PCP cooperate by regulating the spatial distribution of actomyosin networks to promote the cytoskeletal changes required for simultaneous apical constriction and convergent extension. I have addressed this hypothesis through three aims.

First, if the Shroom3 and PCP pathways interact genetically, then modulating the amounts and activities of these pathways *in vivo* should produce neural tube defects. To test this prediction, I have performed a genetic analysis in mice to generate embryos with combinations of mutant alleles of Shroom3 and PCP pathway components and analyzed the associated phenotypes.

The genetic interaction studies indicate crosstalk between Shroom3 and PCP. Thus, the second aim of this dissertation is to determine the molecular basis for pathway integration. I hypothesized that interaction between Dvl2 and Shroom3 would provide a direct connection between PCP signaling and Rock localization and activity. I have performed a biochemical analysis and determined that Dvl2 can physically form a complex with Shroom3 and Rock, thereby providing evidence that these pathways intersect at the level of Dvl2.

The last aim is to understand how the molecular integration of these pathways translates into the cellular behaviors associated with neural tube closure. In this aim, I have evaluated the localization of Shroom3 and PCP pathway components in neural plates of wild type and mutant embryos and assessed the affects of Shroom3 mutation on the planar arrangement of neural plate cells.

2.0 SHROOM3 INTERACTS GENETICALLY WITH PLANAR CELL POLARITY

2.1 INTRODUCTION

To identify novel genetic interactions between Shroom3 and planar cell polarity, I took advantage of one of the most highly studied mouse models of neural tube defects, the *Looptail* (*Lp*) strain. These mice harbor a mutation in the *Vangl2* gene, which encodes a 521 amino acid protein with four predicted transmembrane domains and a cytoplasmic domain containing a PDZ binding motif [304, 305]. Two *Lp* alleles have been described. These alleles contain independent missense mutations, either S464N or D255E, both in the C-terminal cytoplasmic domain [304, 324]. Both alleles result in loss-of-function phenotypes that are gene-dosage dependent. Heterozygous animals (*Vangl2*^{+/*Lp*}) are viable, but exhibit a characteristic looped tail, while homozygotes (*Vangl2*^{*Lp*/*Lp*}) die *in utero* due to craniorachischisis [325, 326]. *Vangl2*^{*Lp*/*Lp*} embryos exhibit dramatic defects in axial elongation due to convergent extension failure [134, 277, 308]. The phenotype associated with loss of *Vangl2* is consistent with convergent extension failure because the body axis is short and wide and the neural plate remains too wide to permit closure.

Several studies have addressed the mechanisms underlying the neural tube defects associated with the *looptail* mutation. The first study examined the ability of wildtype and mutant *Vangl2* proteins to bind to Dvl proteins. *Vangl2* binds all three mammalian Dvl proteins (Dvl1, Dvl2, and Dvl3) *in vitro* through direct interactions between the C-terminal tail of *Vangl2*

and a PDZ domain of Dvl [327]. Both S464N and D255E reduce Vangl2 binding to Dvl proteins *in vitro*, suggesting the phenotypes associated with *Lp* alleles are a consequence of impaired Dvl recruitment. However, two additional studies found that the *Lp* mutations block interaction with Sec24b, a cargo-binding component of COPII vesicles, which normally package and traffic Vangl2 to the plasma membrane. Loss of interaction between Vangl2 and Sec24b prevents Vangl2 from sorting into vesicles *in vitro*, therefore trapping the mutant protein in the endoplasmic reticulum [328, 329]. These results are consistent with previous findings that *Lp* mutant embryos exhibit a loss in Vangl2 protein localized at the plasma membrane, and mutant variants of Vangl2 fail to traffic to the plasma membrane in cell culture systems [330, 331]. In light of these studies, disrupting the interaction between Vangl2 and Dvl proteins is probably secondary to the mechanistic underpinnings of the *Lp* phenotype because Dvl binding only occurs once Vangl2 is properly localized to the membrane.

The Vangl2 homolog, Vangl1, exhibits an overlapping expression pattern with Vangl2 in the neural epithelium, cochlea, and kidneys [332]. *Vangl1* and *Vangl2* genes are found in mice, fish, and humans, whereas, only *Vangl2* orthologs are found in *Drosophila*, *C. elegans*, and *Xenopus* [327]. Mice homozygous mutant for a loss-of-function (lof) *Vangl1* allele (*Vangl1*^{lof/lof}) are normal, except for subtle phenotypes in the orientation of stereocilia in the inner ear. However, *Vangl1*^{+/lof};*Vangl2*^{+/*Lp*} mice exhibit craniorachischisis, indicating a functional relationship between the homologs [332]. Additional evidence supporting a role for Vangl1 in PCP regulation comes from zebrafish, in which ectopic expression of Vangl1 can partially rescue defects associated with Vangl2 depletion [333]. Targeted over-expression of either homolog also causes neural tube defects, indicating that the system is highly sensitive to gene-dosage and

proper PCP establishment has a minimum requirement for combined Vangl1 and Vangl2 activity [334].

2.2 RESULTS

2.2.1 Shroom3 Interacts Genetically With Vangl2

To establish genetic interactions between *Shroom3* and *Vangl2*, I set up crosses to evaluate the phenotypes associated with combined lesions in both genes. Presumably, if the pathways interact to control neural tube closure, then simultaneous modulation of the pathways would result in an increase in severity and penetrance of neural tube defects. The results of this analysis are depicted in Fig. 12. For reference, the phenotypes associated with lesions in either *Shroom3* (*Shroom3*^{gt(rosa53)sor}, *Shroom3*^{gt}) or *Vangl2* are shown in panels B-E. *Vangl2*^{+/*Lp*} animals exhibit urogenital defects and a distinctive looped tail (Figure 12B), *Vangl2*^{*Lp*/*Lp*} embryos die *in utero* due to craniorachischisis (Figure 12C), *Shroom3*^{+/*gt*} animals are normal (Figure 12D), and *Shroom3*^{*gt*/*gt*} embryos exhibit exencephaly (Figure 12E) [182, 326].

Embryos heterozygous for alleles of both *Shroom3* and *Lp* develop spina bifida, a neural tube defect absent from embryos heterozygous for either *Shroom3* or *Lp* alone (Figure 12F). The penetrance of spina bifida in these embryos is 37.5% (9 out of 24). *Shroom3* mutant embryos that are also heterozygous for *Lp* exhibit both exencephaly and severe spina bifida (Figure 12G). The penetrance of spina bifida in these embryos drastically increases to 75% (9 out of 12) as compared to less than 2% of *Shroom3* null mutants (data not shown). *Shroom3*^{*gt*/*gt*};*Vangl2*^{*Lp*/*Lp*} embryos display an open neural tube and a distinct shortening of the anterior-posterior axis

(Figure 12H). The penetrance of the phenotypes associated with each combination are summarized in Table 2.

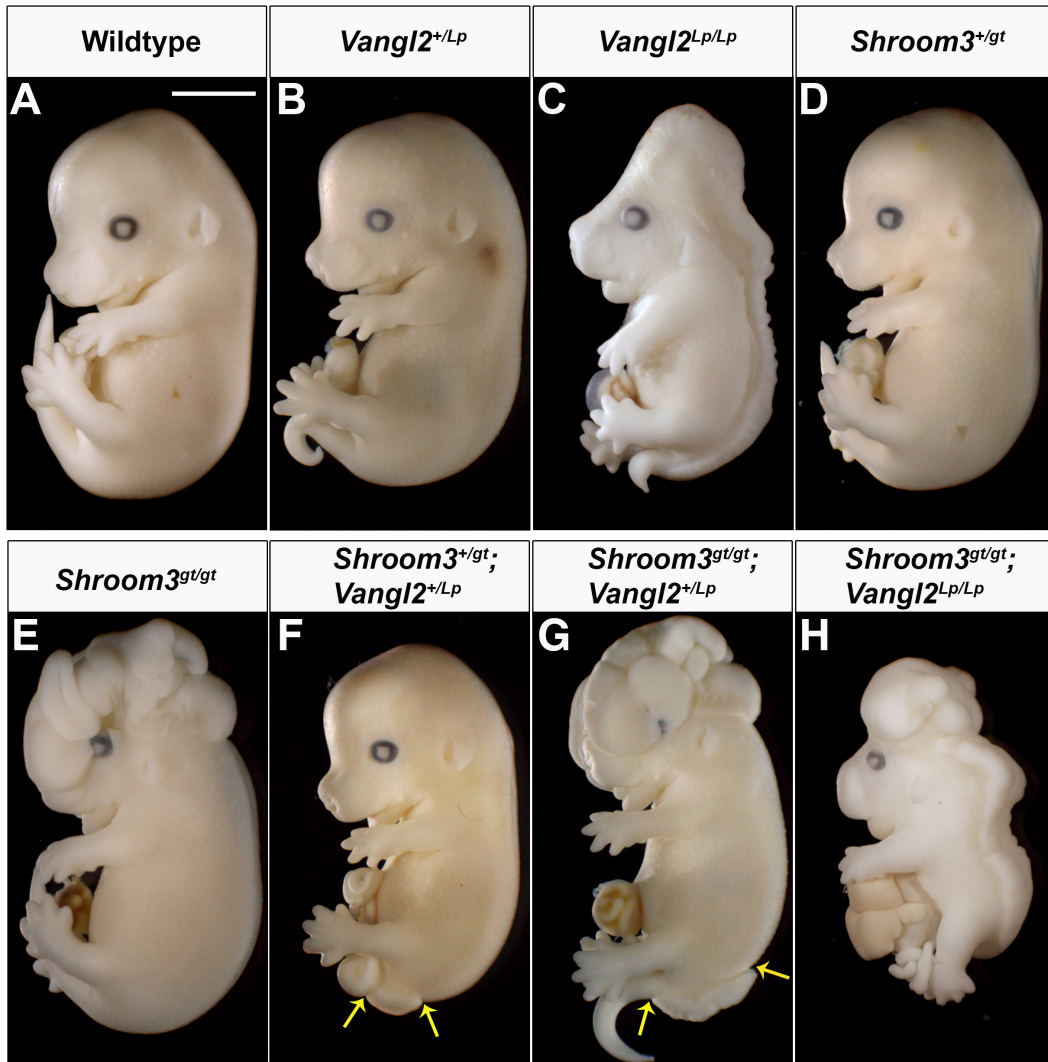


Figure 12. Shroom3 interacts genetically with Vangl2

A-H. Wildtype and mutant embryos of the indicated genotypes were isolated at E13.5 and observed in whole mount. Scale bar: 1 mm, yellow arrows denote spina bifida. *Vangl2*^{+/*Lp*} embryos (**B**) display a characteristic looped tail while *Vangl2*^{*Lp/Lp*} embryos (**C**) exhibit craniorachischisis and a shortened anterior-posterior axis. *Shroom3*^{+/*gt*} embryos are phenotypically normal (**D**) and *Shroom3* mutants exhibit exencephaly (**E**). *Shroom3*^{+/*gt*};*Vangl2*^{+/*Lp*} embryos exhibit spina bifida (**F**) while *Shroom3*^{*gt/gt*};*Vangl2*^{+/*Lp*} embryos display exencephaly and exhibit an increase

in penetrance and severity of spina bifida (**G**). Double mutants exhibit craniorachischisis and a shortened anterior-posterior axis (**H**).

Table 2. The penetrance of the phenotypes upon depletion of Shroom3 and Vangl2.

Genotype	Penetrance of neural tube defects	Sample Size
Wildtype	0%	n > 100
<i>Vangl2</i> ^{+/<i>Lp</i>}	0%	n = 20
<i>Vangl2</i> ^{<i>Lp</i>/<i>Lp</i>}	CR: 100%	n = 5
<i>Shroom3</i> ^{+/<i>gt</i>}	0%	n = 40
<i>Shroom3</i> ^{<i>gt</i>/<i>gt</i>}	SB: 8% EX: 100%	n = 13
<i>Shroom3</i> ^{+/<i>gt</i>} ; <i>Vangl2</i> ^{+/<i>Lp</i>}	SB: 37.5% EX: 8%	n = 24
<i>Shroom3</i> ^{<i>gt</i>/<i>gt</i>} ; <i>Vangl2</i> ^{+/<i>Lp</i>}	SB: 75% EX: 100%	n = 12
<i>Shroom3</i> ^{+/<i>gt</i>} ; <i>Vangl2</i> ^{<i>Lp</i>/<i>Lp</i>}	CR: 100%	n = 2
<i>Shroom3</i> ^{<i>gt</i>/<i>gt</i>} ; <i>Vangl2</i> ^{<i>Lp</i>/<i>Lp</i>}	CR: 100%	n = 4

CR = craniorachischisis, SB = spina bifida, EX = exencephaly

The spina bifida observed in *Shroom3*^{*gt*/*gt*};*Vangl2*^{+/*Lp*} embryos increases in severity compared to *Shroom3*^{+/*gt*};*Vangl2*^{+/*Lp*} embryos as judged by the location in which closure arrests along the body axis. To establish a significant difference between the length of the open neural tube between the two genotypes, I prepared embryos to visualize the fetal cartilaginous skeleton and used ImageJ software (NIH) to measure the length of the open lesion (Figure 13A, red arrows). Spina bifida lengths were normalized to the anterior-posterior axis length of each embryo to control for litter-to-litter variation. The spina bifida:axis length (SB:axis) ratio was used to compare the severity of spina bifida between genotypes. *Shroom3*^{*gt*/*gt*};*Vangl2*^{+/*Lp*} embryos exhibit an increase in the length of the open neural tube as compared to *Shroom3*^{+/*gt*};*Vangl2*^{+/*Lp*} embryos. The SB:axis ratios of at least three embryos of each genotype

were compared using two-tailed, unpaired t-tests, which indicate a significant increase with a p-value of <0.001 (Figure 13B, asterisk). These data suggest that simultaneous depletion of *Shroom3* and *Vangl2* increases the penetrance and severity of neural tube defects, which suggests that *Shroom3* and PCP pathways cooperate during neural tube closure. Additionally this genetic analysis mimics the proposed genetic complexity of human neural tube defect development.

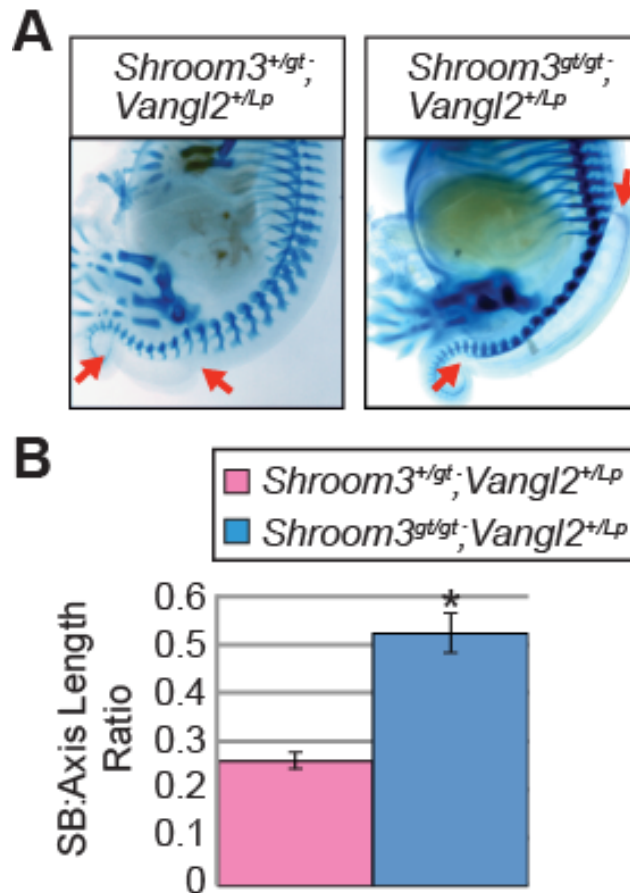


Figure 13. Quantification of spina bifida severity

A. Typical spina bifida (between red arrows) phenotypes seen in *Shroom3*^{+/gt}; *Vangl2*^{+/Lp} and *Shroom3*^{gt/gt}; *Vangl2*^{+/Lp} embryos. **B.** Quantification of spina bifida severity, expressed as the ratio of the length of the open spinal cord to the total length of the body axis. *Shroom3*^{gt/gt}; *Vangl2*^{+/Lp} embryos exhibit a significant increase in the length of the spina bifida compared to transheterozygous embryos. *Shroom3*^{+/gt}; *Vangl2*^{+/Lp} (n=6), *Shroom3*^{gt/gt}; *Vangl2*^{+/Lp} (n=7). Student's *t*-test: p <0 .001 (*). Error bars represent ± s.e.m.

Shroom3^{gt/gt};Vangl2^{Lp/Lp} embryos exhibit a distinct shortening of the anterior-posterior axis compared to wildtype or *Vangl2* mutants. A decrease in anterior-posterior axis length is commonly observed in PCP mutants and is attributed to defective convergent extension [277, 308, 328, 335]. This suggests that *Shroom3* contributes to the elongation of the neural plate. To quantify this phenotype, skeletal preparations of each genotype were used to measure the length of the neural tube from the 2nd cervical vertebrae to the pelvic girdle (Figure 14A, red arrows).

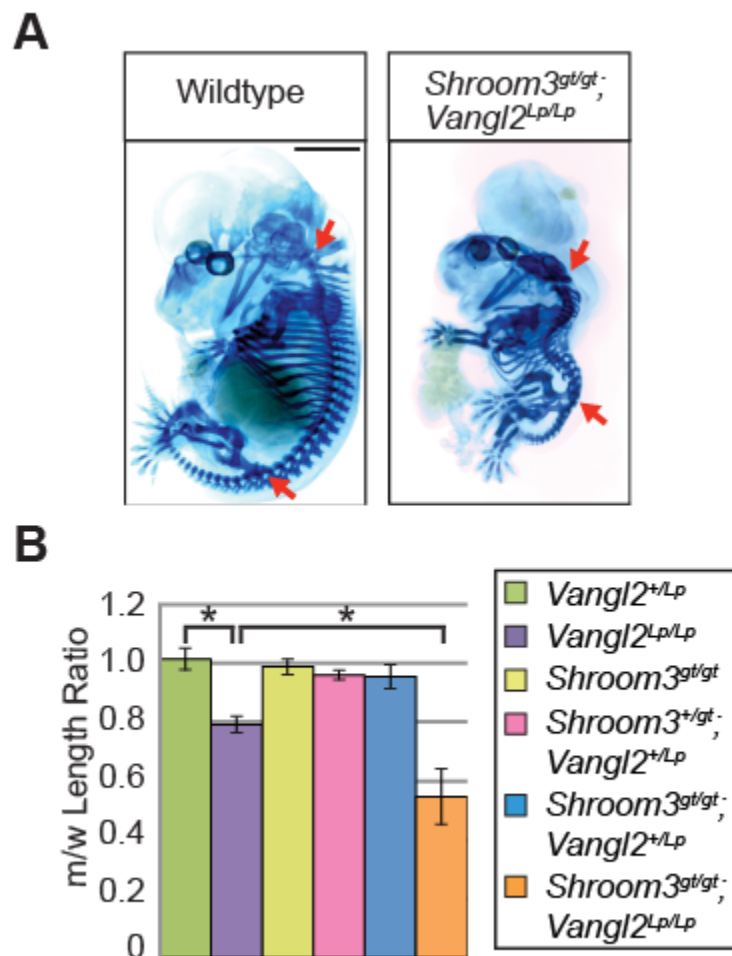


Figure 14. Quantification of body axis length

A. Axis lengths were measured from the 2nd cervical vertebrae to the pelvic girdle (between red arrows on skeleton preparations) and normalized to a wildtype littermate. Scale bar: 1 mm. **B.** Quantification of axis length, expressed

as a mutant to wildtype ratio, m/w, shows a significant decrease in *Vangl2* mutant embryos as compared to wildtype embryos (*, $p < 0.001$) while *Shroom3^{gt/gt};Vangl2^{Lp/Lp}* embryos are significantly shorter than *Vangl2^{Lp/Lp}* embryos (*, $p < 0.001$). *Vangl2^{+Lp}* (n = 6), *Vangl2^{Lp/Lp}* (n = 4), *Shroom3^{gt/gt}* (n = 6), *Shroom3^{+gt}; Vangl2^{+Lp}* (n = 6), *Shroom3^{gt/gt};Vangl2^{+Lp}* (n = 7), *Shroom3^{gt/gt};Vangl2^{Lp/Lp}* (n = 4). Error bars represent \pm s.e.m.

For each genotype, the axis length of mutant embryos was normalized to the axis length of a wildtype littermate to control for litter-to-litter variation. The mutant:wildtype (m/w) ratio was used to compare axis lengths of embryos of different genotypes. To establish significance of this phenotype, the axis lengths of at least three embryos of each genotype were compared using two-tailed unpaired t-tests. These data demonstrate that *Vangl2^{Lp/Lp}* embryos exhibit a significant decrease in axis length compared to wildtype embryos and *Shroom3/Lp* double mutants exhibit a significant decrease in axis length compared to *Lp* mutants. Asterisks show comparisons with a p-value of < 0.001 (Figure 14B). These data indicate that simultaneous disruption of *Shroom3* and PCP induces stronger convergent extension phenotypes than depletion of either one independently, suggesting that loss of *Shroom3* function contributes to convergent extension failure.

2.2.2 *Shroom3* Interacts Genetically With *Wnt5a*

To further establish the interaction between *Shroom3* and the PCP pathway, I employed the same approach described above to assess the genetic interaction between *Shroom3* and *Wnt5a*. In mice, chick, *Xenopus* and zebrafish, convergent extension during gastrulation and neurulation relies heavily on the presence of Wnt ligands, specifically variations of *Wnt5* and/or *Wnt11* [113, 336-339]. In mice, *Wnt5a* is the putative regulator of PCP signaling. Loss of *Wnt5a* causes

perinatal lethality and a wide array of defects including a severely shortened anterior-posterior axis, caudal truncation of the tail, lack of distal elements and shortening of outgrowing structures such as the ear, limbs, snout, mandible, and tongue (Figure 15B) [340]. The structures that do form do not exhibit patterning defects, thus defects in these mutants are attributed to defective cell proliferation and morphogenesis [340]. *Wnt5a*^{-/-} embryos exhibit PCP phenotypes including misoriented stereocilia, loss of convergent extension of the cochlear duct, and neural tube defects albeit at a very low frequency; 1 in 34 exhibit craniorachischisis, 3 in 34 exhibit exencephaly [337]. However, *Wnt5a* null embryos that are heterozygous for the *Vangl2*^{Lp} allele exhibit craniorachischisis with a penetrance of 100%, severely misoriented stereociliary bundles in the inner ear, and convergent extension defects in multiple tissues (Figure 15C) [337]. In the inner ear, loss of *Wnt5a* causes a loss of planar polarization of *Vangl2*. Taken together, these data implicate *Wnt5a* as an upstream regulator of PCP in mammals.

Wnt5a has been linked to signaling through a variety of different receptors. In the Fzd family, *Wnt5a* signals through Fzd3, Fzd4, Fzd5, and Fzd8, but not Fzd6, as determined by several studies [341, 342]. Since Fzd3 and Fzd6 have been implicated in neural tube closure, *Wnt5a* most likely signals through Fzd3 in this context, although direct evidence for this is lacking. In addition to Fzds, Ror2 (receptor tyrosine kinase-like orphan receptor 2) has been shown to function as an essential co-receptor for *Wnt5a* function. Ror2 knockout mice phenocopy *Wnt5a* knockout mice, suggesting that Ror2 is more intimately linked to the specific activation of *Wnt5a* signaling than Fzd [343, 344]. Ror family receptors are also key for transducing non-canonical Wnt signals in both *Xenopus* and zebrafish [345, 346]. Overexpression of Ror2 in *Xenopus* embryos inhibits convergent extension and co-expression of

Ror2 with Wnt11, Fzd7 or both synergistically inhibits convergent extension. Thus, Ror2 in combination with Fzd receptors mediates PCP signaling.

In mice, *Ror2* genetically interacts with *Vangl2*, generating an almost identical suite of phenotypes as combined lesions in *Vangl2* and *Wnt5a* [347]. The best-studied example of Wnt5a-Ror2-PCP signaling is during limb outgrowth, which provides mechanistic insight into how these molecules function together [347]. In outgrowing limbs, a population of chondrocytes exhibit planar polarity along the proximal-distal (P-D) axis of the limb such that outgrowth occurs in the distal direction only. In these cells, Vangl2 exhibits a gradient of asymmetrical localization such that the cells closest to the body exhibit Vangl2 localized to the apical-proximal membrane. This distribution is progressively lost towards the distal end of the developing limb. Vangl2 asymmetry is completely lost along the entire proximal-distal axis in *Wnt5a*^{-/-} or *Ror2*^{-/-} embryos. Wnt5a is expressed in a gradient, with highest levels proximally, thus there is a correlation between the amount of Wnt5a and asymmetric distribution of Vangl2. Wnt5a was shown to bind to Ror2 and induce complex formation between Ror2 and Vangl2, which induces Vangl2 phosphorylation. Phosphorylation of Vangl2 is important for PCP, as constructs that cannot be phosphorylated cannot rescue convergent extension defects in zebrafish [347]. Thus, Wnt5a gradients, together with Ror2 promote asymmetrical localization and activation of Vangl2. Additionally, it was shown that Wnt5a/Ror2 complexes promote Dvl2 phosphorylation in mouse embryonic fibroblasts [348]. Dvl2 phosphorylation is thought to be a read-out of active PCP signaling, thus providing further evidence that Wnt5a/Ror2 signaling is an essential component of vertebrate PCP. Whether this system functions in other tissues such as the neural tube remains to be determined, however, Wnt5a transcripts are expressed in a gradient in the

neural plate along the anterior-posterior axis, with highest expression caudally and medially indicating that a similar mechanism could exist [340].

If *Shroom3* cooperates with PCP during neural tube morphogenesis, then I predicted that *Shroom3* would genetically interact with *Wnt5a* in the same way that *Vangl2* genetically interacts with *Wnt5a*. To identify these interactions, I set up crosses to evaluate the phenotypes associated with simultaneous depletion of both components. *Wnt5a* mutants that are heterozygous for *Shroom3* develop exencephaly with a penetrance of 33% (3 out of 9) (Figure 13D, blue arrows). Additionally, these embryos exhibit spina bifida (Figure 15D, yellow arrows). Thus, as is the case with *Vangl2*, the neural tube defects normally caused by the homozygous condition of *Shroom3* are present in heterozygotes when null for *Wnt5a*.

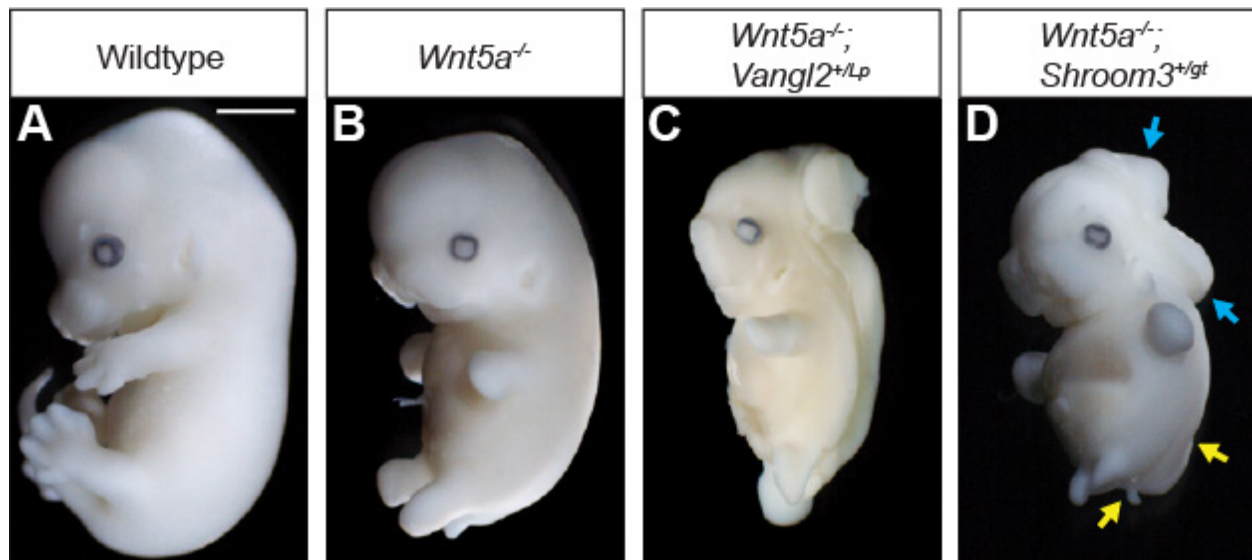


Figure 15. *Shroom3* interacts genetically with *Wnt5a*

A-D. Wildtype and mutant embryos of the indicated genotypes were isolated at E12.5 and observed in whole mount. Scale bar: 1 mm. *Wnt5a* mutant embryos exhibit characteristic convergent extension defects with no neural tube defects (**B**), however *Wnt5a*^{-/-};*Vangl2*^{+/*Lp*} embryos exhibit craniorachischisis (**C**). *Wnt5a*^{-/-};*Shroom3*^{+/*gt*} embryos exhibit exencephaly (**D**, **blue arrows**) and spina bifida (**D**, **yellow arrows**).

To determine if simultaneous depletion of *Shroom3* and *Wnt5a* causes convergent extension defects, I prepared embryos to visualize the skeleton and compared the axis lengths of embryos of each genotype by measuring the length of the vertebral column (Figure 16A-D, red arrows).

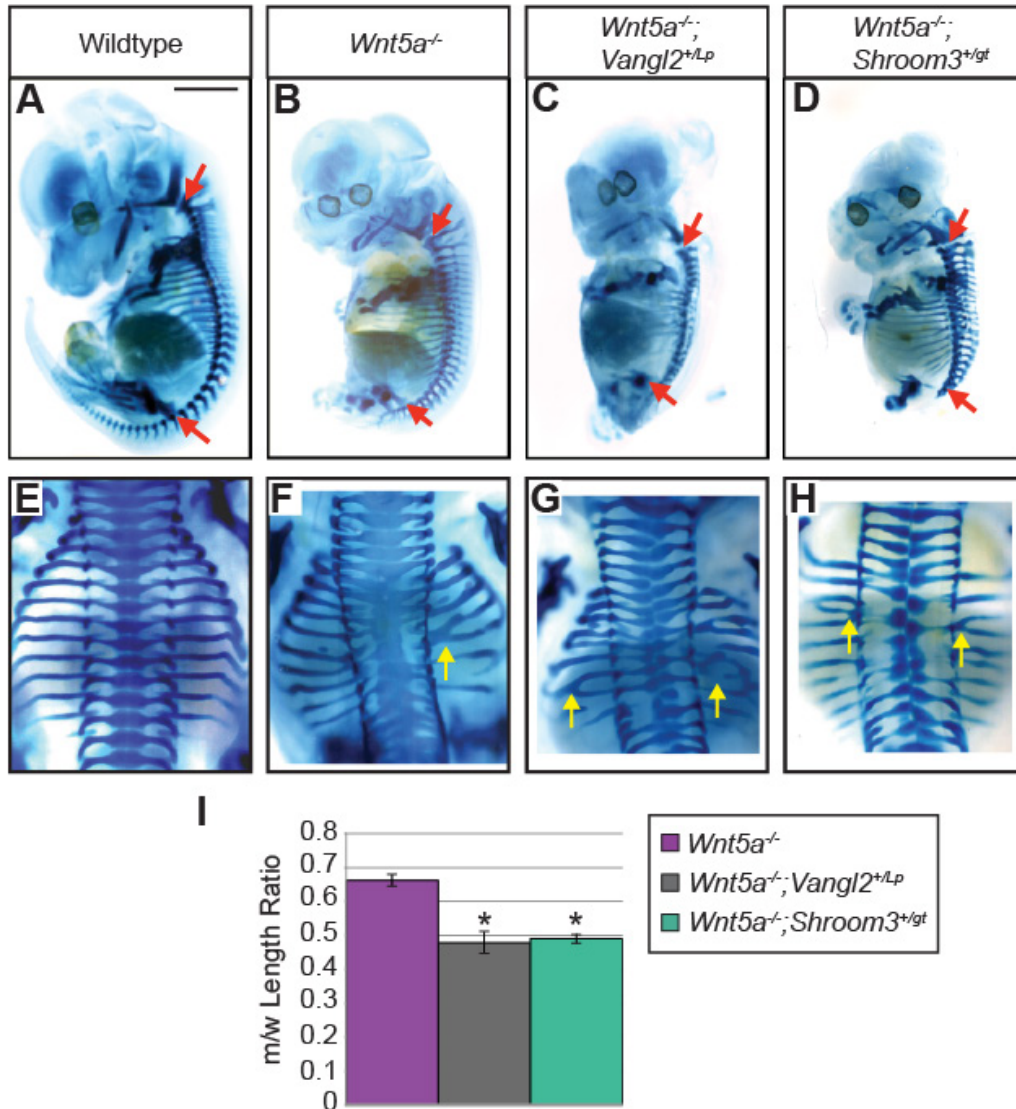


Figure 16. *Wnt5a/Shroom3* embryos exhibit convergent extension and skeletal defects

A-H. Embryos of the indicated genotype were processed to visualize the skeleton. Side (**A-D**) and dorsal (**E-H**) views are pictured. Scale bar: 1 mm. Skeletal staining reveals shortened body axes (**A-D**, red arrows), vertebral

malformations (**E-H**), and rib fusions and bifurcations (**E-H, yellow arrows**). **I**. Axis lengths were measured from the 2nd cervical vertebrae to the pelvic girdle and normalized to a wildtype littermate (m/w mutant to wildtype ratio). The anterior-posterior axis is shortened in both *Wnt5a*^{-/-};*Vangl2*^{+Lp} and *Wnt5a*^{-/-};*Shroom3*^{+Lp} embryos compared to wildtype and *Wnt5a* mutant embryos (red arrows). *Wnt5a*^{-/-} (n = 10), *Wnt5a*^{-/-};*Vangl2*^{+Lp} (n = 5), *Wnt5a*^{-/-};*Shroom3*^{+gt} (n = 4). Student's *t*-Tests compare *Wnt5a*^{-/-};*Vangl2*^{+Lp} and *Wnt5a*^{-/-};*Shroom3*^{+gt} to *Wnt5a* mutants. * = p < 0.001. Error bars: ±s.e.m.

These measurements suggest convergent extension defects in *Wnt5a*^{-/-};*Vangl2*^{+Lp} and *Wnt5a*^{-/-};*Shroom3*^{+gt} embryos as compared to wildtype or *Wnt5a*^{-/-} embryos (Figure 16I, p<0.001). Importantly, mutant embryos lack tail vertebrae but have the same number of cervical, thoracic, and lumbar vertebrae as wildtype, thus the decrease in axis length is due to defective axial extension, not truncation of the anterior-posterior axis (Figure 16A-D). Taken together, these data suggest that when combined with lesions in *Wnt5a*, lesions in *Vangl2* or *Shroom3* confer exacerbated convergent extension phenotypes.

Skeletal preparations revealed skeletal defects that increase in severity upon increasing genetic lesions (Figure 16A-H). These include shortening of the vertebral column, splayed and misaligned vertebrae, and fusions and bifurcations of the ribs (Figure 16E-H, yellow arrows). *Wnt5a*^{-/-} embryos have been shown to exhibit defects in skeletogenesis with aberrant growth plate morphology [349]. These defects are exacerbated in combination with *Vangl2*^{Lp}, which may be attributed to previously described requirements for *Wnt5a/Ror2/Vangl2* in establishing polarity in cartilage growth plates for proper skeletal development [347, 350]. These phenotypes are also seen in *Wnt5a*^{-/-};*Shroom3*^{+gt} embryos, further suggesting cooperation between *Shroom3* and *Vangl2* since they genetically interact with *Wnt5a* in similar ways. Additionally, these phenotypes may result from defective mesoderm migration or patterning due to a deformed

neural tube (Figure 16E-H). *Vangl2*^{Lp/Lp} embryos exhibit shortening of somites along the anterior-posterior axis, indicating PCP function impairs somite morphology, either because of a malformed neural tube or convergent extension defects that fail to properly extend the somites (data not shown). Further studies assessing defects in growth plate morphology and somite patterning and shape are required to fully understand the defects that cause these phenotypes.

No double mutants were recovered at E13.5, indicating that homozygous combination of *Shroom3* and *Wnt5a* null alleles results in embryonic lethality before this stage of development. To address this, I isolated embryos between E10.5 and E11.5 and recovered a small number of *Wnt5a/Shroom3* double mutants, indicating that these embryos die at or before E11.5. These embryos exhibit obvious neural tube defects, severely shortened body axes, and flattening of the neural tube and outgrowing structures (Figure 17A-C). Although the cause of death is unknown, this phenotype is far more severe than what would be expected from either mutation alone, indicating that the phenotypes resulting from this combination are not simply additive, but appear to be synergistic.

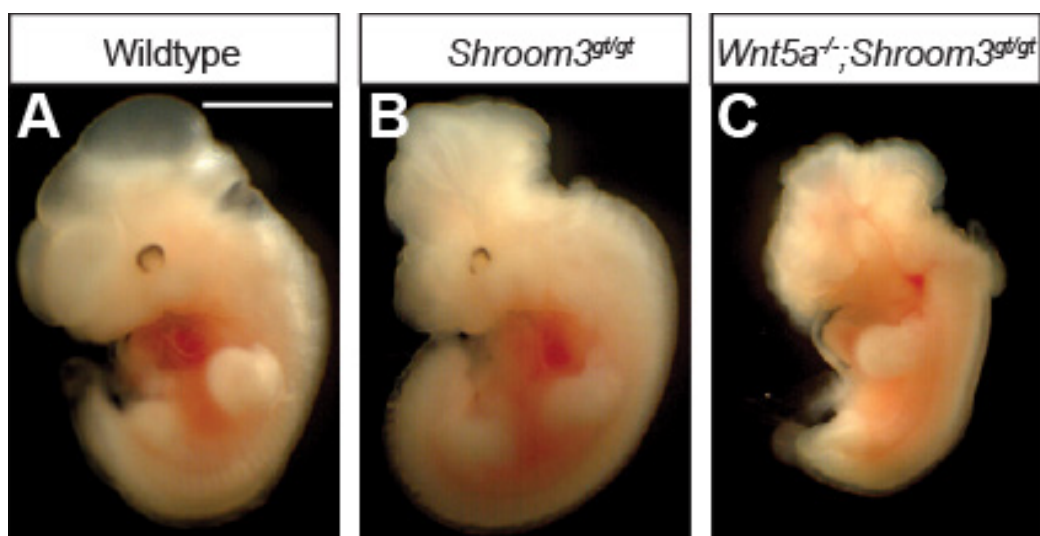


Figure 17. *Wnt5a/Shroom3* double mutants die at or before E11.5

A-C. Embryos of the indicated genotype were isolated at E11.5 and observed in whole mount. *Wnt5a*^{-/-};*Shroom3*^{gt/gt} embryos (**C**) show severe growth defects in addition to the typical phenotypes associated with each individual mutation. Scale bar: 1 mm in all panels.

2.3 DISCUSSION

Using genetic analysis in mice, I have shown that the Shroom3 and PCP pathways cooperate to control neural tube morphogenesis. However, I do not predict that Shroom3 is necessarily a core component of the PCP pathway, as decreased Shroom3 activity either in mice, frogs, or flies does not result in classic PCP phenotypes. In contrast, the genetic interactions suggest that the Shroom3 and PCP pathways are intimately linked to coordinate the tissue changes required to form the neural tube. Depletion of Shroom3 alone does not cause craniorachischisis or a decrease in body axis length, phenotypes most often associated with abnormal PCP in vertebrates. However, when combined with genetic lesions in PCP components, a role for Shroom3 in PCP is revealed. Whether depletion of Shroom3 alone or in combination with PCP causes other characteristic PCP phenotypes such as misoriented hairs in the inner ear remains to be determined. It is likely that these additional PCP phenotypes would be revealed upon simultaneous disruption of Shroom3 and PCP. It should be noted that the lack of PCP phenotypes in *Shroom3* mutants could be the result of some functional redundancy between Shroom2 and Shroom3. For example, in mice both Shroom2 and Shroom3 are expressed in the neural tube and they exhibit a similar subcellular distribution in neural epithelia and both can bind to Rock [191, 199]. However, Shroom2 clearly does not have the ability to fully cover Shroom3 deficiency, suggesting differences in either function, activity, or timing of

expression. Nonetheless, future studies including the generation of a *Shroom2* knockout allele are required to determine whether simultaneous depletion of both *Shroom2* and *Shroom3* causes PCP phenotypes.

Convergent extension and apical constriction have traditionally been thought to contribute independently to the shaping of the neural plate. Disruption of apical constriction through the impairment of actomyosin contractility typically causes exencephaly (e.g. *Shroom3* mutant), whereas disruption of convergent extension through mutation of PCP signaling components always causes craniorachischisis (e.g. *Vangl2* mutant). If the two processes are coupled and both regulated by the same actomyosin components, then one would not expect such a distinct difference in these phenotypes. Perhaps the differences can be attributed to regional differences in the neural plate and the requirement for apical constriction and/or convergent extension varies along the axis of the neural plate. For example, since the cranial neural folds are spaced much farther apart than in the spinal region, the requirement for apical constriction may be greater than in the spinal region. Convergent extension may be required in the spinal region to initiate closure, whereas once the initial contact point has been made, other forces can drive the neural folds together despite a loss of convergent extension. If the molecular machinery that drives these processes is coupled, then disruption of multiple aspects of the machinery may be required to reveal defects along the entire anterior-posterior axis, which is what is observed upon simultaneous depletion of *Shroom3* and planar cell polarity components. Because of the difficulties in interpreting these phenotypes, understanding how the pathways are linked requires a more mechanistic approach to determine biochemical interactions between pathway components and whether *Shroom3* directly influences the cellular behaviors associated with convergent extension.

3.0 SHROOM3 PHYSICALLY INTERACTS WITH DISHEVELLED2

3.1 INTRODUCTION

The genetic experiments described in Chapter 2 suggest that the Shroom3 and PCP pathways intersect (Figure 18).

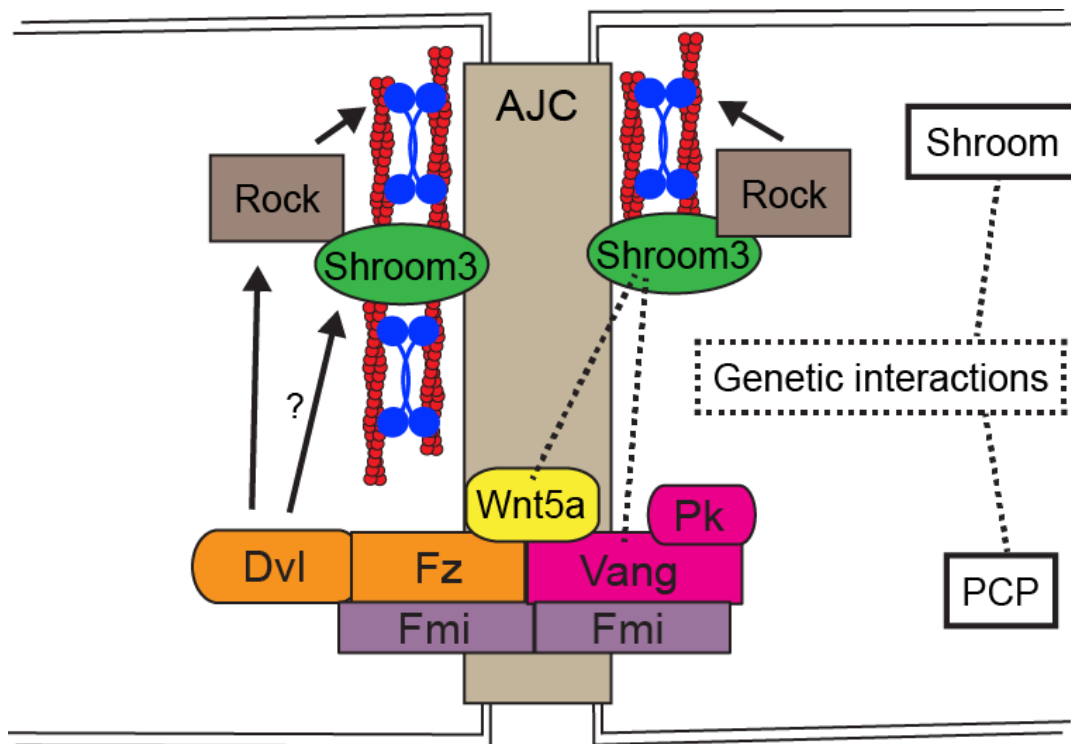


Figure 18. Summary of genetic interactions

A theoretical view of the apical surface of neural epithelial cells shows components of the Shroom3 and PCP pathways localized to the AJC to regulate actomyosin contractility. Chapter 2 described genetic interactions between

Shroom3 and Vangl2 and Wnt5a (dotted lines) indicating a functional relationship between these pathways. Because Shroom3 and Dvl signal to Rock, we hypothesized that the pathways intersect at the level of Dvl (question mark).

Because Dvl is a key downstream effector of PCP that is known to regulate the function of Rock, and Shroom3 is known to bind, recruit and potentially activate Rock, I hypothesized that the intersection of these pathways lies at Dvl2 (Figure 18). Dvl proteins are key signaling components that serve as branch points between canonical and non-canonical Wnt signaling pathways. In mammals, the Dvl family consists of three proteins Dvl1-3. The functions of the mammalian *Dvl* genes have been assessed *in vivo* using mouse knockout strategies. These studies indicate both redundant and divergent functions for *Dvl1-3*. Of the three mammalian Dvl proteins, Dvl2 is sufficient for neural tube closure, as *Dvl1*^{-/-};*Dvl3*^{-/-} embryos do not display neural tube defects, however *Dvl2*^{-/-} in combination with either *Dvl1*^{-/-} or *Dvl3*^{-/-} causes craniorachischisis [275, 277]. *Dvl2*^{-/-} alone results in spina bifida in only 3% of embryos, thus *Dvl1* and *Dvl3* can together compensate for the absence of *Dvl2* [306]. Combinations of Dvl mutations that cause craniorachischisis specifically reduce convergent extension, resulting in embryos with broad, wide neural plates that fail to close [277].

Dvl proteins are characterized by three conserved domains including an N-terminal DIX domain (Disheveled, Axin), a central PDZ domain, and a C-terminal DEP (Dvl, Egl-10, Pleckstrin) domain (reviewed in [351]) (Figure 19). Importantly, these domains bind to a wide array of effector molecules, allowing Dvl proteins to engage multiple pathways and carry out different functions, even in the same tissue [229]. The DIX domain regulates the ability of Dvl to polymerize into protein assemblies, which correlates with the ability to transduce canonical Wnt signaling through β -catenin dependent transcription [352, 353].

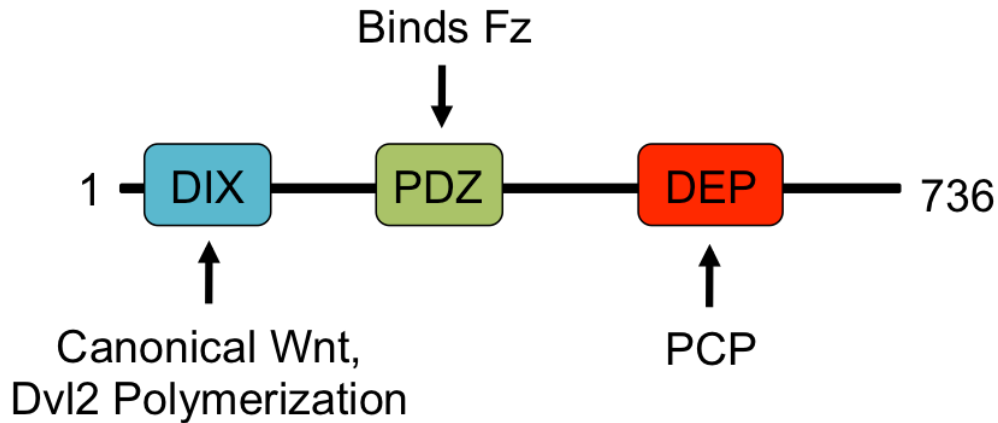


Figure 19. Dvl2 domain structure

Dvl proteins are characterized by a linear array of protein domains including an N-terminal DIX domain, a central PDZ domain, and a C-terminal DEP domain. The DIX domain is required for canonical Wnt signaling and mediates Dvl polymerization into protein assemblies. The PDZ domain binds to Fz receptors to recruit Dvl to membrane-bound signaling complexes. The DEP domain is required for PCP signaling.

As a result of polymerization, both endogenous and ectopically expressed Dvl proteins have been observed in cytoplasmic puncta in numerous model systems including cell culture, frogs, flies, mice, and sea urchins [296, 354-361]. These puncta can be recruited to the plasma membrane of cells through the overexpression of Fzd receptors or through the addition of Wnt ligands [362, 363]. Dvl puncta were initially thought to be vesicles, as Dvl had been shown to mediate endocytosis of Fzd receptors upon Wnt ligand stimulation [364]. Additionally, Dvl is capable of binding phospholipids through its DIX domain, further supporting this hypothesis [352]. However several studies have found that Dvl puncta do not co-localize with any markers for endocytic vesicles or membranes. Moreover, expression of dominant negative proteins that specifically block endocytosis do not influence puncta formation, providing further evidence that Dvl puncta are protein assemblies rather than vesicle associations [365]. Live cell imaging and biochemical analysis of the DIX domain revealed that Dvl puncta are mobile and highly

dynamic, rapidly assembling, growing, and disassembling over time, which can be attributed to the inherent ability of the DIX domain to polymerize in a reversible fashion [353, 365]. The DIX domain of Axin, which is closely related to Dvl DIX, has been crystallized and the structure consists of a novel fold containing multiple β -strands and one α -helix. The β -strands of two DIX domains can arrange in a head-to-tail fashion, facilitating domain packing that allows for polymerization [353]. It has been hypothesized that this polymerization functions to concentrate binding sites for low-affinity Wnt- β -catenin signaling effectors such as Axin and Fzd [353]. Interfering with the ability of Dvl2 to polymerize does not interfere with convergent extension, indicating that this function is only biologically relevant for canonical Wnt signaling [277, 293].

Apical membrane recruitment of Dvl by Fzd is accomplished through direct contact between both the PDZ and DEP domains of Dvl and the third intracellular loop and C-terminal cytoplasmic domain of Fzd [230, 244, 366]. The DEP domain contains a stretch of basic residues that can interact with membrane phospholipids, which could contribute to robust membrane enrichment of Fzd-Dvl complexes during the establishment of planar polarization [367]. During PCP establishment in flies, Dgo and Pk compete for binding to the PDZ of Dsh [233, 248]. The DEP domain is required for PCP in *Drosophila*, as mutations in DEP cause characteristic PCP phenotypes [247]. This is also the case in vertebrates, as constructs that lack the DEP domain fail to rescue convergent extension defects associated with loss of Dvl2 in *Xenopus* or mouse [277, 293]. A Dvl2-DAAM1-RhoGEF pathway has been proposed to link PCP-Dvl2 signaling to the cytoskeleton during *Xenopus* gastrulation and chick neural tube closure. DAAM1 binds to the PDZ and DEP domains of Dvl2. Direct links between Dvl and Rock in mouse neural tube closure have not been determined and whether Shroom3 is involved in linking Dvl2 to Rock in *Xenopus* or Chick has not been addressed.

3.2 RESULTS

3.2.1 Dvl2 Regulates the Distribution of Shroom3 and Rock

To investigate the connection between Shroom3 and Dvl, I tested whether these components co-distribute in cells grown in culture. COS7 fibroblast cells were chosen for these experiments because they are easy to maintain and exhibit robust transfection efficiency. When Shroom3 is expressed in COS7 cells, it localizes to actin filaments through the SD1 (Figure 20A). Consistent with previous results, co-expression of Shroom3 and the central coiled-coil region of Rock results in the co-distribution of these proteins on actin stress fibers through a direct interaction between the SD2 of Shroom3 and the Shroom Binding Domain (SBD) of Rock (Figure 20A) [73, 192]. In contrast, when Dvl2 and Shroom3 are co-expressed in COS7 cells, Shroom3 is recruited to Dvl2 puncta (Figure 20B). When Dvl2 is co-transfected with the SBD of Rock, Rock is distributed in the cytoplasm, indicating that the recruitment of Shroom3 into Dvl2 puncta is specific (Figure 20C). However, when Dvl2, Shroom3, and the Rock SBD are expressed simultaneously in COS7 cells, I observe a clear co-localization of Shroom3 and the Rock SBD in Dvl2 puncta (Figure 20D). These phenomena are also seen in MDCK cells, indicating that the interaction is not cell-type specific (data not shown). Taken together, these data suggest that Dvl2 can regulate the localization of Shroom3 and that Shroom3 can recruit Rock to this new subcellular locale.

To further verify this interaction and determine if Dvl2 and Shroom3 are in a complex *in vivo*, Dvl2 was immunoprecipitated from cells expressing both Dvl2 and Shroom3 and the immune complexes were subjected to Western blotting to detect Shroom3. This analysis shows a

clear enrichment of Shroom3 in the immune complexes containing Dvl2 relative to the control, indicating that a Dvl2-Shroom3 complex can exist *in vivo* (Figure 16E).

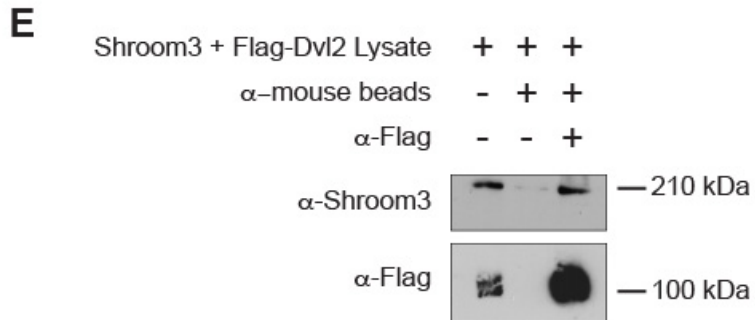
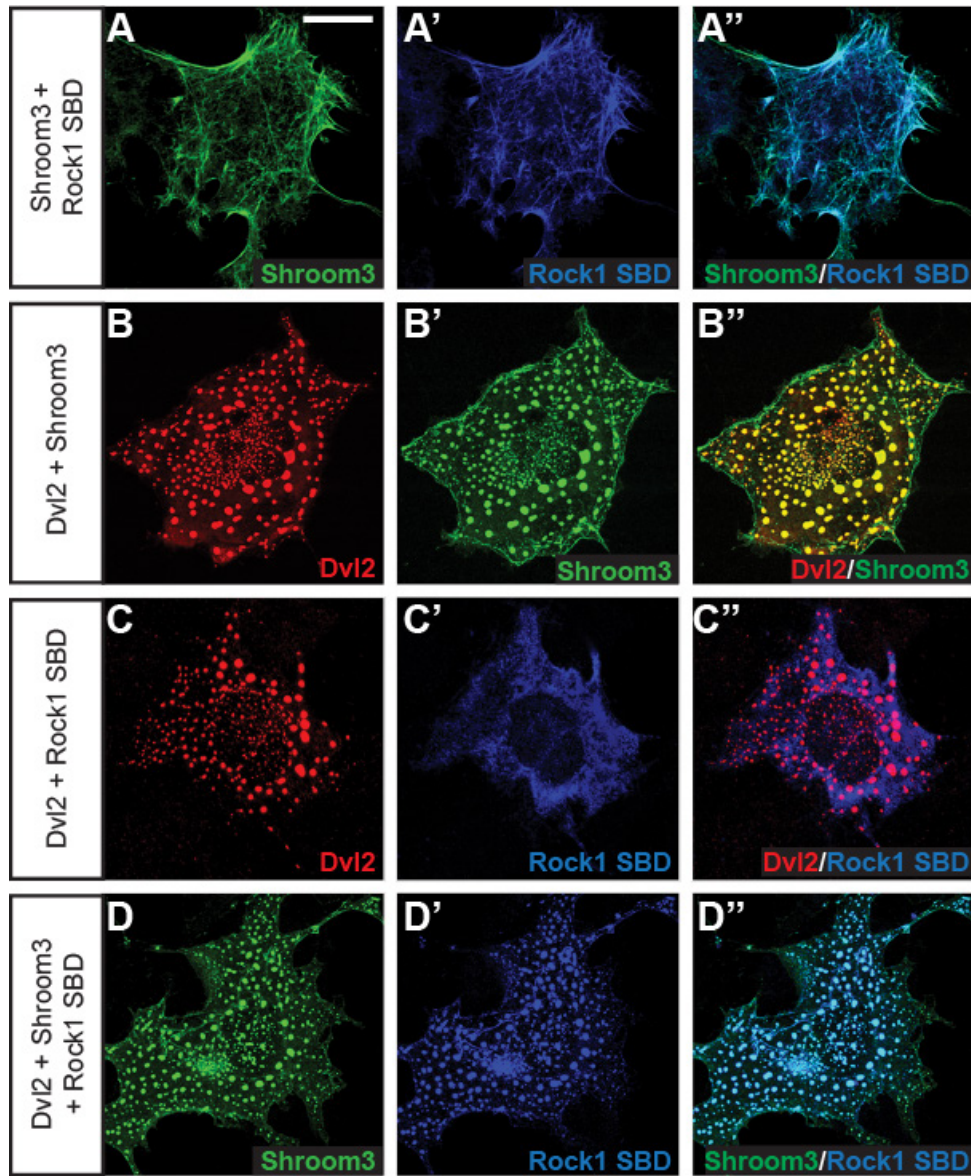


Figure 20. Dvl2 recruits Shroom3 and Rock into cytoplasmic puncta

A-D. COS7 cells transiently expressing either Shroom3, Dvl2, and/or the Shroom Binding Domain (SBD) of Rock were grown on cover slips overnight and stained to detect the indicated proteins. Shroom3 transiently expressed in COS7 cells localizes to F-actin and recruits Rock (**A**). When co-expressed in COS7 cells, Shroom3 and Dvl2 co-localize to cytoplasmic puncta (**B**). COS7 cells expressing Dvl2 and Rock SBD exhibit punctate staining of Dvl2 and cytoplasmic localization of Rock (**C**). COS7 cells expressing Dvl2, Rock SBD, and Shroom3 exhibit co-localization of Shroom3 and Rock in cytoplasmic puncta (**D**). Scale bar: 10 μ m. **E.** Shroom3 and Dvl2 form a complex. Dvl2 was precipitated from lysates of COS7 cells co-expressing Shroom3 and Flag-Dvl2 with anti-flag antibodies bound to agarose beads followed by SDS-PAGE and immunoblotting to detect Shroom3 and Flag. MW markers are indicated to the right.

3.2.2 Dvl2 and Shroom3 Interact Through Specific Protein Domains

To further characterize the interaction between Shroom3 and Dvl2, I used deletion constructs to map the regions of both proteins that are required for recruitment of Shroom3 into Dvl2 puncta. To accomplish this, flag tagged variants of Dvl2 lacking either the DEP or DIX domains were co-expressed with full length Shroom3 in COS7 cells and co-localization was evaluated by immunohistochemistry (Figure 21A). As expected, based on previous studies, the Δ DEP protein retains the ability to form cytoplasmic puncta while the Δ DIX protein no longer forms puncta and is largely cytoplasmic (Figure 21B and 21C) [365]. When assessed for Shroom3 distribution, the Δ DEP protein fails to recruit Shroom3 into these puncta, suggesting that the DEP domain is required for this activity (Figure 21B). In contrast, in cells expressing the Δ DIX protein Shroom3 is largely localized to actin-rich structures and appears to co-distribute with a population of Dvl2 (Figure 21C, white arrows). To quantify this data, the percent of cells that show localization of Dvl2 and/or Shroom3 to cytoplasmic puncta was determined by counting 200 cells in three independent experiments. Deletion of the DEP domain prevents

recruitment of Shroom3 into cytoplasmic puncta in nearly 100% of the cells (Figure 21D). Taken together, these data suggest that the DEP domain is required for the co-distribution of Shroom3 and Dvl2.

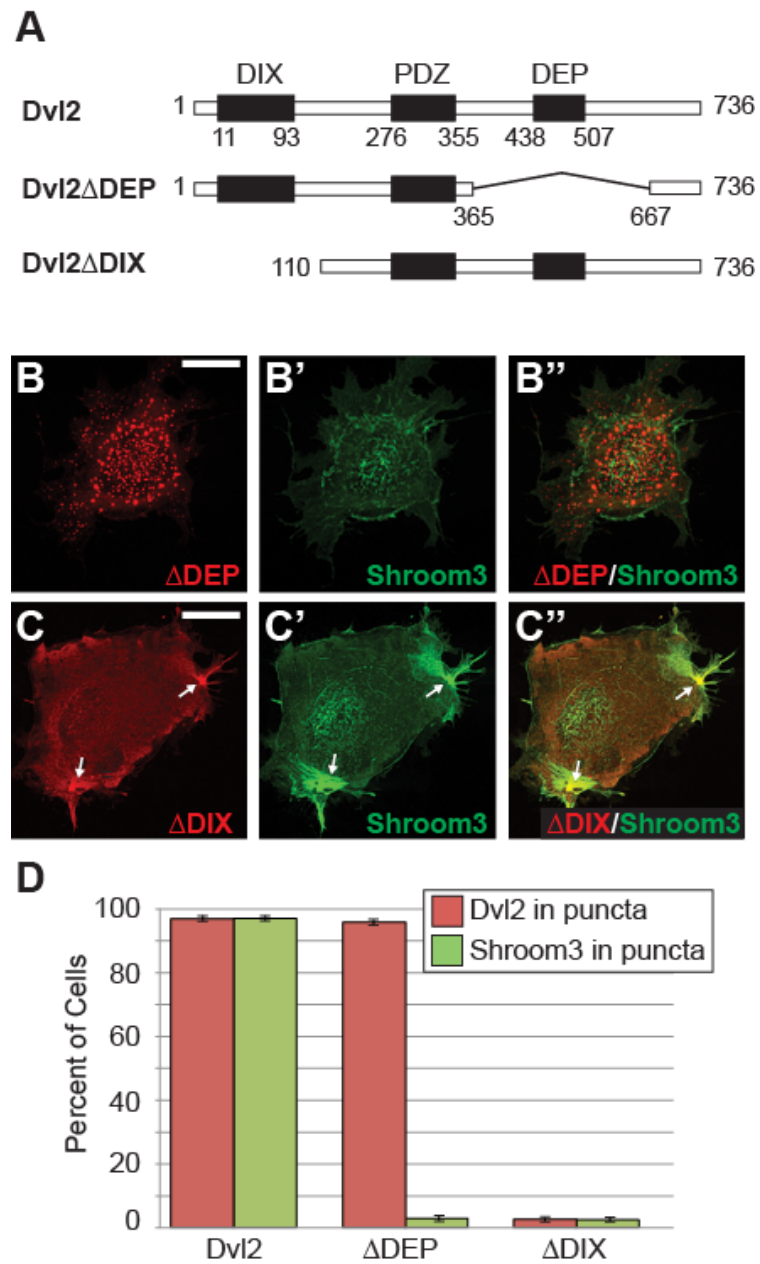


Figure 21. The DEP domain of Dvl2 facilitates interaction with Shroom3

A-C. Mapping the Shroom3 binding region of Dvl2. Indicated deletion mutants of Dvl2 (**A**) and Shroom3 were transiently co-expressed in COS7 cells and detected via immunofluorescent microscopy (**B and C**). Deletion of the DEP domain prevents recruitment of Shroom3 into puncta. Deletion of the DIX domain prevents Dvl2 polymerization and thus no puncta are observed. Some Dvl2/Shroom3 co-localization is observed at actin stress fibers (**C**, arrowheads) Scale bar: 10 μ m. **D.** Quantification of Shroom3 recruitment into puncta. Graph shows the percent of cells that show Dvl2 or Shroom3 localized to puncta in 200 cells from three independent experiments. Error bars: \pm s.e.m.

Next, a series of deletion constructs of myc-Shroom3 were used to determine the region of Shroom3 that interacts with Dvl2 (Figure 22A). The expression and stability of these constructs was confirmed via Western analysis of transfected cell lysates (Figure 22B). Each construct was co-expressed with full length Flag-tagged Dvl2 and their co-localization to puncta was evaluated by immunofluorescence. Co-localization of Shroom3 and Dvl2 is maintained in the absence of the PDZ, SPR, SD1, and SD2 domains, implicating a previously uncharacterized region spanning amino acids 286-776 in mediating the interaction between Shroom3 and Dvl2 (Figure 22C-F). Constructs that disrupt this region, 286-523 or 510-779, reduce co-localization with Dvl2 (Figure 22G and 22H).

I quantified this data by counting the number of cells in which the indicated Shroom3 protein is recruited to Dvl2 puncta (Figure 22I). These results suggest that the smallest fragment necessary to mediate co-localization with Dvl2 consists of the region between the SPR and SD1. Finally, to show that this region of Shroom3 can form a complex with Dvl2, a GST fusion containing amino acids 286-881 of Shroom3 was used to perform a pull down assay from cell lysates containing Flag tagged Dvl2 (Figure 22J). Data from these experiments show that this region of Shroom3 can form a complex containing Dvl2.

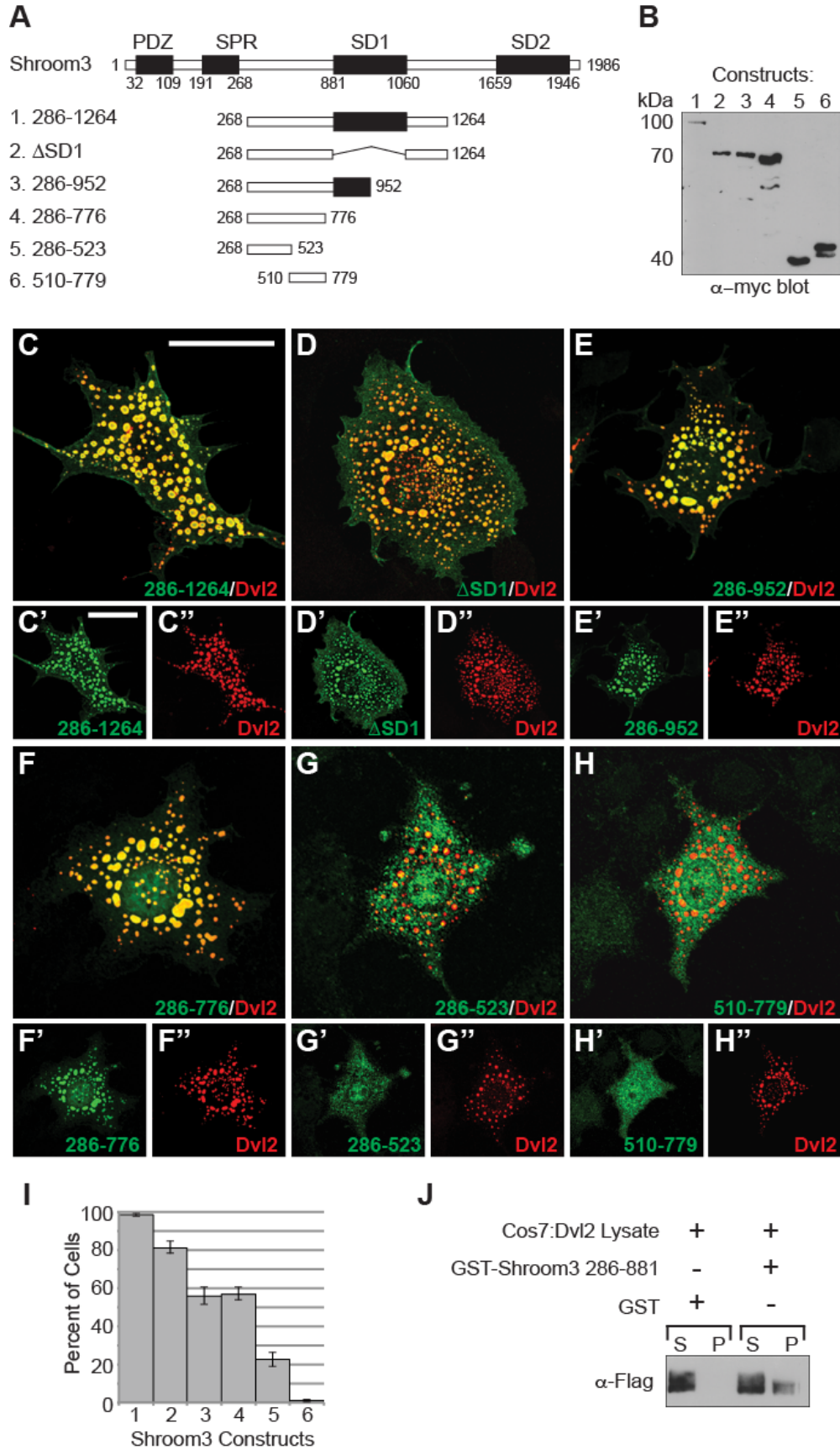


Figure 22. An uncharacterized region of Shroom3 mediates co-localization with Dvl2

A-H. Dvl2 and the indicated myc-tagged Shroom3 proteins (**A**) were co-expressed in COS7 cells and were detected via Western blotting (anti-Myc blot, **B**) or immunofluorescent microscopy and analyzed for co-localization in puncta. Merged images are shown in large panels, individual fluorescent channels are shown below the merged images (**C-H**). The smallest region of Shroom3 that mediates interaction with Dvl2 ranges from amino acids 286 to 776. Scale Bars: 10 μm **I.** Quantification of Shroom3 recruitment into puncta. Graph shows the percent of cells that show Dvl2/Shroom3 co-localization in puncta in 200 cells from three independent experiments. Error bars: \pm s.e.m. **J.** Amino acids 286-881 of Shroom3 forms a complex with Dvl2. GST or GST-Shroom3 286-881 bound to beads were added to COS7 lysate containing Dvl2, incubated, washed, pelleted, resolved by SDS-PAGE, and subjected to western blotting to detect Flag-tagged Dvl2. S, supernatant; P, pellet.

Taken together, results from these experiments indicate that Shroom3 and Dvl2 can form a complex *in vivo* and that this complex may serve to link PCP signaling to Rock and subsequent regulation of actomyosin contractility during neural tube morphogenesis.

3.3 DISCUSSION

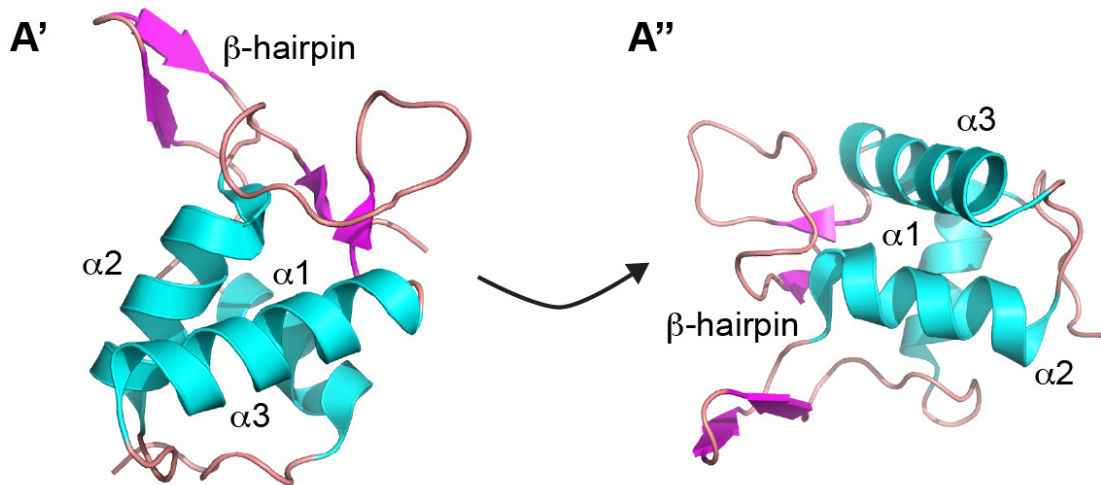
I have shown that in cells, Dvl2 can direct the distribution of a Shroom3-Rock complex. This would provide a direct mechanism to connect the PCP pathway to localized Rock activity and would suggest that Shroom3 is downstream of Dvl2. These data also indicate that Shroom3 and Dvl2 can exist in a complex *in vivo* and that this requires the DEP domain of Dvl and an N-terminal region of Shroom3 located between the SPR domain and the SD1. Future experiments would require the construction of a Shroom3 construct that lacks this region to confirm that it is solely responsible for binding Dvl2. The GST-pull down assay (Figure 22J) does not confirm that the interaction between Dvl2-DEP and Shroom3 is direct; there may be other cellular

constituents present in the COS7 lysate that mediate interaction with GST-Shroom3 286-881. Treatment of cells overexpressing full length Dvl2 and Shroom3 with small molecule inhibitors of F-actin (Cytochalasin D or Latrunculin A), microtubules (Nocodazole), or Rock (Y26732) does not block co-localization of Dvl2 and Shroom3 into puncta (data not shown), indicating that the interaction occurs independently of cytoskeletal elements. However, further studies are still required to determine whether the DEP domain directly binds to Shroom3.

While a clear function for the region of Shroom3 between the SPR and SD1 has not been identified previously, it has been shown to interact directly with the adaptor protein Posh and participate in signaling during axon growth [206]. Interestingly, the corresponding region of Shroom2 has been shown to bind to ZO1 and Myosin VIIA [197]. Therefore, the N-terminal region of Shroom3, and other Shroom proteins may represent another binding surface that links Shroom to either upstream regulators or downstream effectors. This region of Shroom3 is not well conserved among family members, thus Dvl2 binding may be a specific characteristic of Shroom3. Whether other Shroom family members interact with Dvl2 remains to be determined.

It is intriguing that the DEP domain is both required to bind Shroom3 and required for PCP signaling. The structure of the Dvl2 DEP domain has been extensively studied through x-ray crystallography and biochemical techniques [368] (Figure 23). The DEP domain is approximately 86 amino acids long and is comprised of an α -helical core with a protruding β -hairpin arm that is highly similar in sequence and structure to DEP domains from a variety of other proteins [369] (Figure 23A). This characteristic structure provides several binding interfaces that could be used to interact with various effector molecules [368] (Figure 23B). Dvl2 DEP has been shown to bind frizzled receptors and facilitate membrane recruitment during signaling.

A. Dvl DEP Structure



B. Putative binding surfaces

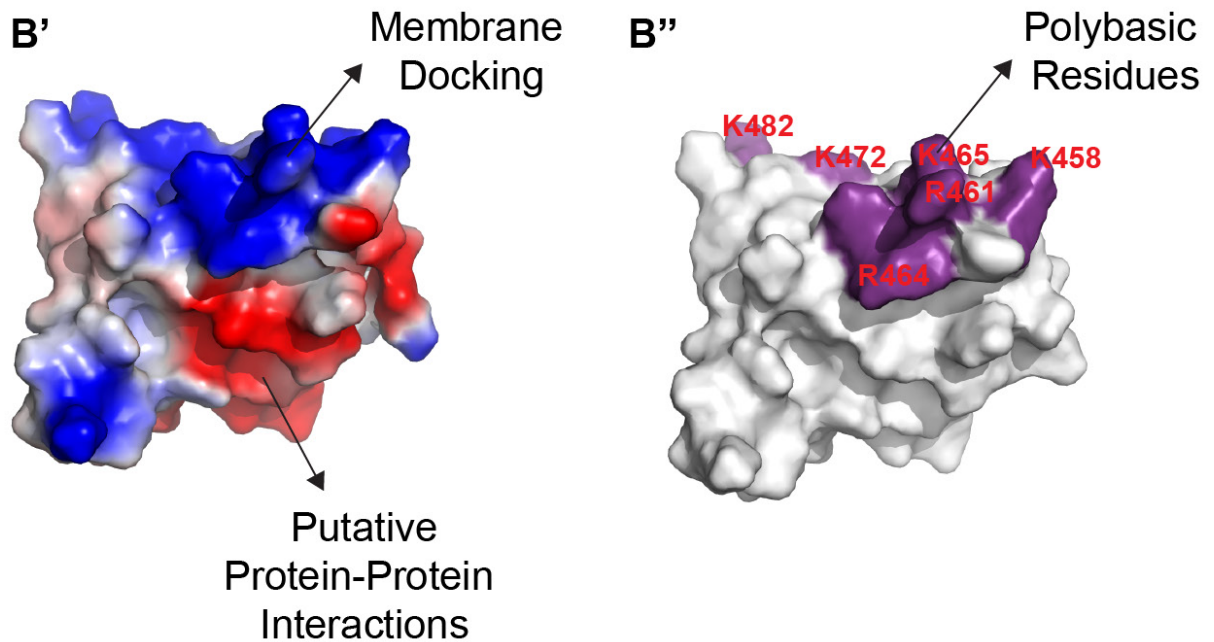


Figure 23. Dvl DEP structure and binding interfaces

A. The solution structure of the Dvl DEP domain shows a characteristic fold composed of three α -helices and a β -hairpin arm. The rotated structure in **A''** represents the same orientation as the surface models in panel **B**. **B'**. Surface model colored by electrostatic potential (blue = positive, red = negative). A positively charged interface composed of lysine and arginine residues (**B''**) has been shown to participate in membrane docking through

interactions with negatively charged phospholipids. A negatively charged patch has been hypothesized to facilitate protein-protein interactions (**B'**). Images are based on the Protein Data Bank (PDB) entry 1fsh of Dvl and were color-coded using Pymol software.

One common characteristic among DEP domains is the presence of a series of polybasic residues that bind to negatively charged phospholipids in the plasma membrane to anchor membrane-bound Dvl signaling complexes [247, 367, 370] (Figure 23B''). A region below the membrane-docking interface has been hypothesized to mediate interactions between Dvl and other proteins such as Fz. This region has been shown to bind a clathrin-adaptor complex that facilitates endocytosis of frizzled receptors to desensitize Wnt signaling [371]. Dvl proteins are key to specifying signaling specificity between canonical and non-canonical pathways. Signaling specificity is likely achieved through specific binding partners and subcellular localization, both of which are conferred by interactions between Dvl binding interfaces and effector molecules [351]. Thus, interactions between Dvl2 and Shroom3 may help to facilitate which signaling pathway is utilized downstream of Dvl2 activation.

Whether Shroom3 and Dvl2 interact in the neural plate remains to be determined. Co-localization studies to identify overlapping subcellular locales of these two proteins are made difficult by the lack of antibodies raised in different species that effectively detect endogenous Dvl2 and Shroom3 proteins. Additional experiments to co-immunoprecipitate Dvl2 and Shroom3 from neural plate lysates would provide evidence that this interaction occurs *in vivo*. Whether binding of Shroom3 and Dvl2 is required for neural tube closure also remains to be determined. Genetic interaction studies using *Dvl* mutant mice may be useful in further understanding the interplay between these two molecules. The challenge, however, is in the redundancy between the three mammalian *Dvl* homologs, which cause varying degrees of phenotypes when depleted

and will likely cause varying phenotypes in combination with mutations in *Shroom3*. Thus, the complicated genetics and the fact that some *Dvl* mutant phenotypes are attributed to canonical Wnt signaling pathways would make the interpretation of phenotypes challenging.

4.0 A PCP-SHROOM3 PATHWAY CONTROLS PLANAR CELL ARRANGEMENT

4.1 INTRODUCTION

In the case of both neural plate morphogenesis and *Drosophila* germband extension, polarized junctional remodeling and multicellular rosette formation drives cellular intercalation. In these cases, rosettes form through the polarized accumulation of actomyosin networks along mediolateral or dorsoventral cell-cell junctions, respectively [98, 130]. Additionally, neural plate bending occurs only along the mediolateral axis, indicating that actomyosin contractility driving apical constriction is also polarized along the mediolateral axis. Thus, the enrichment of contractile networks along mediolateral axes is essential for both apical constriction and convergent extension.

Based on the genetic and biochemical interactions described above, I hypothesized that PCP and Shroom3 signaling cooperate during mouse neural tube closure to regulate the distribution of contractile networks to promote both cellular organization into rosettes and directional bending of the neural plate. The interactions between Dvl2 and Shroom3 suggest that Shroom3 is downstream of PCP, such that Dvl2 mediates recruitment of Shroom3-Rock complexes to the apical membrane. If PCP establishes mediolateral accumulation of Dvl2, then a Dvl2-Shroom3 complex could establish mediolateral accumulation of Rock and subsequent activation of actomyosin contractility preferentially along mediolateral junctions. Thus, I

predicted that components of the Shroom3 and PCP pathways are localized at mediolaterally oriented cell-cell junctions. Additionally, if Shroom3 is important for establishing polarized contractile networks, then I should be able to detect defects in the arrangement of cells into rosettes that drive convergent extension.

4.2 RESULTS

4.2.1 Shroom3 Pathway Components Are Planarly Polarized

To determine if Shroom3 pathway components exhibit a polarized distribution in the neural plate, I stained neural plates from wildtype mouse embryos at E8.5 to detect ZO1, Shroom3, and F-actin (Figure 24A-D). Unlike other epithelial tissues used to assess the planar distribution of PCP components, such as *Drosophila* ommatidia, *Drosophila* ectoderm, and cells of the inner ear in mice, the cells of the neural plate in mouse E8.5 embryos do not appear to be highly organized, but instead exhibit a variety of shapes and sizes at their apical surface (Figure 24B). Furthermore, groups of neighboring cells are typically linearly aligned and linked together across several cells to form a contiguous cable oriented along the mediolateral axis (Figure 24B, red arrows). Both Shroom3 and F-actin accumulate along these linked mediolateral junctions (Figure 24C and 24D, red arrows). This distribution is most apparent within the region of the neural plate located between the midline and the future dorsolateral hinge point (boxed region in Figure 24A). Interestingly, the linear cables are most commonly seen directly adjacent to the medial hinge point, suggesting that their formation is important in regions of the neural plate that are actively bending.

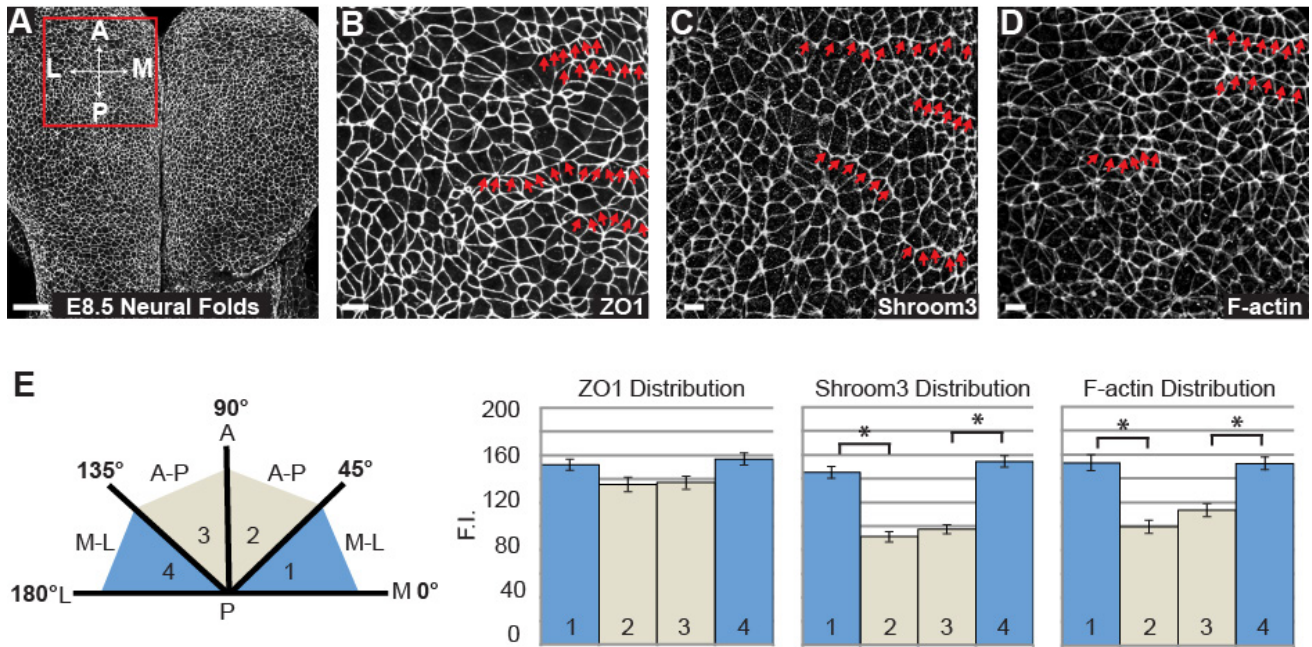


Figure 24. Shroom3 and F-actin are planarly polarized during neural plate bending

A. Schematic of analytical approach. Wildtype E8.5 embryos were stained in whole mount to detect ZO1 and visualize apical cell junctions of neural epithelial cells. Scale bar: 50 μm . M = medial, L = lateral, A = anterior, P = posterior. Box indicates the region of the embryo shown in panels B-D and used for quantification in panel E. **B-D.** Embryos were stained to detect ZO1 (**B**) Shroom3 (**C**) or F-actin (**D**). Red arrows show examples of cells linked linearly along their mediolateral junctions. Shroom3 and F-actin are enriched along mediolateral junctions closest to the midline (**C and D**). Scale bar: 10 μm . **E.** Quantification of polarized protein distribution of ZO1, Shroom3, and F-actin. The angle of each junction was measured relative to the mediolateral axis. Those junctions between 0° and 45° or between 135° and 180° (Bins 1 and 4, blue) were considered to be oriented along the mediolateral axis. Those between 45° and 135° (Bins 2 and 3, beige) were considered to be oriented along the anterior-posterior axis (panel E). Using ImageJ software, user-drawn lines across cell junctions were analyzed to determine the mean grey value and orientation relative to the mediolateral axis of each junction. Junctions were binned according to their angle and the fluorescence intensities (F.I.) in each bin were averaged. At least 200 junctions were analyzed from three wildtype embryos. Error bars: \pm s.e.m.; Student's *t*-tests: $p < 0.001$ (*).

I quantified this data using ImageJ software (NIH) by measuring the fluorescence intensity of each cell-cell junction of at least 200 cells within this region in three wildtype embryos and determined the angle of each junction relative to the mediolateral axis of the embryo (Figure 24E). Junctions positioned between either 0° and 45° or 135° and 180° (Figure 19E, blue) were considered oriented towards the mediolateral axis, while those junctions positioned between 45° and 135° (Figure 24E, beige) were considered oriented towards the anterior-posterior axis. Average measurements for mediolateral and anterior-posterior bins were compared using two-tailed, unpaired t-tests and significance was determined by a p-value of <0.001 . These data show a significant enrichment of Shroom3 and F-actin in the junctions oriented along the mediolateral axis (Figure 24E). In contrast, ZO1 is not significantly enriched at mediolateral junctions, indicating that the asymmetric distribution of Shroom3 and F-actin is specific.

In light of previous work showing the genetic and biochemical interactions between Shroom3, Dvl2, and Rock and the fact that activation of Rock results in the assembly of actomyosin networks, I hypothesized that Dvl2, Rock, and Myosin II would be similarly planarly distributed in the neural epithelium. Using the same techniques as described above, I observed that Dvl2, Rock1 and Myosin IIb are all planar distributed in wildtype E8.5 neural plates such that they are enriched at mediolateral cell junctions of the neural epithelium (Figure 25A-C). As is the case for Shroom3 and F-actin, enrichment of these components along mediolateral junctions is most apparent in the region adjacent to the medial hinge point. I quantified the fluorescent intensities of cell-cell junctions as described above and found that mediolateral enrichment of Dvl2, Rock1, and Myosin IIb is statistically significant with a p-value <0.001 .

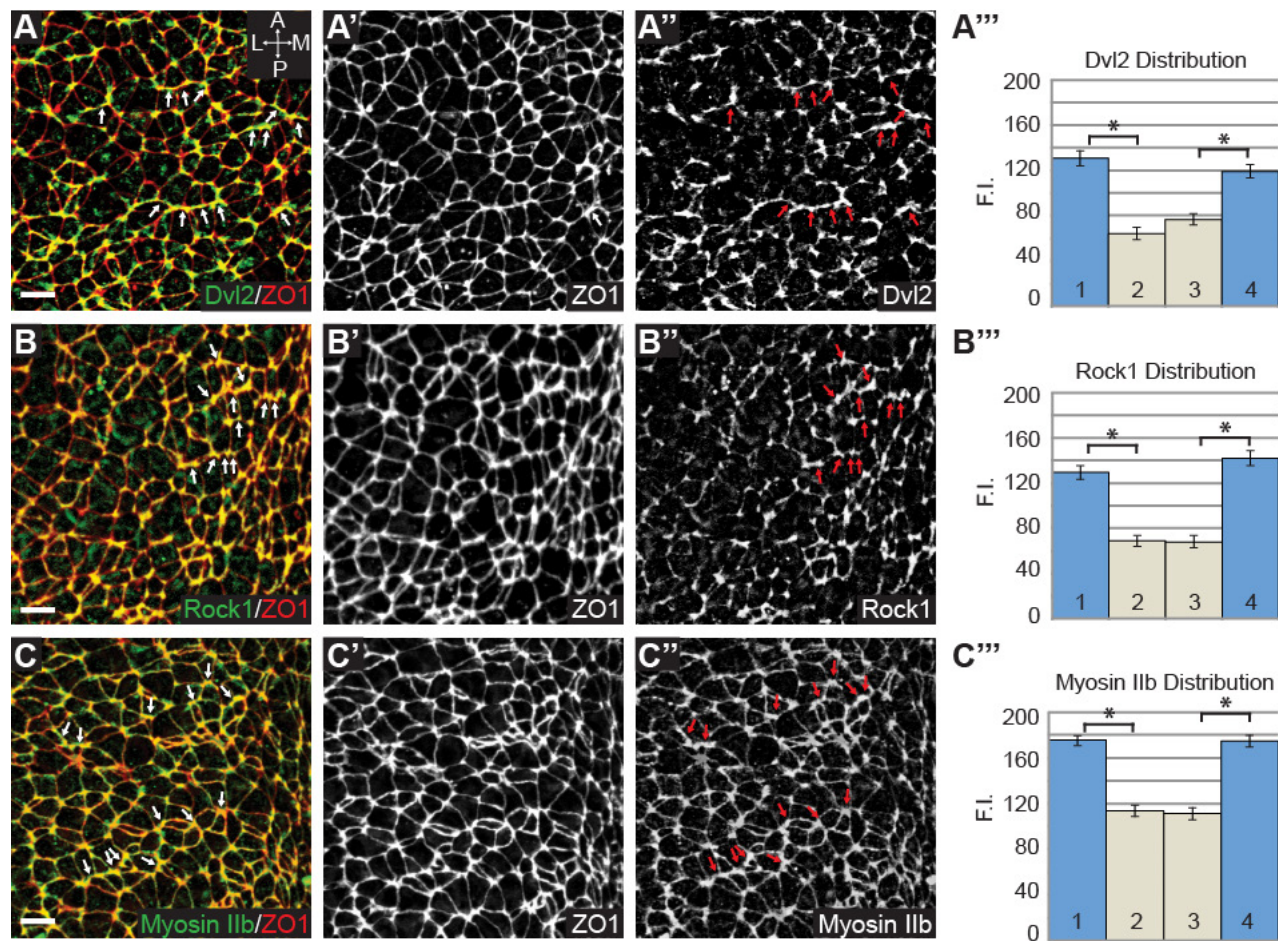


Figure 25. Dvl2, Rock1, and Myosin IIb are planarly polarized during neural plate bending

A-C. Wildtype E8.5 embryos were co-stained to visualize ZO1 with Dvl2, Rock1, or Myosin IIb. Arrows show enrichment along mediolateral junctions; scale bars: 10 μ m. Graphs show quantification of planar distribution analysis. F.I. = fluorescence intensity. Student's *t*-tests: $p < 0.001$ (*); Error bars: \pm s.e.m.

4.2.2 PCP is Upstream of the Shroom3 Pathway

I next wanted to order Shroom3 function relative to the PCP pathway and determine if Shroom3 localization is downstream of PCP. To accomplish this, I stained the neural plates of *Shroom3* and *Vangl2* mutant embryos to detect various components of these pathways (Figure 26A and 26B and Figure 27A-F). In *Vangl2* mutants, Shroom3 and F-actin are localized to cell-

cell junctions but are no longer enriched at mediolateral junctions, suggesting that the general localization signals are intact, but that mediolateral asymmetry of the adherens junctions specified by PCP signaling is lost (Figure 26A-C).

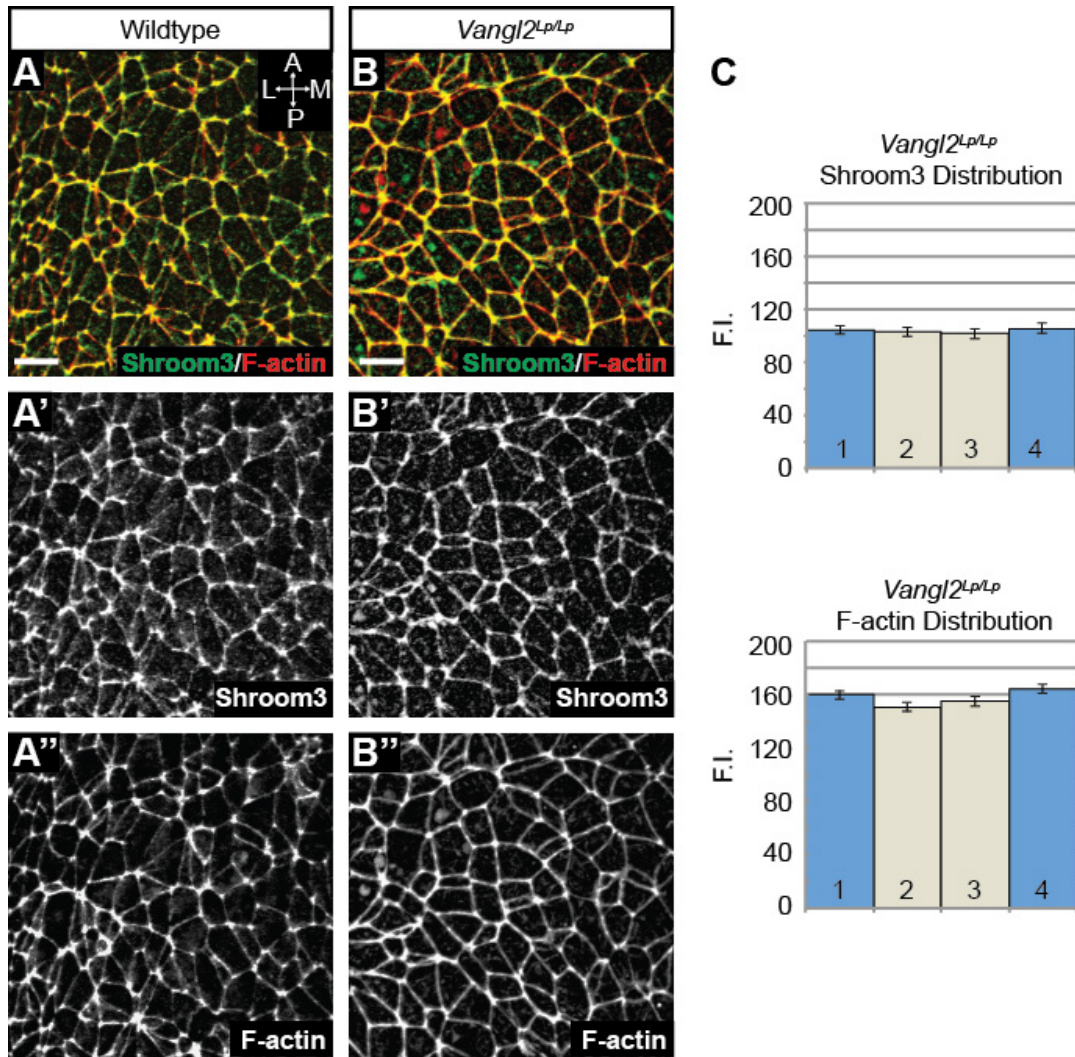


Figure 26. Planar polarity of Shroom3 and F-actin is lost in *Vangl2* mutants

A-B. Wildtype and *Vangl2* mutant E8.5 embryos were co-stained in whole mount to visualize the distribution of Shroom3 and F-actin. Scale Bars: 10 μ m. **C.** Quantification of planar distribution of Shroom3 and F-actin in *Lp* mutants. There is no significant difference in fluorescence intensity (F.I.) between mediolateral and anterior-posterior junctions.

In *Shroom3* mutant embryos, ZO1 staining is comparable to wildtype (data not shown) and Dvl2 remains planarly polarized (Figure 27A and 27B). This would suggest that neither apical-basal polarity nor planar asymmetry require *Shroom3*. Interestingly, based on our quantification, it appears that the amount of Dvl2 recruited to cell junctions is decreased in *Shroom3* mutants (Figure 27G vs Figure 25A’’’).

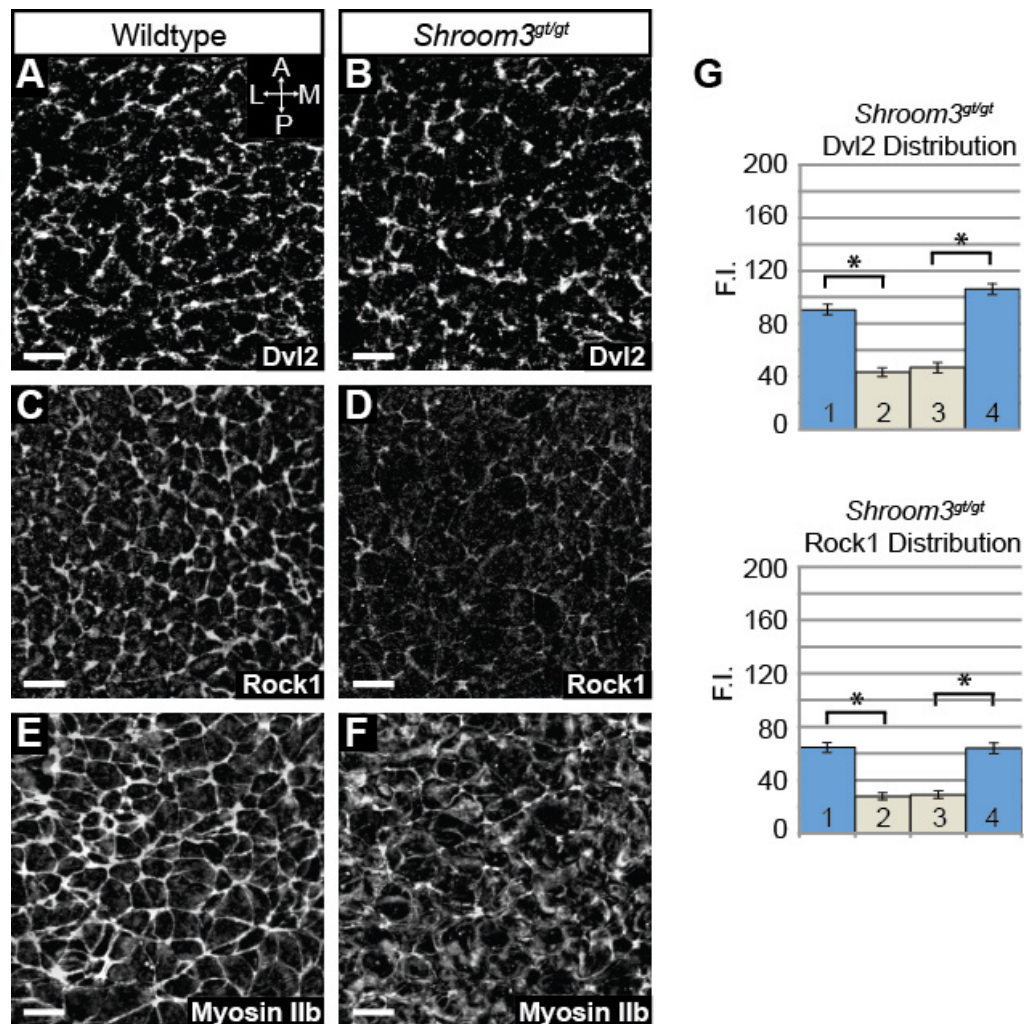


Figure 27. Analysis of PCP pathway components in *Shroom3* mutant embryos

A-F. Wildtype (**A,C,E**) and *Shroom3* (**B,D,F**) mutant neural plates were stained to visualize the planar distribution of Dvl2 (**A and B**), Rock1 (**C and D**), and Myosin IIb (**E and F**). Scale bars: 10 μ m. **G.** Quantification of planar

distribution of Dvl2 and Rock1. Dvl2 and Rock1 exhibit planar polarization, however a loss in total fluorescence intensity is apparent. Student's *t*-test: $p < 0.001$ (*); error bars: \pm s.e.m.

In contrast to Dvl2, I observed that Rock1 and Myosin IIb localization to the adherens junctions is significantly impaired in Shroom3 deficient embryos (Figure 27C-F). The small amount of Rock1 that retains its localization at cell junctions in the absence of Shroom3 is still mediolaterally enriched, suggesting there are other mechanisms to recruit Rock1 to cell junctions (Figure 27G). Consistent with the loss of Rock1 at cell junctions, I observed a significant reduction in Myosin IIb localization to cell junctions and an increase in the amount of cytoplasmic Myosin IIb (Figure 27E and 27F). This increased cytoplasmic staining prevents accurate quantification of the Myosin IIb remaining at cell junctions. Taken together, these results provide evidence that Shroom3 recruits Rock1 and Myosin IIb to adherens junctions while the PCP pathway refines the spatial distribution of the pathway.

Based on the above results showing the mislocalization of Rock1 and Myosin II in *Shroom3* mutants, I assessed the impact that Shroom3 loss has on the apical actin cytoskeleton of the neural epithelium. Consistent with the localization of Rock1 and Myosin IIb, Shroom3 deficiency results in a diffuse, discontinuous apical-junctional actin network and the appearance of a medial population of F-actin (Figure 28A and 28B). At the current resolution, it does not appear that this medial F-actin exhibits a defined organization. These data are consistent with the strong interplay between Shroom3 function and F-actin architecture that has been described in a wide range of tissues. Shroom3 can bundle actin *in vitro* and ectopic expression of Shroom3 increases F-actin accumulation at apical junctions in several experimental systems. Shroom3 constructs that target Shroom3 to various cellular locales such as the mitochondrial membrane robustly recruit actin to ectopic sites, thereby actively directing the subcellular distribution of F-

actin [182]. Thus, the redistribution of F-actin seen in *Shroom3* mutant neural plates is consistent with previous findings.

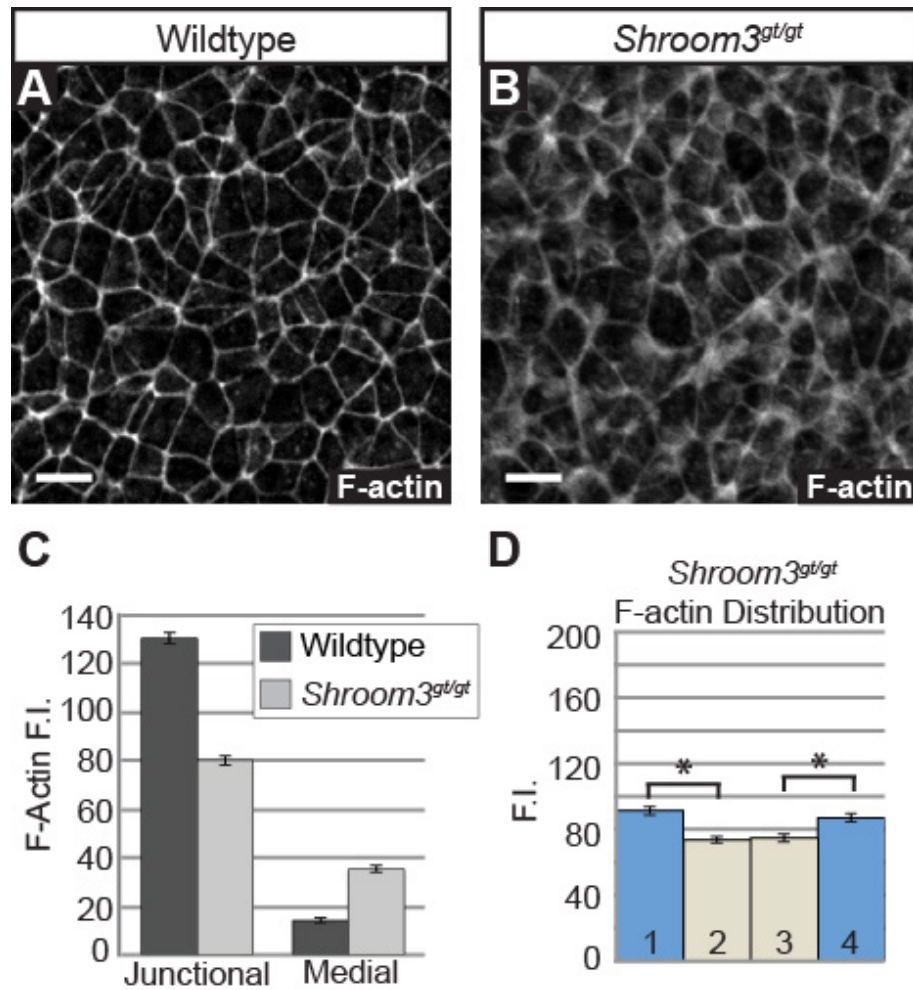


Figure 28. The apical F-actin network is disrupted in *Shroom3* mutants

A and B. Wildtype (**A**) and *Shroom3* (**B**) mutant neural plates were stained to visualize the planar distribution of F-actin. Scale bars: 10 μ m. **C and D.** Quantification of F-actin distribution in *Shroom3* mutant neural plates. User-drawn ROIs for the cell junctions of 200 cells in three wildtype and 3 *Shroom3* mutant embryos were used to determine the fluorescence intensity (F.I.) of F-actin at cell-cell junctions. ROIs within the cell borders were used to determine the F-actin fluorescence intensity of medial F-actin. Graph in (**C**) shows a loss of F-actin at apical junctions and an increase in medial actin populations in *Shroom3* mutant neural plates compared to wildtype. The remaining junctional F-actin is mediolaterally enriched in *Shroom3* mutants (**D**). Student's *t*-test: $p < 0.001$ (*), error bars: \pm s.e.m.

To quantify this redistribution of F-actin, I measured the fluorescence intensity of junctional and medial F-actin in 300 cells from 3 wildtype and 3 *Shroom3* mutant embryos (Figure 28C). In wildtype embryos, 90% of the F-actin fluorescence is localized along cell-cell junctions. *Shroom3* mutant embryos exhibit an approximate 40% decrease in the fluorescence intensity of junctional F-actin and there is a concomitant increase in the diffuse intracellular population. However, consistent with what I observe for Rock1 distribution, the F-actin that remains localized to the junctions in the *Shroom3* mutants exhibits a mediolateral distribution bias, indicating that the PCP signaling is still intact (Figure 28D).

These experiments demonstrate that Dvl2, Shroom3, Rock1, Myosin IIb, and F-actin are enriched at mediolateral cell-cell junctions of the neural epithelium (Figure 29). The asymmetric localization of Shroom3 pathway components depends on the PCP pathway, suggesting that Shroom3 functions downstream of PCP to regulate the distribution of Rock, Myosin II, and F-actin.

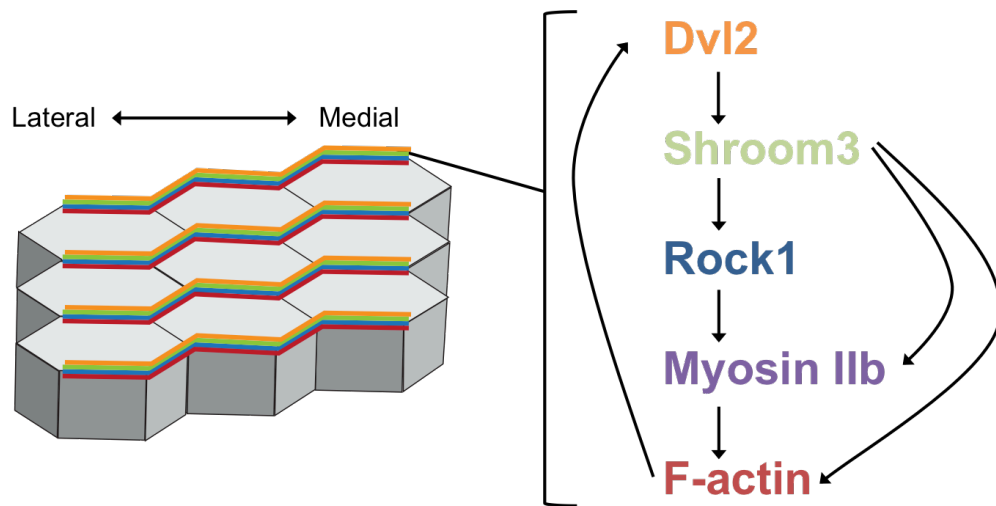


Figure 29. Summary model of results

Shroom3 pathway components are enriched at mediolateral cell junctions in a PCP-dependent manner. Shroom3 influences the actomyosin network, which may feedback to stabilize Dvl2 localization at the apical membrane.

The fact that I see a loss of Dvl2 apical recruitment in Shroom3 mutants indicates that Shroom3 pathway function is necessary to maintain Dvl2 at the apical membrane. Proper actomyosin localization may help to stabilize Dvl2 localization, thus when Shroom3 is lost, the resultant disturbance in the actomyosin network causes a loss of apical Dvl2. The fact that both Rock1 and F-actin maintain some level of planar distribution in Shroom3 mutants could be due to functional redundancy with Shroom2, which is expressed in the neural epithelium during closure. In the *Drosophila* germband, where dShroom is required for planar polarization of dRok and Myosin II, loss of dShroom is sufficient to cause a loss of planar distribution of dRok and Myosin II [131]. Since *Drosophila* only has one *Shroom* gene, functional redundancy is not an issue.

4.2.3 Loss of Shroom3 Disrupts Planar Cell Arrangement

Based on the observed genetic interactions between *Shroom3* and *Vangl2* and the polarized distribution of the Shroom pathway components Rock and Myosin II, it is possible that Shroom3 plays a direct role in cell arrangements associated with convergent extension. Specifically, I hypothesized that Shroom3-induced tension at mediolateral junctions participates in convergent extension by facilitating the arrangement of neural epithelial cells into rosettes and rosette-like clusters. To test this hypothesis, I stained E8.5 embryos in whole mount to detect ZO1 in order to visualize the planar arrangement of neural epithelial cells prior to neural tube closure (Figure 30A). Wildtype neural epithelial cells are arranged into rosettes that vary in complexity (Figure 30B). Structures that resemble rosettes that are forming and resolving are easily identified in wildtype neural plates, indicating that rosette formation occurs during convergent extension of the mouse neural plate (Figure 30C).

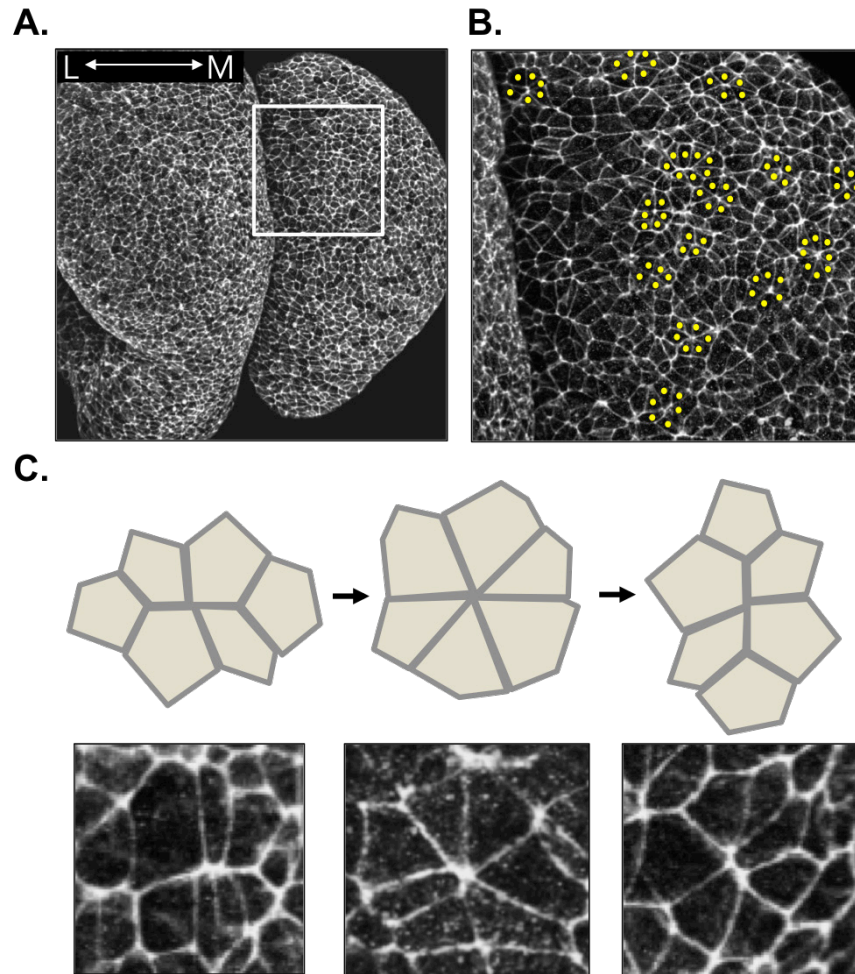


Figure 30. Wildtype neural epithelial cells are arranged in rosettes

A. E8.5 mouse embryos were stained in whole mount using antibodies against ZO1 to evaluate planar cell arrangement. **B.** Zoom-in of the boxed region in panel A shows cells arranged into rosette-like clusters. **C.** Rosettes that appear to be forming and resolving are easily identified in wildtype neural plates.

To automate the analysis of planar cell arrangement, images from five wildtype and five *Shroom3* mutant embryos were segmented (Seedwater Segmenter, [372]) to produce separate Regions of Interest (ROI) for each cell (Figure 31A and 31B). Analysis of each ROI indicates that neural epithelial cells of *Shroom3* mutants exhibit a 48% increase in apical area (Figure 31C). This is consistent with the role of *Shroom3* in regulating apical constriction.

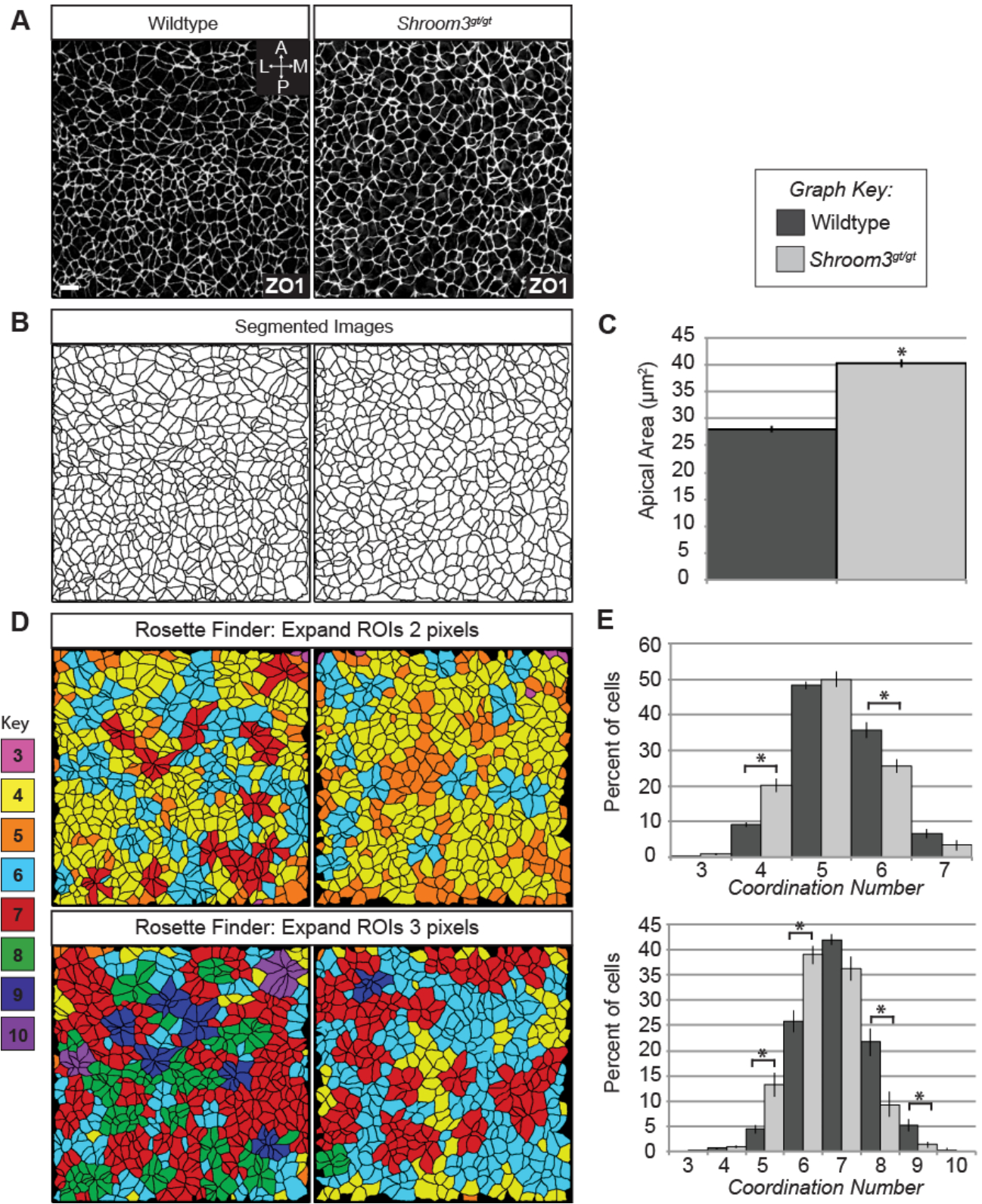


Figure 31. *Shroom3* mutants exhibit defective planar cell arrangement

A and B. Image processing to detect rosettes. Wildtype and *Shroom3^{gt/gt}* E8.5 embryos were stained to detect ZO1 to visualize the apical junctions in the neural plate. Scale bar: 10 μm . **(A).** Seedwater Segmenter was used to segment images from wildtype and *Shroom3* mutant embryos **(B)**. These segmented images were imported into ImageJ software (NIH) and an automated system was used to convert the segments into ROIs. **C.** Graph shows average apical area of neural plate cells in 3 wildtype and *Shroom3* mutant embryos, $n \geq 300$ cells. **D.** A rosette finding macro was used in ImageJ to analyze the segmented images. ROIs were expanded by either 2 or 3 pixels and cells were color-coded based on the number of cells that meet at shared vertices (referred to as the coordination number). **E.** Cells were binned based on their coordination number and the percent of cells in each bin was plotted to compare the complexity of cell clusters between wildtype and *Shroom3* mutant embryos. The overlap threshold was set at either 2 or 3 pixels and the results from both analyses are presented (top panels, 2 pixel overlap; bottom panels, 3 pixel overlap). Graphs show analysis from images from five wildtype and *Shroom3* mutant embryos. Student's *t*-Tests: $p < 0.001$ (*), error bars: \pm s.e.m.

Sets of ROIs were then analyzed with a custom image analysis tool to determine the number of cells that meet at shared vertices, referred to as the coordination number (see Experimental Procedures). This method is based on the notion that cells clustered in rosettes will have a higher number of cells that share a common vertex. For this analysis, multi-cell junctions were found by counting the number of cells that overlap after their ROIs were expanded by either 2 or 3 pixels. The coordination number present in each of the shared vertices was calculated and cell clusters were either color coded (Figure 31D) or binned (Figure 31E) based on their coordination number. If a given cell is in multiple clusters, it is assigned the highest coordination number. In practice I found that changing the overlap threshold from 2 to 3 pixels significantly increased the number of rosettes as well as the coordination number of each rosette. For comparison I present the results of both analyses (Figure 31D and 31E) and find they both report qualitatively similar differences between wildtype and *Shroom3^{gt/gt}* cell arrays.

Neural epithelial cells in both wildtype embryos and *Shroom3* mutant embryos form cellular clusters ranging from 3-10 cells, suggesting that Shroom3 is not required for the formation of clusters or rosettes (Figure 31D). However, wildtype neural epithelial cells form significantly more rosettes/clusters with a higher complexity based on the number of participating cells (Figure 31D).

Because *Shroom3*^{gt/gt} cells are less apically constricted, the field of view contains fewer cells than wildtype. Thus, the percent of cells with each coordination number relative to the total number of cells in the field was graphed and used to compare the percent of cells in each bin between wildtype and *Shroom3* mutant embryos (Figure 31E). This analysis demonstrates that in *Shroom3* mutants there is a significant decrease in the percent of cells that participate in cell clusters with high coordination numbers. This suggests that loss of Shroom3 function reduces the degree of cellular remodeling and neighbor exchange. The fact that I do not observe a complete loss of rosette formation in the absence of Shroom3, but rather a reduction in the complexity of the rosettes is consistent with recent studies indicating that rosette formation and resolution in the mouse neural plate is not driven solely by apical contractility, but also relies on the formation of basolateral lamellipodia that guide mediolateral intercalations [134]. Taken together, these data indicate that Shroom3 participates in the planar organization of the Rock-Myosin II pathway and that this localization is required for the planar organization of cells that facilitates convergent extension and subsequent neural tube closure.

4.3 DISCUSSION

These experiments clearly demonstrate that Shroom3 is preferentially recruited to mediolateral cell junctions in a PCP-dependent manner. Taken together with the genetic analysis and biochemical interaction between Shroom3 and Dvl2, these data suggest a model in which the Shroom3 and PCP pathways work together during neural tube closure to define the subcellular distribution of activated, contractile actomyosin networks (Figure 32).

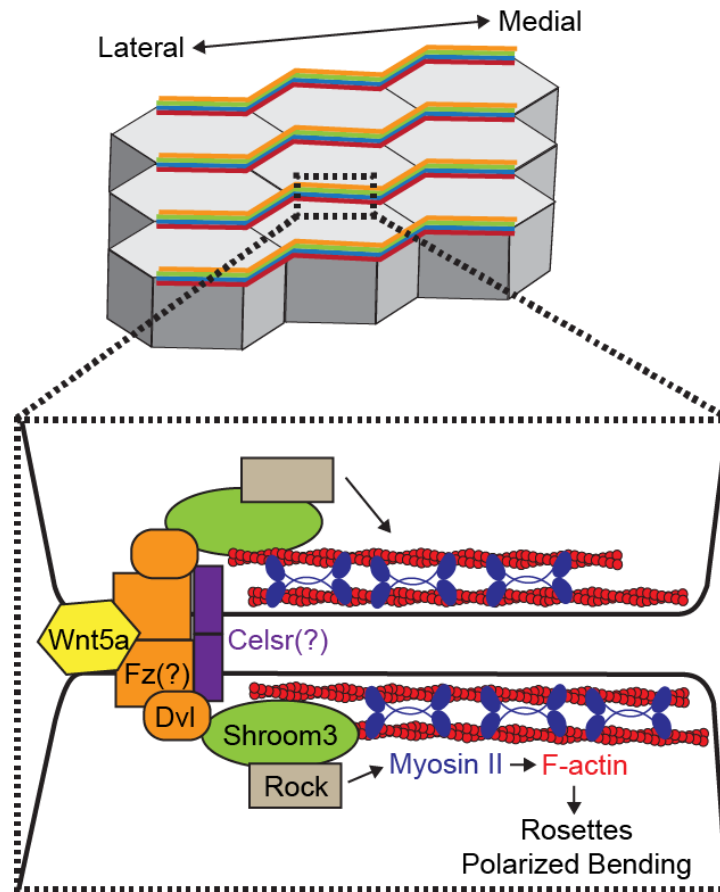


Figure 32. Model of Shroom3 and PCP pathway integration

PCP components are enriched at mediolateral cell-cell junctions in the mouse neural plate. Dvl2 promotes mediolateral accumulation of Shroom3, which recruits and potentially activates Rock to elicit actomyosin

contraction along mediolateral junctions. Polarized contraction drives both polarized neural plate bending and rosette formation, thereby coupling apical constriction and convergent extension during neural tube morphogenesis.

PCP signaling results in the accumulation of Dvl2 at mediolateral junctions. Dvl2 facilitates the enrichment of Shroom3 at these same junctions, resulting in an increased population of Rock along the mediolateral axis of the neural plate. At the current resolution, it is difficult to determine whether Dvl2, Shroom3, and Rock are localized to all mediolateral junctions or restricted to one side. Whether medial and lateral protein complexes of Fz/Dvl and Vang/Pk comparable to the proximal and distal complexes described in the *Drosophila* wing exist in the neural plate remains to be determined. However, an enrichment of Shroom3, Rock, and Myosin II along both sides would provide an active actomyosin network that could drive both polarized apical constriction and convergent extension. Rock-mediated activation of Myosin II along mediolateral junctions would provide contractility specifically along the mediolateral axis, which could facilitate apical constriction that preferentially causes cells to shorten along the mediolateral axis and less so along the anterior-posterior axis. The contiguous actomyosin cables that I observed at cell junctions aligned linearly along the mediolateral axis close to the medial hinge point could promote either elevation or bending of the neural folds prior to closure.

Additionally, contraction of mediolateral junctions could promote elongation of the body axis via the formation of higher order rosettes that facilitate directional cell rearrangements and neighbor exchange. Finally, these contractile cables could provide tissue rigidity to withstand the external forces that are thought to promote neural tube closure. While Shroom3 is enriched at mediolateral junctions, it is also localized to anterior-posterior junctions, indicating that in addition to its role in rosette formation and bending, it may provide tension along both axes of

the neural plate. Shroom3-induced contractility is required for apical constriction, polarized bending, and cellular arrangement into rosettes, thus Shroom3 in conjunction with PCP signaling provides a mechanism to couple apical constriction and convergent extension and thus offers a cohesive story of how the neural tube is shaped.

The establishment of mediolateral actomyosin networks by Shroom3 and PCP may involve several levels of feedback to stabilize planar distribution. The fact that there appears to be a loss of Dvl2 membrane recruitment in *Shroom3* mutants suggests that Shroom3 may reinforce Dvl localization or junctional architecture. It is possible that the decreased junctional F-actin in *Shroom3* mutants could influence Dvl2 distribution as it has been shown to co-localize with F-actin [352, 373]. Additionally, it is possible that there is feedback regulation such that the recruitment of Rock by Shroom3 results in increased junctional F-actin, which allows for additional Dvl2 recruitment. This concept of feedback regulation between Shroom, Rock, and F-actin is supported by experiments in *Drosophila* [131].

The rosette studies performed in this work were done in fixed tissue. Just because rosettes are capable of forming does not mean that they are able to resolve in the correct direction. Live imaging of *Shroom3* mutant embryos would allow the tracking of individual rosettes to further characterize the exact nature of the role of Shroom3 in rosette formation. The rosette defects are likely a result of reduced actomyosin contractility. In the *Drosophila* germband, it was shown that larger order rosettes require more force generation for formation than smaller rosettes. Multicellular actomyosin cables are under a higher level of tension and accumulate more Myosin II and F-actin than single junctions [86]. Thus, in *Shroom3* mutants, the loss of junctional localization of Myosin II, Rock, and F-actin would prevent the generation of enough force to allow for the formation of high order rosette structures.

A study published this year by Williams et al. examined cell intercalation in the mouse neural plate using live time-lapse imaging of whole mount embryos [134]. This study found that *Vangl2*^{Lp/Lp} neural plates can form cellular rosettes that resolve in the correct direction. Frequency of neighbor exchange, however, occurs much less than wildtype, such that half of the rosettes that form fail to resolve. Thus, the defect associated with loss of Vangl2 is in the ability of rosettes to resolve, not in their directionality. Contrary to studies done in *Drosophila* and the mammalian inner ear that have established a direct role for Vangl2 in establishing planar polarity, this study proposes that Vangl2 is not essential for the establishment of polarity within the mouse neural plate. Furthermore, zero studies to date have shown planar polarized distribution of Vangl2 in the neural plate. However, a common characteristic of *Vangl2*^{Lp/Lp} mutants is a loss of planar distribution of other PCP components or downstream effectors. Consistent with this, I observed a loss of planar polarity of Shroom3 and F-actin, suggesting that planar polarity of the neural plate is lost in *Vangl2* mutants. Perhaps the rosettes that do resolve in the correct orientation in the *Vangl2*^{Lp/Lp} neural plate can be explained by functional redundancy between Vangl1 and Vangl2. Data from this same report also suggests that apical Myosin IIb is not planar polarized in the neural plate. This discrepancy appears to result from differences in what portion of the embryo was analyzed, as I focused on the cranial neural tube, while these data appear to be collected from the spinal region. Thus, regional differences may account for apparent differences in the cellular and molecular mechanisms of neurulation.

There are likely to be additional factors that regulate the distribution of Shroom3 that were not addressed in this study. For example, Lulu and F-actin have been shown to be important in determining Shroom3 distribution [189, 195]. This is consistent with my observation that Shroom3 localization to the AJC is not lost in *Vangl2*^{Lp/Lp} mutants. Additionally, the roles of

other PCP components such as *Celsr1* and *Fzd3* were not addressed by this study, thus how they are involved still remains to be determined. A mechanistic understanding for the role of *Wnt5a* in neural tube closure also remains elusive. Additionally, a role for *Rho* in connecting PCP to *Rock* as in the case of the chick neural plate has not been addressed. The studies done in chick did not assess the role of *Shroom3* in the proposed *Dvl2*-*PDZ**Rho**GEF* pathway, thus it still remains to be determined whether the *Dvl2*-*PDZ**Rho**GEF* pathway and *Dvl2*-*Shroom3*-*Rock* pathways are independent or linked. Additionally, *Ptk7* is required for neural tube closure, and a *Ptk7*-*Src*-*Rock* pathway has also been suggested to play a role in regulating the spatial distribution of actomyosin networks [286]. Based on the data herein and that of others, it is likely that there are redundant mechanisms in neurulation that ensure robustness of the process. This redundancy may account for the observations that in humans, neural tube defects, while relatively common, exhibit such a complex etiology. It will be interesting to determine the genetic interactions that exist between these various pathways and explore how these networks may interact in the etiology of disease that impacts human neural development.

5.0 CONCLUSIONS AND FUTURE PROSPECTIVES

How signaling events are translated into changes in cell shape, cell topography, and contractility during epithelial morphogenesis is an important area of research due to its relevance to human disease conditions, tissue engineering, and regeneration. This work investigates the mechanism by which signaling pathways are coordinated during the development of the mouse neural tube using genetic, biochemical, and cell-based approaches. Previous work has suggested that Shroom3 utilizes the activity of Rock to regulate actomyosin contractility that drives apical constriction and facilitates neural tube closure. Prior to this study, however, it was unclear if Shroom3 activity is regulated. I have shown that the Shroom3 and PCP pathways interact to control the planar distribution of apical contractile actomyosin networks in neural epithelial cells and suggest that PCP may be an upstream regulator of Shroom3 activity to provide directionality to contractile force. Based on the analysis herein, I predict that the asymmetric distribution of the Shroom3-Rock-Myosin II pathway facilitates the directional bending of the neural plate and the topographical organization of cells into rosettes, both of which are implicated in neural tube closure (Figure 33). The data presented suggest that the intersection of the Shroom3 and PCP pathways controls neural tube morphogenesis and represents a model of how the simultaneous reduction of multiple pathways can cause neural tube defects, which mimics the genetic nature of neural tube defects in humans.

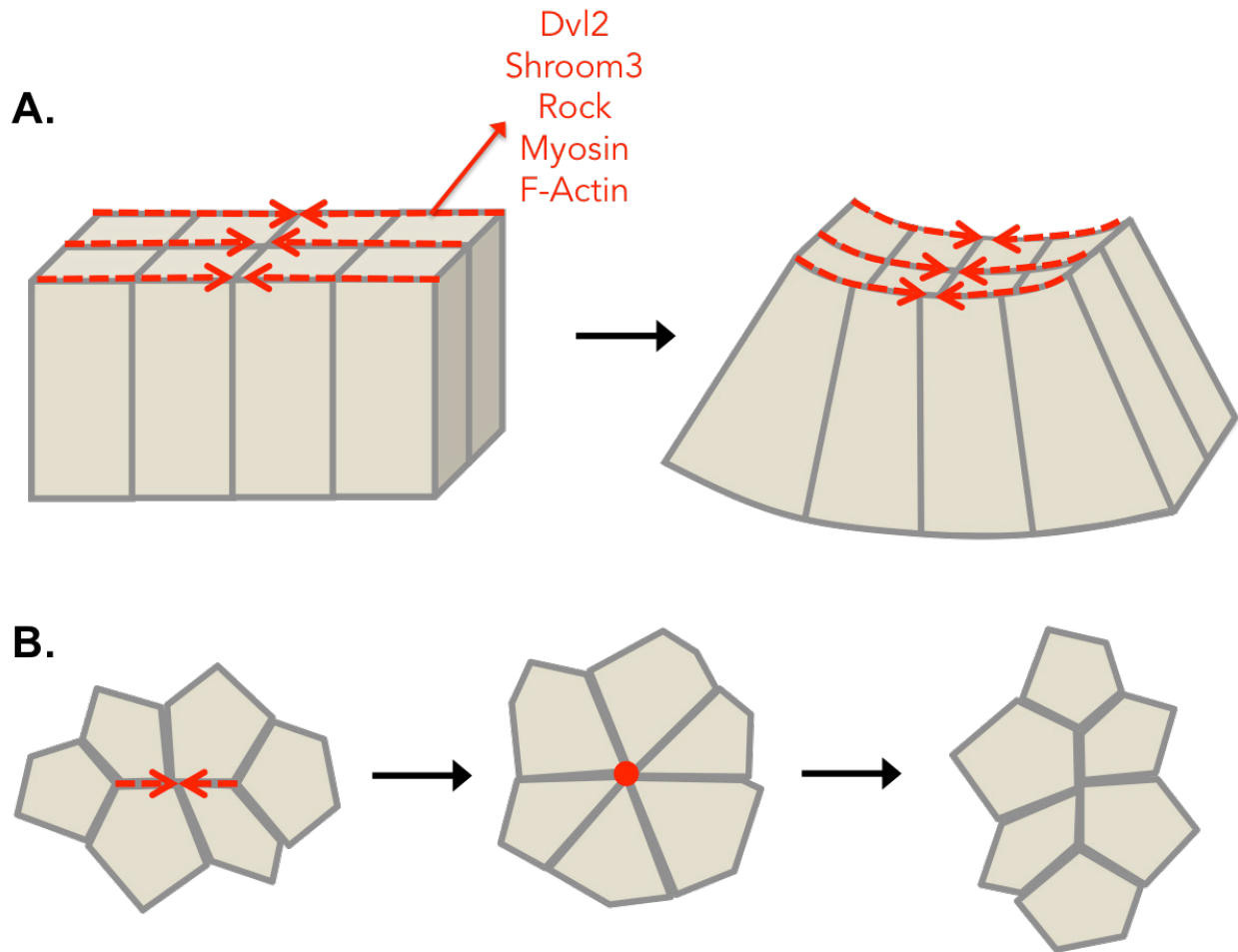


Figure 33. Morphogenetic consequences of PCP-Shroom3 interactions

The enrichment of PCP and Shroom3 pathway components at mediolateral cell-cell junctions provides a mechanism to couple apical constriction (**A**) and convergent extension (**B**) during neural tube closure.

Through this work, I have identified both novel and redundant mechanisms regulating cell behavior in the mouse neural plate. In the past few years, developmental biologists have elucidated the mechanisms of cellular intercalation in a wide array of model tissues. Polarized junctional remodeling has emerged as a highly conserved cellular mechanism for intercalation in epithelial tissues and the examples studied thus far rely on molecular inputs from various molecules including PCP, RhoGEF, Rho, Rock, Myosin II, and adherens junction components

such as Cadherin and Par3. The work herein adds Shroom3 to the list of regulators of cell intercalation and helps to define the interplay between the various molecules involved in regulating convergent extension. Because Shroom3 functions in this capacity in the mouse neural plate and *Drosophila* germband, it is likely that Shroom3 represents a conserved molecular pathway that functions in other tissues to link PCP establishment to actomyosin contractility to promote junctional remodeling. In addition to further defining the spatial distribution of other PCP components such as Fzd and Celsr1 in the mouse neural plate, future work aims to understand the interplay between PCP, Shroom3, and components of adherens junctions. Based on previous studies that identified genetic interactions between Shroom3 and n-Cadherin and between Vangl2 and Cofilin, it is likely that the PCP-Shroom3 pathway is intimately linked to adherens junction architecture and regulation of the actin cytoskeleton [187, 335]. Because cadherin turnover is thought to play an important role in polarized junctional remodeling in the *Drosophila* germband, it may also play a role in neural tube morphogenesis. Whether adherens junction components and apical-basal polarity complexes are excluded from mediolateral junctions in the neural plate or preferentially enriched in opposing junctions remains to be determined.

The Shroom3 and PCP pathways are both critical modulators of epithelial morphogenesis in a wide array of tissues. The neural tube is just one of many potential scenarios where Shroom3 and PCP might cooperate to regulate the subcellular distribution of actomyosin networks. Thus, future experiments that characterize the roles of Shroom3 and PCP in other tissues would lend insight into the ways in which these pathways cooperate in various contexts. For example, several recent studies have shown that disruption of PCP leads to defects in kidney tubule morphogenesis. *Vangl2*^{Lp/Lp} mice exhibit kidney tubule branching defects due to defective

convergent extension within the extending tubules [128, 374]. Wnt9b mutants exhibit decreased tubule branching with increased tubule diameter, which phenocopies the effect of treating kidneys with a Rock inhibitor [375]. It is clear that PCP is required for proper kidney development and that it functions to regulate convergent extension through actomyosin contractility. Preliminary data suggests that Shroom3 is expressed in kidneys and *Shroom3* mutant kidneys display a decreased overall organ size (unpublished observations). Thus, Shroom3 may be involved in kidney morphogenesis by facilitating branching and/or tubulogenesis through the regulation of actomyosin contractility. Polymorphisms in human SHROOM3 have recently been associated with kidney disease, thus understanding the roles of Shroom3 and PCP in kidney morphogenesis would not only lend insight into pathway function but would also be relevant to human disease conditions. Kidneys can be cultured *in vitro* and manipulated using si-RNA mediated gene knockdown, thus investigating potential interactions between Shroom3 and PCP in this tissue provides more effective techniques for dissecting the molecular interactions between pathway components than the neural plate.

The work described in this dissertation supports previous models of Shroom3 and PCP function and adds new insight into the interplay between the pathways. The model presented provides a number of testable hypotheses for future work aimed to fully understand the connections between various molecular regulators of epithelial morphogenesis in a wide array of contexts.

6.0 EXPERIMENTAL PROCEDURES

6.1 MICE AND EMBRYOS

The *Shroom3* null allele (*Shroom3*^{gt(ROSA)53sor}, *Shroom3*^{+ /gt}) has been described previously (Hildebrand, 99). LPT/LeJ (*Vangl2*^{+ /Lp}) and B6;129S7-*Wnt5*^{atm1Amc}/J (*Wnt5a*^{- /-}) [140, 340] mice were obtained from the Jackson Laboratory (Bar Harbor, ME, USA). Matings were set up overnight and checked daily for copulation plugs. The day of finding a copulation plug was designated embryonic day 0.5 (E0.5). For genetic studies, embryos were dissected in PBS + 0.2% BSA between E9.5 and E13.5. For visualization of phenotypes, embryos were fixed in Bouin's Fixative for 2 hours, washed with 70% ethanol plus 0.1% NH₄OH until white and photographed with an S6D dissecting scope equipped with a DFC 300F camera (Leica Microsystems, Wetzlar, Germany). Animal care and use was in accordance with the guidelines established by the University of Pittsburgh's Institutional Animal Care and Use Committee.

6.2 GENOTYPING

PCR genotyping was performed using DNA from ear clippings from adult mice or yolk sacs from embryos. Tissue samples were heat denatured at 95°C for five minutes in digest buffer (1X GB buffer (670mM Tris pH8.8, 166mM (NH₄)₂SO₄, 65mM MgCl₂), 1% Triton, 1% BME), and

incubated with 1µg/µl proteinase K at 55°C for 50 minutes. *Shroom3* and *Wnt5a* mice and embryos were PCR genotyped using the primers listed in Table 3 with the following conditions: 1mM dNTPs, 1X GB buffer, 10% DMSO, 0.1µM of each primer, and 0.5% BME. To genotype the LPT allele, mismatched PCR primers were designed to create a restriction endonuclease-sensitive site including the LPT mutation [376]. This line was genotyped by PCR amplification using the above conditions followed by digestion with HpaI. Mutant and wildtype alleles differing by 20 base pairs after HpaI digestion were separated on 3% high resolution Metaphor agarose gel (Lonza, Rockland, ME, USA).

Table 3. PCR primers used for mouse genotyping of *Wnt5a*, *Shroom3*, and *Vangl2* alleles

Primer Name	Sequence
Wnt5a_Forward_wildtype allele	5' - GAGGAGAAGCGCAGTCAATC -3'
Wnt5a_Forward_TM1 allele	5' - GCCAGAGGCCACTTGTGTAG -3'
Wnt5a_Reverse	5' - CATCTCAACAAGGGCCTCAT -3'
Shroom3_Forward	5' - GGTGACTGAGGAGTAGAGTCC -3'
Shroom3_Reverse_wildtype allele	5' - GAGCACTGGCTGCTCTTCATG -3'
Shroom3_Reverse_gene trap allele	5' - GAGTTTGTCTCAACCGCGAGC -3'
Lp_Forward_HPAI site, cuts Lp allele	5' - GCTGGCCAAACAGTGGACCTTGGTTA -3'
Lp_Reverse	5' - ACTGGCAGAAATGTGTCAGGGCCAG -3'

6.3 AXIS LENGTH MEASUREMENTS

To compare the axis length of embryos of each genotype, embryos were stained with alcian blue to visualize the fetal cartilaginous skeleton as previously described [377]. Images were taken using a Leica S6D dissecting scope equipped with a DFC 300F camera and axis lengths were measured by drawing a line from the 2nd cervical vertebrae to the pelvic girdle using ImageJ software (National Institutes of Health, Bethesda, MD, USA). For each genotype, the axis length was taken as a ratio to the axis length of a wildtype littermate. The length of spina bifida in *Shroom3*^{+/*gt*};*Vangl2*^{+/*Lp*} and *Shroom3*^{*gt/gt*};*Vangl2*^{+/*Lp*} embryos were measured using skeleton stained embryos and taken as a ratio to the overall axis length. A minimum of four embryos per genotype were quantified.

6.4 CELL CULTURE AND TRANSFECTION

COS7 fibroblasts were maintained in DMEM supplemented with 10% fetal bovine serum, penicillin/streptomycin, and L-glutamine at 37°C and 5% CO₂. Cells were transiently transfected in suspension with 1-2µg of plasmid using Lipofectamine 2000 according to manufacturer's instructions (Invitrogen, Carlsbad, CA, USA). For immunohistochemistry, cells were plated on fibronectin coated glass cover slips at a density of 4x10⁵ cells per cover slip and allowed to grow for 18 - 24 hours before staining.

6.5 IMMUNOHISTOCHEMISTRY

Cells were washed with PBS and fixed with either -20° MeOH for 5 minutes or 4% PFA for 15 min, and stained as previously described [189]. The following antibodies were used: rabbit anti-Shroom3 (1:200, UPT132, [189]), mouse anti-myc (1:200, 9E10, Developmental Studies Hybridoma Bank, Iowa City, IA, USA), mouse anti-Flag (1:200, Sigma, St Louis, MO, USA), and Alexa 488 or 568 conjugated secondary antibodies (1:400, Invitrogen). Cells were imaged using an Olympus Fluoview 1000 confocal microscope equipped with a 40X oil immersion objective with scan speed 244 Hz (Olympus America, Center Valley, PA, USA). Two-dimensional projections were generated from z-series (0.5 µm steps) and images were processed using ImageJ software (National Institutes of Health).

6.6 CO-IMMUNOPRECIPITATION

pCS2-Shroom3L [189] and pCS2-flag-Dvl2 [299] plasmids were transiently transfected into COS7 cells and lysates were made in IP buffer (40mM Tris pH 8.0, 5mM EDTA pH 8.0, 10mM EGTA pH 8.0, 100mM NaCl, 0.5% Nonidet P-40) containing protease inhibitor cocktail (Sigma). Lysates were precleared with anti-mouse agarose beads and then incubated with mouse anti-flag antibody (Sigma) overnight at 4°C with constant rotation. Lysates were incubated with anti-mouse agarose beads while rotating for 4 hours at 4°C. The beads were washed extensively in IP buffer, collected by centrifugation, resuspended in SDS sample buffer (62.5 mM Tris-HCL, pH 6.8, 2% SDS, 10% glycerol, 50 mM dithiothreitol), and resolved on an 8% denaturing polyacrylamide gel. Proteins were transferred to a nitrocellulose membrane and detected using

rabbit anti-Shroom3 (UPT132, 1:300) or mouse anti-flag (1:1000, Sigma) primary antibodies, horseradish peroxidase-conjugated goat anti-rabbit or mouse IgG secondary antibodies (1:2,500, GE Healthcare Life Sciences, Pittsburgh, PA, USA) and ECL reagent (Thermo Fisher Scientific, Rockford, IL USA).

6.7 MOLECULAR BIOLOGY

The Flag-tagged Dvl2 constructs were a gift from Raymond Habas (Temple University, Philadelphia, PA, USA) [299]. pCS2 plasmids containing Shroom3L, Shroom3S, and myc-Shroom3S Δ SD1 constructs have been previously described [182, 191]. To generate Shroom3 deletion constructs, mShroom3 cDNA corresponding to amino acids 286-952, 286-776, 286-523, and 510-779 were cut from pCS2-Shroom3S plasmids and ligated into empty pCS3mt vectors in frame with the myc tags. To generate GST-Shroom3 286-881, the cDNA of Shroom3 encoding amino acids 286-881 was PCR amplified using primers that engineered BamHI and EcoRI sites on either side: 5'-GTAACAGGATCCCTACCTTAGATGAGAAC-3' and 5'-CGTTCCTGAATTCAAGAAACCTTCTCCAG -3' The product was digested and ligated into a pGEX-3X vector.

6.8 GST PULL DOWN

For GST-pull down experiments, pGEX-3X-Shroom3 286-881 plasmid was transformed into RIPL *E. coli* cells and protein expression was induced in log phase cell cultures with 0.5mM

isopropyl β -D-1-thiogalactopyranoside (IPTG) for 4 hours. Cells were collected by centrifugation and lysed in NETN buffer (100 mM NaCl, 1 mM EDTA, 20 mM Tris, pH 8.0, 0.05% Nonidet P-40, protease inhibitor cocktail) followed by sonication. GST-Shroom 286-881 protein and GST alone were incubated with glutathione sepharose beads (GE Healthcare Life Sciences) for 1 hr at 4°C. Beads were collected by centrifugation, washed with NETN, and added to pre-cleared lysates made from COS7 cells transiently expressing pCS2-flag-Dvl2 overnight at 4°C with constant rotation. Beads were collected, washed, and resuspended in SDS sample buffer. Proteins were resolved on an 8% denaturing polyacrylamide gel and analyzed via western blot using mouse anti-Flag (1:1,000, Sigma), horseradish peroxidase-conjugated goat anti-mouse IgG (1:2,500, GE Healthcare Life Sciences) and ECL reagent (Thermo Fisher Scientific).

6.9 MOUSE WHOLE MOUNT IMMUNOHISTOCHEMISTRY

E8.5 embryos were dissected in PBS + 0.1% FBS and processed for immunohistochemistry (IHC) (Figure 34). For Shroom3 and F-actin IHC, embryos were fixed in 4% paraformaldehyde in PBS overnight at 4°C and permeabilized in PBS + 0.5% Triton (PBT) for 30 minutes. For ZO1, Myosin IIb, Rock1, and Dvl2 IHC, embryos were fixed in freshly prepared, ice cold 80:20 Methanol:DMSO overnight at 4°C and rehydrated in 50% MeOH for 30 minutes, followed by two 30 minute washes in PBT. Non-specific antibody binding was blocked by incubating in PBS + 5% BSA + 10% heat-inactivated FBS for 1 hour. Embryos were incubated in primary antibody diluted 1:100 in block solution overnight at 4°C with rotation. Antibodies used were rabbit anti-Shroom3 (UPT132; [189]), rat anti-ZO1 (R26.4C,

Developmental Studies Hybridoma Bank), mouse anti-Myosin IIb (CMII23, Developmental Studies Hybridoma Bank), rabbit anti-Myosin IIb (Covance, Princeton, NJ, USA) rabbit anti-Rock1 (Bethyl Labs, Montgomery, TX, USA), and rabbit anti-Dvl2 (Enzo Life Sciences, Farmingdale, NY, USA). Embryos were washed in PBT 3-5 times for 30 minutes each and incubated with secondary antibodies diluted in PBT overnight at 4°C with rotation. Secondary antibodies used were Alexa 488 or 568-conjugated goat anti-rabbit, rat, or mouse (1:400, Invitrogen). TRITC-phalloidin (1:500, Sigma) was used to detect actin. Embryos were washed with PBT three times for 30 minutes each and mounted face down in 2% agarose for imaging (Figure 34). Imaging was done using a Leica TCS SP5 confocal microscope equipped with an APO L 20X/1.00 water immersion objective. Z-series (1µm steps) were collected and projections were generated using ImageJ software (NIH) (Figure 34).

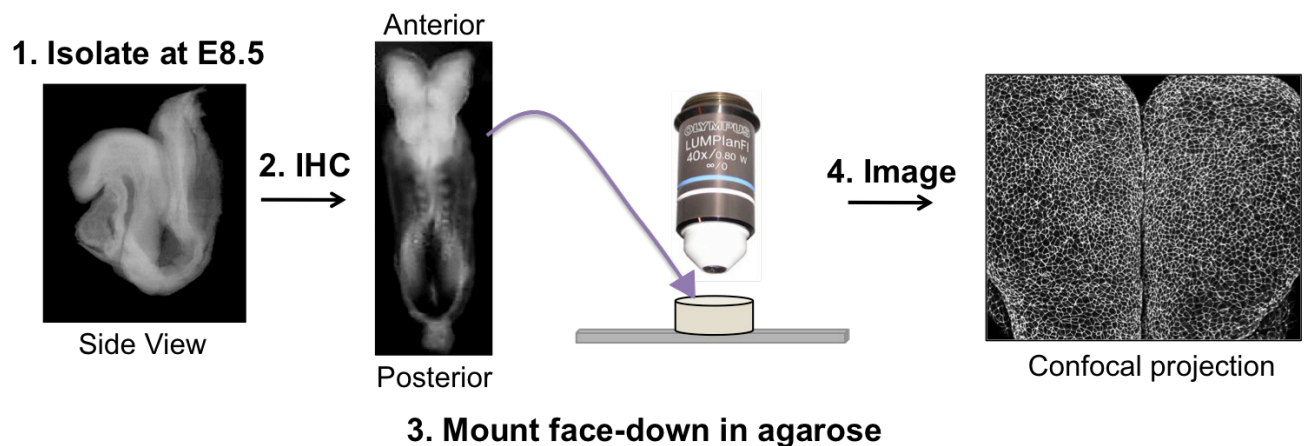


Figure 34. Whole mount immunohistochemistry methods

Embryos were isolated at E8.5, processed for immunohistochemistry (IHC), mounted face-down, and imaged using a Leica TCS SP5 confocal microscope.

6.10 PLANAR DISTRIBUTION ANALYSES

The semi-automated image segmenting program Seedwater Segmenter [372] was used to segment images to produce separate Regions of Interest (ROI) for each cell (Figure 35A). Using ImageJ software, 1-pixel wide user-drawn lines across cell junctions of subsaturated confocal projections were analyzed to determine the mean grey value and orientation relative to the mediolateral axis of the embryo (Figure 35B-D). Junctions were binned according to their angle and the fluorescence intensities in each bin were averaged. To quantify junctional versus medial F-actin fluorescence, the average fluorescence intensity was measured for regions of interest (ROIs) along the junctions at the apical surface and within ROIs medial to the apical cell junctions. For each experiment, at least 200 junctions were analyzed from each of three embryos.

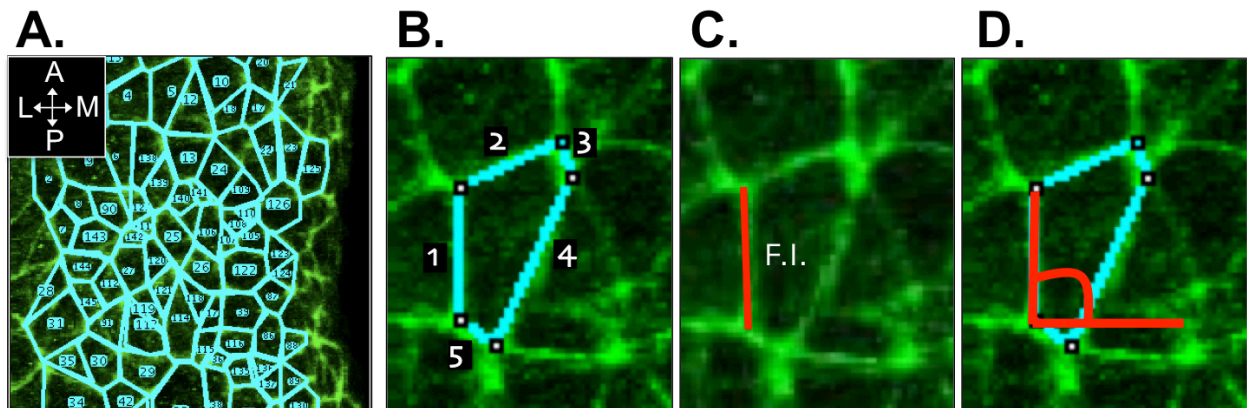


Figure 35. Fluorescence intensity measurements at cell-cell junctions

A. Regions of interest (ROIs) were generated for each cell boundary using Seedwater Segmenter. Each cell boundary was assigned a number (B) and the fluorescence intensity (C) and angle relative to the mediolateral axis (D) of each boundary was calculated using ImageJ software.

A. Cells that are linearly arranged are assigned low coordination numbers. An ROI set (**A'**) is imported into ImageJ. The coordination number of a given cell (**A''**, **yellow**) is defined as the maximum number of neighboring cells that share a vertex. The highlighted cell in **A''** shares five vertices with neighboring cells (pink dots). To calculate the coordination number of this cell, a custom macro was used in ImageJ to expand each ROI (**A'''**, **red**) to determine the number of expanded ROIs that overlap at each vertex. Each cell is assigned the maximum possible coordination number (**A''''**). **B.** Cells that are arranged into rosettes are assigned high coordination numbers.

6.12 STATISTICAL ANALYSES

All statistics were computed using Microsoft Excel software. Measures of significance were determined by two-tailed, unpaired, Student's *t*-Tests. For all graphs, error bars represent standard error of mean (\pm s.e.m.) and significant differences were determined by p-values less than 0.001.

BIBLIOGRAPHY

1. Andrew, D.J. and A.J. Ewald, *Morphogenesis of epithelial tubes: Insights into tube formation, elongation, and elaboration*. Dev Biol, 2010. **341**(1): p. 34-55.
2. St Johnston, D. and B. Sanson, *Epithelial polarity and morphogenesis*. Curr Opin Cell Biol, 2011. **23**(5): p. 540-6.
3. Cavey, M. and T. Lecuit, *Molecular bases of cell-cell junctions stability and dynamics*. Cold Spring Harb Perspect Biol, 2009. **1**(5): p. a002998.
4. Meng, W. and M. Takeichi, *Adherens junction: molecular architecture and regulation*. Cold Spring Harb Perspect Biol, 2009. **1**(6): p. a002899.
5. Schneeberger, E.E. and R.D. Lynch, *The tight junction: a multifunctional complex*. Am J Physiol Cell Physiol, 2004. **286**(6): p. C1213-28.
6. Anderson, J.M., *Molecular structure of tight junctions and their role in epithelial transport*. News Physiol Sci, 2001. **16**: p. 126-30.
7. Miyaguchi, K., *Ultrastructure of the zonula adherens revealed by rapid-freeze deep-etching*. J Struct Biol, 2000. **132**(3): p. 169-78.
8. Hartsock, A. and W.J. Nelson, *Adherens and tight junctions: structure, function and connections to the actin cytoskeleton*. Biochim Biophys Acta, 2008. **1778**(3): p. 660-9.
9. Furuse, M., et al., *Claudin-1 and -2: novel integral membrane proteins localizing at tight junctions with no sequence similarity to occludin*. J Cell Biol, 1998. **141**(7): p. 1539-50.
10. Furuse, M., et al., *Occludin: a novel integral membrane protein localizing at tight junctions*. J Cell Biol, 1993. **123**(6 Pt 2): p. 1777-88.
11. Martin-Padura, I., et al., *Junctional adhesion molecule, a novel member of the immunoglobulin superfamily that distributes at intercellular junctions and modulates monocyte transmigration*. J Cell Biol, 1998. **142**(1): p. 117-27.
12. Haskins, J., et al., *ZO-3, a novel member of the MAGUK protein family found at the tight junction, interacts with ZO-1 and occludin*. J Cell Biol, 1998. **141**(1): p. 199-208.
13. Jesaitis, L.A. and D.A. Goodenough, *Molecular characterization and tissue distribution of ZO-2, a tight junction protein homologous to ZO-1 and the Drosophila discs-large tumor suppressor protein*. J Cell Biol, 1994. **124**(6): p. 949-61.
14. Stevenson, B.R., et al., *Identification of ZO-1: a high molecular weight polypeptide associated with the tight junction (zonula occludens) in a variety of epithelia*. J Cell Biol, 1986. **103**(3): p. 755-66.
15. Fanning, A.S., et al., *The tight junction protein ZO-1 establishes a link between the transmembrane protein occludin and the actin cytoskeleton*. J Biol Chem, 1998. **273**(45): p. 29745-53.
16. Itoh, M., et al., *Direct binding of three tight junction-associated MAGUKs, ZO-1, ZO-2, and ZO-3, with the COOH termini of claudins*. J Cell Biol, 1999. **147**(6): p. 1351-63.

17. Itoh, M., K. Morita, and S. Tsukita, *Characterization of ZO-2 as a MAGUK family member associated with tight as well as adherens junctions with a binding affinity to occludin and alpha catenin*. J Biol Chem, 1999. **274**(9): p. 5981-6.
18. Wittchen, E.S., J. Haskins, and B.R. Stevenson, *Protein interactions at the tight junction. Actin has multiple binding partners, and ZO-1 forms independent complexes with ZO-2 and ZO-3*. J Biol Chem, 1999. **274**(49): p. 35179-85.
19. Yamamoto, T., et al., *The Ras target AF-6 interacts with ZO-1 and serves as a peripheral component of tight junctions in epithelial cells*. J Cell Biol, 1997. **139**(3): p. 785-95.
20. Roh, M.H., et al., *The carboxyl terminus of zona occludens-3 binds and recruits a mammalian homologue of discs lost to tight junctions*. J Biol Chem, 2002. **277**(30): p. 27501-9.
21. Sotillos, S., et al., *DaPKC-dependent phosphorylation of Crumbs is required for epithelial cell polarity in Drosophila*. J Cell Biol, 2004. **166**(4): p. 549-57.
22. Wodarz, A., et al., *Expression of crumbs confers apical character on plasma membrane domains of ectodermal epithelia of Drosophila*. Cell, 1995. **82**(1): p. 67-76.
23. Chalmers, A.D., et al., *aPKC, Crumbs3 and Lgl2 control apicobasal polarity in early vertebrate development*. Development, 2005. **132**(5): p. 977-86.
24. Itoh, M., et al., *Junctional adhesion molecule (JAM) binds to PAR-3: a possible mechanism for the recruitment of PAR-3 to tight junctions*. J Cell Biol, 2001. **154**(3): p. 491-7.
25. Tanentzapf, G. and U. Tepass, *Interactions between the crumbs, lethal giant larvae and bazooka pathways in epithelial polarization*. Nat Cell Biol, 2003. **5**(1): p. 46-52.
26. Takeichi, M., *The cadherins: cell-cell adhesion molecules controlling animal morphogenesis*. Development, 1988. **102**(4): p. 639-55.
27. Overduin, M., et al., *Solution structure of the epithelial cadherin domain responsible for selective cell adhesion*. Science, 1995. **267**(5196): p. 386-9.
28. Pokutta, S., et al., *Conformational changes of the recombinant extracellular domain of E-cadherin upon calcium binding*. Eur J Biochem, 1994. **223**(3): p. 1019-26.
29. Kobiela, A. and E. Fuchs, *Alpha-catenin: at the junction of intercellular adhesion and actin dynamics*. Nat Rev Mol Cell Biol, 2004. **5**(8): p. 614-25.
30. Yap, A.S., M.S. Crampton, and J. Hardin, *Making and breaking contacts: the cellular biology of cadherin regulation*. Curr Opin Cell Biol, 2007. **19**(5): p. 508-14.
31. Kasza, K.E. and J.A. Zallen, *Dynamics and regulation of contractile actin-myosin networks in morphogenesis*. Curr Opin Cell Biol, 2011. **23**(1): p. 30-8.
32. Salbreux, G., G. Charras, and E. Paluch, *Actin cortex mechanics and cellular morphogenesis*. Trends Cell Biol, 2012. **22**(10): p. 536-45.
33. Wear, M.A., D.A. Schafer, and J.A. Cooper, *Actin dynamics: assembly and disassembly of actin networks*. Curr Biol, 2000. **10**(24): p. R891-5.
34. Bray, D. and J.G. White, *Cortical flow in animal cells*. Science, 1988. **239**(4842): p. 883-8.
35. Pollard, T.D. and G.G. Borisy, *Cellular motility driven by assembly and disassembly of actin filaments*. Cell, 2003. **112**(4): p. 453-65.
36. Stewart, M.P., et al., *Hydrostatic pressure and the actomyosin cortex drive mitotic cell rounding*. Nature, 2011. **469**(7329): p. 226-30.

37. Zhou, J., H.Y. Kim, and L.A. Davidson, *Actomyosin stiffens the vertebrate embryo during crucial stages of elongation and neural tube closure*. *Development*, 2009. **136**(4): p. 677-88.
38. Borisy, G.G. and T.M. Svitkina, *Actin machinery: pushing the envelope*. *Curr Opin Cell Biol*, 2000. **12**(1): p. 104-12.
39. Holmes, K.C., et al., *Atomic model of the actin filament*. *Nature*, 1990. **347**(6288): p. 44-9.
40. Tooley, A.J., et al., *Amoeboid T lymphocytes require the septin cytoskeleton for cortical integrity and persistent motility*. *Nat Cell Biol*, 2009. **11**(1): p. 17-26.
41. Harris, T.J. and U. Tepass, *Adherens junctions: from molecules to morphogenesis*. *Nat Rev Mol Cell Biol*, 2010. **11**(7): p. 502-14.
42. Nishimura, T. and M. Takeichi, *Remodeling of the adherens junctions during morphogenesis*. *Curr Top Dev Biol*, 2009. **89**: p. 33-54.
43. Cooper, J.A. and D.A. Schafer, *Control of actin assembly and disassembly at filament ends*. *Curr Opin Cell Biol*, 2000. **12**(1): p. 97-103.
44. Uribe, R. and D. Jay, *A review of actin binding proteins: new perspectives*. *Mol Biol Rep*, 2009. **36**(1): p. 121-5.
45. Hartwig, J.H., J. Tyler, and T.P. Stossel, *Actin-binding protein promotes the bipolar and perpendicular branching of actin filaments*. *J Cell Biol*, 1980. **87**(3 Pt 1): p. 841-8.
46. Stossel, T.P., et al., *Filamins as integrators of cell mechanics and signalling*. *Nat Rev Mol Cell Biol*, 2001. **2**(2): p. 138-45.
47. Small, J.V., et al., *The lamellipodium: where motility begins*. *Trends Cell Biol*, 2002. **12**(3): p. 112-20.
48. Bear, J.E., et al., *Antagonism between Ena/VASP proteins and actin filament capping regulates fibroblast motility*. *Cell*, 2002. **109**(4): p. 509-21.
49. Kobiela, A., H.A. Pasolli, and E. Fuchs, *Mammalian formin-1 participates in adherens junctions and polymerization of linear actin cables*. *Nat Cell Biol*, 2004. **6**(1): p. 21-30.
50. Meyer, R.K. and U. Aebi, *Bundling of actin filaments by alpha-actinin depends on its molecular length*. *J Cell Biol*, 1990. **110**(6): p. 2013-24.
51. Lazarides, E., *Actin, alpha-actinin, and tropomyosin interaction in the structural organization of actin filaments in nonmuscle cells*. *J Cell Biol*, 1976. **68**(2): p. 202-19.
52. Lo, S.H., et al., *Interactions of tensin with actin and identification of its three distinct actin-binding domains*. *J Cell Biol*, 1994. **125**(5): p. 1067-75.
53. Andre, E., et al., *Severin, gelsolin, and villin share a homologous sequence in regions presumed to contain F-actin severing domains*. *J Biol Chem*, 1988. **263**(2): p. 722-7.
54. Lappalainen, P. and D.G. Drubin, *Cofilin promotes rapid actin filament turnover in vivo*. *Nature*, 1997. **388**(6637): p. 78-82.
55. Krendel, M. and M.S. Mooseker, *Myosins: tails (and heads) of functional diversity*. *Physiology (Bethesda)*, 2005. **20**: p. 239-51.
56. Maravillas-Montero, J.L. and L. Santos-Argumedo, *The myosin family: unconventional roles of actin-dependent molecular motors in immune cells*. *J Leukoc Biol*, 2012. **91**(1): p. 35-46.
57. Conti, M.A. and R.S. Adelstein, *Nonmuscle myosin II moves in new directions*. *J Cell Sci*, 2008. **121**(Pt 1): p. 11-8.
58. Vicente-Manzanares, M., et al., *Non-muscle myosin II takes centre stage in cell adhesion and migration*. *Nat Rev Mol Cell Biol*, 2009. **10**(11): p. 778-90.

59. Niederman, R. and T.D. Pollard, *Human platelet myosin. II. In vitro assembly and structure of myosin filaments*. J Cell Biol, 1975. **67**(1): p. 72-92.
60. Verkhovsky, A.B., T.M. Svitkina, and G.G. Borisy, *Myosin II filament assemblies in the active lamella of fibroblasts: their morphogenesis and role in the formation of actin filament bundles*. J Cell Biol, 1995. **131**(4): p. 989-1002.
61. Umemoto, S., A.R. Bengur, and J.R. Sellers, *Effect of multiple phosphorylations of smooth muscle and cytoplasmic myosins on movement in an in vitro motility assay*. J Biol Chem, 1989. **264**(3): p. 1431-6.
62. Adelstein, R.S. and M.A. Conti, *Phosphorylation of platelet myosin increases actin-activated myosin ATPase activity*. Nature, 1975. **256**(5518): p. 597-8.
63. Amano, M., et al., *Phosphorylation and activation of myosin by Rho-associated kinase (Rho-kinase)*. J Biol Chem, 1996. **271**(34): p. 20246-9.
64. Ito, M., et al., *Myosin phosphatase: structure, regulation and function*. Mol Cell Biochem, 2004. **259**(1-2): p. 197-209.
65. Kovacs, M., et al., *Functional divergence of human cytoplasmic myosin II: kinetic characterization of the non-muscle IIA isoform*. J Biol Chem, 2003. **278**(40): p. 38132-40.
66. Wang, A., et al., *Distinct and redundant roles of the non-muscle myosin II isoforms and functional domains*. Biochem Soc Trans, 2011. **39**(5): p. 1131-5.
67. Wang, F., et al., *Kinetic mechanism of non-muscle myosin IIB: functional adaptations for tension generation and maintenance*. J Biol Chem, 2003. **278**(30): p. 27439-48.
68. Amano, M., M. Nakayama, and K. Kaibuchi, *Rho-kinase/ROCK: A key regulator of the cytoskeleton and cell polarity*. Cytoskeleton (Hoboken), 2010. **67**(9): p. 545-54.
69. Kimura, K., et al., *Regulation of myosin phosphatase by Rho and Rho-associated kinase (Rho-kinase)*. Science, 1996. **273**(5272): p. 245-8.
70. Fujisawa, K., et al., *Identification of the Rho-binding domain of p160ROCK, a Rho-associated coiled-coil containing protein kinase*. J Biol Chem, 1996. **271**(38): p. 23022-8.
71. Leung, T., et al., *The p160 RhoA-binding kinase ROK alpha is a member of a kinase family and is involved in the reorganization of the cytoskeleton*. Mol Cell Biol, 1996. **16**(10): p. 5313-27.
72. Matsui, T., et al., *Rho-associated kinase, a novel serine/threonine kinase, as a putative target for small GTP binding protein Rho*. EMBO J, 1996. **15**(9): p. 2208-16.
73. Mohan, S., et al., *Structure of a highly conserved domain of Rock1 required for Shroom-mediated regulation of cell morphology*. PLoS One, 2013. **8**(12): p. e81075.
74. Amano, M., et al., *The COOH terminus of Rho-kinase negatively regulates rho-kinase activity*. J Biol Chem, 1999. **274**(45): p. 32418-24.
75. Ishizaki, T., et al., *The small GTP-binding protein Rho binds to and activates a 160 kDa Ser/Thr protein kinase homologous to myotonic dystrophy kinase*. EMBO J, 1996. **15**(8): p. 1885-93.
76. Citi, S., et al., *Regulation of small GTPases at epithelial cell-cell junctions*. Mol Membr Biol, 2011. **28**(7-8): p. 427-44.
77. Spiering, D. and L. Hodgson, *Dynamics of the Rho-family small GTPases in actin regulation and motility*. Cell Adh Migr, 2011. **5**(2): p. 170-80.
78. Gibbs, J.B., et al., *Modulation of guanine nucleotides bound to Ras in NIH3T3 cells by oncogenes, growth factors, and the GTPase activating protein (GAP)*. J Biol Chem, 1990. **265**(33): p. 20437-42.

79. Rossman, K.L., C.J. Der, and J. Sondek, *GEF means go: turning on RHO GTPases with guanine nucleotide-exchange factors*. Nat Rev Mol Cell Biol, 2005. **6**(2): p. 167-80.
80. Coleman, M.L., et al., *Membrane blebbing during apoptosis results from caspase-mediated activation of ROCK I*. Nat Cell Biol, 2001. **3**(4): p. 339-45.
81. Riento, K., et al., *RhoE binds to ROCK I and inhibits downstream signaling*. Mol Cell Biol, 2003. **23**(12): p. 4219-29.
82. Sebbagh, M., et al., *Direct cleavage of ROCK II by granzyme B induces target cell membrane blebbing in a caspase-independent manner*. J Exp Med, 2005. **201**(3): p. 465-71.
83. Ward, Y., et al., *The GTP binding proteins Gem and Rad are negative regulators of the Rho-Rho kinase pathway*. J Cell Biol, 2002. **157**(2): p. 291-302.
84. Bertet, C., M. Rauzi, and T. Lecuit, *Repression of Wasp by JAK/STAT signalling inhibits medial actomyosin network assembly and apical cell constriction in intercalating epithelial cells*. Development, 2009. **136**(24): p. 4199-212.
85. Bertet, C., L. Sulak, and T. Lecuit, *Myosin-dependent junction remodelling controls planar cell intercalation and axis elongation*. Nature, 2004. **429**(6992): p. 667-71.
86. Fernandez-Gonzalez, R., et al., *Myosin II dynamics are regulated by tension in intercalating cells*. Dev Cell, 2009. **17**(5): p. 736-43.
87. Heller, E., et al., *Forces generated by cell intercalation tow epidermal sheets in mammalian tissue morphogenesis*. Dev Cell, 2014. **28**(6): p. 617-32.
88. Martin, A.C., M. Kaschube, and E.F. Wieschaus, *Pulsed contractions of an actin-myosin network drive apical constriction*. Nature, 2009. **457**(7228): p. 495-9.
89. Mason, F.M., M. Tworoger, and A.C. Martin, *Apical domain polarization localizes actin-myosin activity to drive ratchet-like apical constriction*. Nat Cell Biol, 2013. **15**(8): p. 926-36.
90. Tamada, M., et al., *Two distinct modes of myosin assembly and dynamics during epithelial wound closure*. J Cell Biol, 2007. **176**(1): p. 27-33.
91. Parsons, J.T., A.R. Horwitz, and M.A. Schwartz, *Cell adhesion: integrating cytoskeletal dynamics and cellular tension*. Nat Rev Mol Cell Biol, 2010. **11**(9): p. 633-43.
92. Martin, A.C. and B. Goldstein, *Apical constriction: themes and variations on a cellular mechanism driving morphogenesis*. Development, 2014. **141**(10): p. 1987-98.
93. Baker, P.C. and T.E. Schroeder, *Cytoplasmic filaments and morphogenetic movement in the amphibian neural tube*. Dev Biol, 1967. **15**(5): p. 432-50.
94. Owaribe, K. and H. Masuda, *Isolation and characterization of circumferential microfilament bundles from retinal pigmented epithelial cells*. J Cell Biol, 1982. **95**(1): p. 310-5.
95. Pilot, F. and T. Lecuit, *Compartmentalized morphogenesis in epithelia: from cell to tissue shape*. Dev Dyn, 2005. **232**(3): p. 685-94.
96. Barrett, K., M. Leptin, and J. Settleman, *The Rho GTPase and a putative RhoGEF mediate a signaling pathway for the cell shape changes in Drosophila gastrulation*. Cell, 1997. **91**(7): p. 905-15.
97. Hacker, U. and N. Perrimon, *DRhoGEF2 encodes a member of the Dbl family of oncogenes and controls cell shape changes during gastrulation in Drosophila*. Genes Dev, 1998. **12**(2): p. 274-84.
98. Nishimura, T., H. Honda, and M. Takeichi, *Planar cell polarity links axes of spatial dynamics in neural-tube closure*. Cell, 2012. **149**(5): p. 1084-97.

99. Plageman, T.F., Jr., et al., *A Trio-RhoA-Shroom3 pathway is required for apical constriction and epithelial invagination*. *Development*, 2011. **138**(23): p. 5177-88.
100. Kam, Z., et al., *Drosophila gastrulation: analysis of cell shape changes in living embryos by three-dimensional fluorescence microscopy*. *Development*, 1991. **112**(2): p. 365-70.
101. Sweeton, D., et al., *Gastrulation in Drosophila: the formation of the ventral furrow and posterior midgut invaginations*. *Development*, 1991. **112**(3): p. 775-89.
102. Manning, A.J., et al., *Regulation of epithelial morphogenesis by the G protein-coupled receptor mist and its ligand fog*. *Sci Signal*, 2013. **6**(301): p. ra98.
103. Homem, C.C. and M. Peifer, *Diaphanous regulates myosin and adherens junctions to control cell contractility and protrusive behavior during morphogenesis*. *Development*, 2008. **135**(6): p. 1005-18.
104. Costa, M., E.T. Wilson, and E. Wieschaus, *A putative cell signal encoded by the folded gastrulation gene coordinates cell shape changes during Drosophila gastrulation*. *Cell*, 1994. **76**(6): p. 1075-89.
105. Dawes-Hoang, R.E., et al., *folded gastrulation, cell shape change and the control of myosin localization*. *Development*, 2005. **132**(18): p. 4165-78.
106. Kolsch, V., et al., *Control of Drosophila gastrulation by apical localization of adherens junctions and RhoGEF2*. *Science*, 2007. **315**(5810): p. 384-6.
107. Davidson, L.A., *No strings attached: new insights into epithelial morphogenesis*. *BMC Biol*, 2012. **10**: p. 105.
108. Keller, R., *Shaping the vertebrate body plan by polarized embryonic cell movements*. *Science*, 2002. **298**(5600): p. 1950-4.
109. Blankenship, J.T., et al., *Multicellular rosette formation links planar cell polarity to tissue morphogenesis*. *Dev Cell*, 2006. **11**(4): p. 459-70.
110. Elul, T. and R. Keller, *Monopolar protrusive activity: a new morphogenic cell behavior in the neural plate dependent on vertical interactions with the mesoderm in Xenopus*. *Dev Biol*, 2000. **224**(1): p. 3-19.
111. Ettensohn, C.A., *Gastrulation in the sea urchin embryo is accompanied by the rearrangement of invaginating epithelial cells*. *Dev Biol*, 1985. **112**(2): p. 383-90.
112. Glickman, N.S., et al., *Shaping the zebrafish notochord*. *Development*, 2003. **130**(5): p. 873-87.
113. Heisenberg, C.P., et al., *Silberblick/Wnt11 mediates convergent extension movements during zebrafish gastrulation*. *Nature*, 2000. **405**(6782): p. 76-81.
114. Irvine, K.D. and E. Wieschaus, *Cell intercalation during Drosophila germband extension and its regulation by pair-rule segmentation genes*. *Development*, 1994. **120**(4): p. 827-41.
115. Munro, E.M. and G.M. Odell, *Polarized basolateral cell motility underlies invagination and convergent extension of the ascidian notochord*. *Development*, 2002. **129**(1): p. 13-24.
116. Shih, J. and R. Keller, *Cell motility driving mediolateral intercalation in explants of Xenopus laevis*. *Development*, 1992. **116**(4): p. 901-14.
117. Warga, R.M. and C.B. Kimmel, *Cell movements during epiboly and gastrulation in zebrafish*. *Development*, 1990. **108**(4): p. 569-80.
118. Williams-Masson, E.M., et al., *The cellular mechanism of epithelial rearrangement during morphogenesis of the Caenorhabditis elegans dorsal hypodermis*. *Dev Biol*, 1998. **204**(1): p. 263-76.

119. Yamanaka, Y., et al., *Live imaging and genetic analysis of mouse notochord formation reveals regional morphogenetic mechanisms*. *Dev Cell*, 2007. **13**(6): p. 884-96.
120. Yen, W.W., et al., *PTK7 is essential for polarized cell motility and convergent extension during mouse gastrulation*. *Development*, 2009. **136**(12): p. 2039-48.
121. Yin, C., et al., *Cooperation of polarized cell intercalations drives convergence and extension of presomitic mesoderm during zebrafish gastrulation*. *J Cell Biol*, 2008. **180**(1): p. 221-32.
122. Zallen, J.A. and E. Wieschaus, *Patterned gene expression directs bipolar planar polarity in Drosophila*. *Dev Cell*, 2004. **6**(3): p. 343-55.
123. Caussinus, E., J. Colombelli, and M. Affolter, *Tip-cell migration controls stalk-cell intercalation during Drosophila tracheal tube elongation*. *Curr Biol*, 2008. **18**(22): p. 1727-34.
124. Davidson, L.A. and R.E. Keller, *Neural tube closure in Xenopus laevis involves medial migration, directed protrusive activity, cell intercalation and convergent extension*. *Development*, 1999. **126**(20): p. 4547-56.
125. Harrington, M.J., K. Chalasani, and R. Brewster, *Cellular mechanisms of posterior neural tube morphogenesis in the zebrafish*. *Dev Dyn*, 2010. **239**(3): p. 747-62.
126. Keller, R., J. Shih, and A. Sater, *The cellular basis of the convergence and extension of the Xenopus neural plate*. *Dev Dyn*, 1992. **193**(3): p. 199-217.
127. Lengyel, J.A. and D.D. Iwaki, *It takes guts: the Drosophila hindgut as a model system for organogenesis*. *Dev Biol*, 2002. **243**(1): p. 1-19.
128. Lienkamp, S.S., et al., *Vertebrate kidney tubules elongate using a planar cell polarity-dependent, rosette-based mechanism of convergent extension*. *Nat Genet*, 2012. **44**(12): p. 1382-7.
129. Keller, R., et al., *Mechanisms of convergence and extension by cell intercalation*. *Philos Trans R Soc Lond B Biol Sci*, 2000. **355**(1399): p. 897-922.
130. Simoes Sde, M., et al., *Rho-kinase directs Bazooka/Par-3 planar polarity during Drosophila axis elongation*. *Dev Cell*, 2010. **19**(3): p. 377-88.
131. Simoes Sde, M., A. Mainieri, and J.A. Zallen, *Rho GTPase and Shroom direct planar polarized actomyosin contractility during convergent extension*. *J Cell Biol*, 2014. **204**(4): p. 575-89.
132. Tamada, M., D.L. Farrell, and J.A. Zallen, *Abl regulates planar polarized junctional dynamics through beta-catenin tyrosine phosphorylation*. *Dev Cell*, 2012. **22**(2): p. 309-19.
133. Levayer, R., A. Pelissier-Monier, and T. Lecuit, *Spatial regulation of Dia and Myosin-II by RhoGEF2 controls initiation of E-cadherin endocytosis during epithelial morphogenesis*. *Nat Cell Biol*, 2011. **13**(5): p. 529-40.
134. Williams, M., et al., *Distinct apical and basolateral mechanisms drive planar cell polarity-dependent convergent extension of the mouse neural plate*. *Dev Cell*, 2014. **29**(1): p. 34-46.
135. Nishimura, T. and M. Takeichi, *Shroom3-mediated recruitment of Rho kinases to the apical cell junctions regulates epithelial and neuroepithelial planar remodeling*. *Development*, 2008. **135**(8): p. 1493-502.
136. Copp, A.J. and N.D. Greene, *Genetics and development of neural tube defects*. *J Pathol*, 2010. **220**(2): p. 217-30.

137. Copp, A.J., N.D. Greene, and J.N. Murdoch, *The genetic basis of mammalian neurulation*. Nat Rev Genet, 2003. **4**(10): p. 784-93.
138. Copp, A.J., P. Stanier, and N.D. Greene, *Neural tube defects: recent advances, unsolved questions, and controversies*. Lancet Neurol, 2013. **12**(8): p. 799-810.
139. Greene, N.D. and A.J. Copp, *Development of the vertebrate central nervous system: formation of the neural tube*. Prenat Diagn, 2009. **29**(4): p. 303-11.
140. Yamaguchi, Y., et al., *Live imaging of apoptosis in a novel transgenic mouse highlights its role in neural tube closure*. J Cell Biol, 2011. **195**(6): p. 1047-60.
141. Massarwa, R. and L. Niswander, *In toto live imaging of mouse morphogenesis and new insights into neural tube closure*. Development, 2013. **140**(1): p. 226-36.
142. Blom, H.J., et al., *Neural tube defects and folate: case far from closed*. Nat Rev Neurosci, 2006. **7**(9): p. 724-31.
143. Juriloff, D.M., et al., *Normal mouse strains differ in the site of initiation of closure of the cranial neural tube*. Teratology, 1991. **44**(2): p. 225-33.
144. Schoenwolf, G.C., *Shaping and bending of the avian neuroepithelium: morphometric analyses*. Dev Biol, 1985. **109**(1): p. 127-39.
145. Van Straaten, H.W., et al., *Neural tube closure in the chick embryo is multiphasic*. Dev Dyn, 1996. **207**(3): p. 309-18.
146. Rolo, A., P. Skoglund, and R. Keller, *Morphogenetic movements driving neural tube closure in Xenopus require myosin IIB*. Dev Biol, 2009. **327**(2): p. 327-38.
147. Lowery, L.A. and H. Sive, *Strategies of vertebrate neurulation and a re-evaluation of teleost neural tube formation*. Mech Dev, 2004. **121**(10): p. 1189-97.
148. Pierpont, M.E., et al., *Genetic basis for congenital heart defects: current knowledge: a scientific statement from the American Heart Association Congenital Cardiac Defects Committee, Council on Cardiovascular Disease in the Young: endorsed by the American Academy of Pediatrics*. Circulation, 2007. **115**(23): p. 3015-38.
149. Mitchell, L.E., *Epidemiology of neural tube defects*. Am J Med Genet C Semin Med Genet, 2005. **135C**(1): p. 88-94.
150. Stiefel, D., et al., *Tethering of the spinal cord in mouse fetuses and neonates with spina bifida*. J Neurosurg, 2003. **99**(2 Suppl): p. 206-13.
151. Cai, C. and O. Shi, *Genetic evidence in planar cell polarity signaling pathway in human neural tube defects*. Front Med, 2014. **8**(1): p. 68-78.
152. Alwan, S., et al., *Use of selective serotonin-reuptake inhibitors in pregnancy and the risk of birth defects*. N Engl J Med, 2007. **356**(26): p. 2684-92.
153. Brender, J.D., et al., *Maternal pesticide exposure and neural tube defects in Mexican Americans*. Ann Epidemiol, 2010. **20**(1): p. 16-22.
154. Grewal, J., et al., *Neural tube defects: an analysis of neighbourhood- and individual-level socio-economic characteristics*. Paediatr Perinat Epidemiol, 2009. **23**(2): p. 116-24.
155. Gurvich, N., et al., *Association of valproate-induced teratogenesis with histone deacetylase inhibition in vivo*. FASEB J, 2005. **19**(9): p. 1166-8.
156. Loeken, M.R., *Current perspectives on the causes of neural tube defects resulting from diabetic pregnancy*. Am J Med Genet C Semin Med Genet, 2005. **135C**(1): p. 77-87.
157. Moretti, M.E., et al., *Maternal hyperthermia and the risk for neural tube defects in offspring: systematic review and meta-analysis*. Epidemiology, 2005. **16**(2): p. 216-9.

158. Njamnshi, A.K., et al., *Neural tube defects are rare among black Americans but not in sub-Saharan black Africans: the case of Yaounde - Cameroon*. J Neurol Sci, 2008. **270**(1-2): p. 13-7.
159. Pitkin, R.M., *Folate and neural tube defects*. Am J Clin Nutr, 2007. **85**(1): p. 285S-288S.
160. Ray, J.G., et al., *Greater maternal weight and the ongoing risk of neural tube defects after folic acid flour fortification*. Obstet Gynecol, 2005. **105**(2): p. 261-5.
161. Vieira, A.R. and S. Castillo Taucher, [*Maternal age and neural tube defects: evidence for a greater effect in spina bifida than in anencephaly*]. Rev Med Chil, 2005. **133**(1): p. 62-70.
162. Leck, I., *Causation of neural tube defects: clues from epidemiology*. Br Med Bull, 1974. **30**(2): p. 158-63.
163. Detrait, E.R., et al., *Human neural tube defects: developmental biology, epidemiology, and genetics*. Neurotoxicol Teratol, 2005. **27**(3): p. 515-24.
164. Risch, N., *Linkage strategies for genetically complex traits. I. Multilocus models*. Am J Hum Genet, 1990. **46**(2): p. 222-8.
165. Kibar, Z., V. Capra, and P. Gros, *Toward understanding the genetic basis of neural tube defects*. Clin Genet, 2007. **71**(4): p. 295-310.
166. Allache, R., et al., *Role of the planar cell polarity gene CELSR1 in neural tube defects and caudal agenesis*. Birth Defects Res A Clin Mol Teratol, 2012. **94**(3): p. 176-81.
167. Robinson, A., et al., *Mutations in the planar cell polarity genes CELSR1 and SCRIB are associated with the severe neural tube defect craniorachischisis*. Hum Mutat, 2012. **33**(2): p. 440-7.
168. Harris, M.J. and D.M. Juriloff, *An update to the list of mouse mutants with neural tube closure defects and advances toward a complete genetic perspective of neural tube closure*. Birth Defects Res A Clin Mol Teratol, 2010. **88**(8): p. 653-69.
169. Harris, M.J. and D.M. Juriloff, *Mouse mutants with neural tube closure defects and their role in understanding human neural tube defects*. Birth Defects Res A Clin Mol Teratol, 2007. **79**(3): p. 187-210.
170. Zohn, I.E., *Mouse as a model for multifactorial inheritance of neural tube defects*. Birth Defects Res C Embryo Today, 2012. **96**(2): p. 193-205.
171. Chen, Z.F. and R.R. Behringer, *twist is required in head mesenchyme for cranial neural tube morphogenesis*. Genes Dev, 1995. **9**(6): p. 686-99.
172. Lakhwani, S., P. Garcia-Sanz, and M. Vallejo, *Alx3-deficient mice exhibit folic acid-resistant craniofacial midline and neural tube closure defects*. Dev Biol, 2010. **344**(2): p. 869-80.
173. Zhao, Q., R.R. Behringer, and B. de Crombrughe, *Prenatal folic acid treatment suppresses acrania and meroanencephaly in mice mutant for the Cart1 homeobox gene*. Nat Genet, 1996. **13**(3): p. 275-83.
174. Zohn, I.E., K.V. Anderson, and L. Niswander, *The Hectd1 ubiquitin ligase is required for development of the head mesenchyme and neural tube closure*. Dev Biol, 2007. **306**(1): p. 208-21.
175. Ybot-Gonzalez, P. and A.J. Copp, *Bending of the neural plate during mouse spinal neurulation is independent of actin microfilaments*. Dev Dyn, 1999. **215**(3): p. 273-83.
176. Morriss-Kay, G. and F. Tuckett, *The role of microfilaments in cranial neurulation in rat embryos: effects of short-term exposure to cytochalasin D*. J Embryol Exp Morphol, 1985. **88**: p. 333-48.

177. Schoenwolf, G.C., D. Folsom, and A. Moe, *A reexamination of the role of microfilaments in neurulation in the chick embryo*. *Anat Rec*, 1988. **220**(1): p. 87-102.
178. Gurniak, C.B., E. Perlas, and W. Witke, *The actin depolymerizing factor n-cofilin is essential for neural tube morphogenesis and neural crest cell migration*. *Dev Biol*, 2005. **278**(1): p. 231-41.
179. Lanier, L.M., et al., *Mena is required for neurulation and commissure formation*. *Neuron*, 1999. **22**(2): p. 313-25.
180. Kinoshita, N., et al., *Apical accumulation of Rho in the neural plate is important for neural plate cell shape change and neural tube formation*. *Mol Biol Cell*, 2008. **19**(5): p. 2289-99.
181. Haigo, S.L., et al., *Shroom induces apical constriction and is required for hinge point formation during neural tube closure*. *Curr Biol*, 2003. **13**(24): p. 2125-37.
182. Hildebrand, J.D. and P. Soriano, *Shroom, a PDZ domain-containing actin-binding protein, is required for neural tube morphogenesis in mice*. *Cell*, 1999. **99**(5): p. 485-97.
183. Bolinger, C., et al., *Specific isoforms of drosophila shroom define spatial requirements for the induction of apical constriction*. *Dev Dyn*, 2010. **239**(7): p. 2078-93.
184. Chung, M.I., et al., *Direct activation of Shroom3 transcription by Pitx proteins drives epithelial morphogenesis in the developing gut*. *Development*, 2010. **137**(8): p. 1339-49.
185. Ernst, S., et al., *Shroom3 is required downstream of FGF signalling to mediate proneuromast assembly in zebrafish*. *Development*, 2012. **139**(24): p. 4571-81.
186. Plageman, T.F., Jr., et al., *Pax6-dependent Shroom3 expression regulates apical constriction during lens placode invagination*. *Development*, 2010. **137**(3): p. 405-15.
187. Plageman, T.F., Jr., et al., *Shroom3 and a Pitx2-N-cadherin pathway function cooperatively to generate asymmetric cell shape changes during gut morphogenesis*. *Dev Biol*, 2011. **357**(1): p. 227-34.
188. Grosse, A.S., et al., *Cell dynamics in fetal intestinal epithelium: implications for intestinal growth and morphogenesis*. *Development*, 2011. **138**(20): p. 4423-32.
189. Hildebrand, J.D., *Shroom regulates epithelial cell shape via the apical positioning of an actomyosin network*. *J Cell Sci*, 2005. **118**(Pt 22): p. 5191-203.
190. Lee, C., H.M. Scherr, and J.B. Wallingford, *Shroom family proteins regulate gamma-tubulin distribution and microtubule architecture during epithelial cell shape change*. *Development*, 2007. **134**(7): p. 1431-41.
191. Dietz, M.L., et al., *Differential actin-dependent localization modulates the evolutionarily conserved activity of Shroom family proteins*. *J Biol Chem*, 2006. **281**(29): p. 20542-54.
192. Mohan, S., et al., *Structure of Shroom domain 2 reveals a three-segmented coiled-coil required for dimerization, Rock binding, and apical constriction*. *Mol Biol Cell*, 2012. **23**(11): p. 2131-42.
193. Brouns, M.R., et al., *The adhesion signaling molecule p190 RhoGAP is required for morphogenetic processes in neural development*. *Development*, 2000. **127**(22): p. 4891-903.
194. Lee, J.D., et al., *The FERM protein Epb4.115 is required for organization of the neural plate and for the epithelial-mesenchymal transition at the primitive streak of the mouse embryo*. *Development*, 2007. **134**(11): p. 2007-16.
195. Chu, C.W., et al., *Lulu regulates Shroom-induced apical constriction during neural tube closure*. *PLoS One*, 2013. **8**(11): p. e81854.

196. Nakajima, H. and T. Tanoue, *Epithelial cell shape is regulated by Lulu proteins via myosin-II*. J Cell Sci, 2010. **123**(Pt 4): p. 555-66.
197. Etournay, R., et al., *Shroom2, a myosin-VIIa- and actin-binding protein, directly interacts with ZO-1 at tight junctions*. J Cell Sci, 2007. **120**(Pt 16): p. 2838-50.
198. Fairbank, P.D., et al., *Shroom2 (APXL) regulates melanosome biogenesis and localization in the retinal pigment epithelium*. Development, 2006. **133**(20): p. 4109-18.
199. Farber, M.J., R. Rizaldy, and J.D. Hildebrand, *Shroom2 regulates contractility to control endothelial morphogenesis*. Mol Biol Cell, 2011. **22**(6): p. 795-805.
200. Lee, C., et al., *Changes in localization and expression levels of Shroom2 and spectrin contribute to variation in amphibian egg pigmentation patterns*. Dev Genes Evol, 2009. **219**(6): p. 319-30.
201. Dye, D.E., et al., *hShroom1 links a membrane bound protein to the actin cytoskeleton*. Cell Mol Life Sci, 2009. **66**(4): p. 681-96.
202. Lee, C., M.P. Le, and J.B. Wallingford, *The shroom family proteins play broad roles in the morphogenesis of thickened epithelial sheets*. Dev Dyn, 2009. **238**(6): p. 1480-91.
203. Yoder, M. and J.D. Hildebrand, *Shroom4 (Kiaa1202) is an actin-associated protein implicated in cytoskeletal organization*. Cell Motil Cytoskeleton, 2007. **64**(1): p. 49-63.
204. Hagens, O., et al., *Disruptions of the novel KIAA1202 gene are associated with X-linked mental retardation*. Hum Genet, 2006. **118**(5): p. 578-90.
205. Schiaffino, M.V., et al., *Cloning of a human homologue of the Xenopus laevis APX gene from the ocular albinism type 1 critical region*. Hum Mol Genet, 1995. **4**(3): p. 373-82.
206. Taylor, J., et al., *The scaffold protein POSH regulates axon outgrowth*. Mol Biol Cell, 2008. **19**(12): p. 5181-92.
207. Nubler-Jung, K., R. Bonitz, and M. Sonnenschein, *Cell polarity during wound healing in an insect epidermis*. Development, 1987. **100**(1): p. 163-70.
208. Klein, T.J. and M. Mlodzik, *Planar cell polarization: an emerging model points in the right direction*. Annu Rev Cell Dev Biol, 2005. **21**: p. 155-76.
209. Devenport, D. and E. Fuchs, *Planar polarization in embryonic epidermis orchestrates global asymmetric morphogenesis of hair follicles*. Nat Cell Biol, 2008. **10**(11): p. 1257-68.
210. Guo, N., C. Hawkins, and J. Nathans, *Frizzled6 controls hair patterning in mice*. Proc Natl Acad Sci U S A, 2004. **101**(25): p. 9277-81.
211. Ravní, A., et al., *Planar cell polarity cadherin Celsr1 regulates skin hair patterning in the mouse*. J Invest Dermatol, 2009. **129**(10): p. 2507-9.
212. Aldaz, S., L.M. Escudero, and M. Freeman, *Live imaging of Drosophila imaginal disc development*. Proc Natl Acad Sci U S A, 2010. **107**(32): p. 14217-22.
213. Maung, S.M. and A. Jenny, *Planar cell polarity in Drosophila*. Organogenesis, 2011. **7**(3): p. 165-79.
214. Guild, G.M., et al., *Actin filament bundles in Drosophila wing hairs: hairs and bristles use different strategies for assembly*. Mol Biol Cell, 2005. **16**(8): p. 3620-31.
215. Mitchell, H.K., J. Roach, and N.S. Petersen, *The morphogenesis of cell hairs on Drosophila wings*. Dev Biol, 1983. **95**(2): p. 387-98.
216. Turner, C.M. and P.N. Adler, *Distinct roles for the actin and microtubule cytoskeletons in the morphogenesis of epidermal hairs during wing development in Drosophila*. Mech Dev, 1998. **70**(1-2): p. 181-92.

217. Garcia-Bellido, A. and J.R. Merriam, *Parameters of the wing imaginal disc development of Drosophila melanogaster*. Dev Biol, 1971. **24**(1): p. 61-87.
218. Schubiger, M. and J. Palka, *Changing spatial patterns of DNA replication in the developing wing of Drosophila*. Dev Biol, 1987. **123**(1): p. 145-53.
219. Peng, Y. and J.D. Axelrod, *Asymmetric protein localization in planar cell polarity: mechanisms, puzzles, and challenges*. Curr Top Dev Biol, 2012. **101**: p. 33-53.
220. Chae, J., et al., *The Drosophila tissue polarity gene starry night encodes a member of the protocadherin family*. Development, 1999. **126**(23): p. 5421-9.
221. Gubb, D. and A. Garcia-Bellido, *A genetic analysis of the determination of cuticular polarity during development in Drosophila melanogaster*. J Embryol Exp Morphol, 1982. **68**: p. 37-57.
222. Taylor, J., et al., *Van Gogh: a new Drosophila tissue polarity gene*. Genetics, 1998. **150**(1): p. 199-210.
223. Theisen, H., et al., *dishevelled is required during wingless signaling to establish both cell polarity and cell identity*. Development, 1994. **120**(2): p. 347-60.
224. Usui, T., et al., *Flamingo, a seven-pass transmembrane cadherin, regulates planar cell polarity under the control of Frizzled*. Cell, 1999. **98**(5): p. 585-95.
225. Vinson, C.R. and P.N. Adler, *Directional non-cell autonomy and the transmission of polarity information by the frizzled gene of Drosophila*. Nature, 1987. **329**(6139): p. 549-51.
226. Wolff, T. and G.M. Rubin, *Strabismus, a novel gene that regulates tissue polarity and cell fate decisions in Drosophila*. Development, 1998. **125**(6): p. 1149-59.
227. Wong, L.L. and P.N. Adler, *Tissue polarity genes of Drosophila regulate the subcellular location for prehair initiation in pupal wing cells*. J Cell Biol, 1993. **123**(1): p. 209-21.
228. Clevers, H., *Wnt/beta-catenin signaling in development and disease*. Cell, 2006. **127**(3): p. 469-80.
229. Boutros, M. and M. Mlodzik, *Dishevelled: at the crossroads of divergent intracellular signaling pathways*. Mech Dev, 1999. **83**(1-2): p. 27-37.
230. Axelrod, J.D., *Unipolar membrane association of Dishevelled mediates Frizzled planar cell polarity signaling*. Genes Dev, 2001. **15**(10): p. 1182-7.
231. Das, G., et al., *Diego interacts with Prickle and Strabismus/Van Gogh to localize planar cell polarity complexes*. Development, 2004. **131**(18): p. 4467-76.
232. Strutt, D.I., *Asymmetric localization of frizzled and the establishment of cell polarity in the Drosophila wing*. Mol Cell, 2001. **7**(2): p. 367-75.
233. Tree, D.R., et al., *Prickle mediates feedback amplification to generate asymmetric planar cell polarity signaling*. Cell, 2002. **109**(3): p. 371-81.
234. Wu, J. and M. Mlodzik, *The frizzled extracellular domain is a ligand for Van Gogh/Stbm during nonautonomous planar cell polarity signaling*. Dev Cell, 2008. **15**(3): p. 462-9.
235. Chen, W.S., et al., *Asymmetric homotypic interactions of the atypical cadherin flamingo mediate intercellular polarity signaling*. Cell, 2008. **133**(6): p. 1093-105.
236. Strutt, H. and D. Strutt, *Differential stability of flamingo protein complexes underlies the establishment of planar polarity*. Curr Biol, 2008. **18**(20): p. 1555-64.
237. Shimada, Y., et al., *Polarized transport of Frizzled along the planar microtubule arrays in Drosophila wing epithelium*. Dev Cell, 2006. **10**(2): p. 209-22.
238. Wu, C.H. and R. Nusse, *Ligand receptor interactions in the Wnt signaling pathway in Drosophila*. J Biol Chem, 2002. **277**(44): p. 41762-9.

239. Wu, J., et al., *Wg and Wnt4 provide long-range directional input to planar cell polarity orientation in Drosophila*. *Nat Cell Biol*, 2013. **15**(9): p. 1045-55.
240. Aigouy, B., et al., *Cell flow reorients the axis of planar polarity in the wing epithelium of Drosophila*. *Cell*, 2010. **142**(5): p. 773-86.
241. Sagner, A., et al., *Establishment of global patterns of planar polarity during growth of the Drosophila wing epithelium*. *Curr Biol*, 2012. **22**(14): p. 1296-301.
242. Strutt, H., S.J. Warrington, and D. Strutt, *Dynamics of core planar polarity protein turnover and stable assembly into discrete membrane subdomains*. *Dev Cell*, 2011. **20**(4): p. 511-25.
243. Struhl, G., J. Casal, and P.A. Lawrence, *Dissecting the molecular bridges that mediate the function of Frizzled in planar cell polarity*. *Development*, 2012. **139**(19): p. 3665-74.
244. Wong, H.C., et al., *Direct binding of the PDZ domain of Dishevelled to a conserved internal sequence in the C-terminal region of Frizzled*. *Mol Cell*, 2003. **12**(5): p. 1251-60.
245. Bastock, R., H. Strutt, and D. Strutt, *Strabismus is asymmetrically localised and binds to Prickle and Dishevelled during Drosophila planar polarity patterning*. *Development*, 2003. **130**(13): p. 3007-14.
246. Jenny, A., et al., *Prickle and Strabismus form a functional complex to generate a correct axis during planar cell polarity signaling*. *EMBO J*, 2003. **22**(17): p. 4409-20.
247. Axelrod, J.D., et al., *Differential recruitment of Dishevelled provides signaling specificity in the planar cell polarity and Wingless signaling pathways*. *Genes Dev*, 1998. **12**(16): p. 2610-22.
248. Jenny, A., et al., *Diego and Prickle regulate Frizzled planar cell polarity signalling by competing for Dishevelled binding*. *Nat Cell Biol*, 2005. **7**(7): p. 691-7.
249. Amonlirdviman, K., et al., *Mathematical modeling of planar cell polarity to understand domineering nonautonomy*. *Science*, 2005. **307**(5708): p. 423-6.
250. Adler, P.N., C. Zhu, and D. Stone, *Inturned localizes to the proximal side of wing cells under the instruction of upstream planar polarity proteins*. *Curr Biol*, 2004. **14**(22): p. 2046-51.
251. Collier, S. and D. Gubb, *Drosophila tissue polarity requires the cell-autonomous activity of the fuzzy gene, which encodes a novel transmembrane protein*. *Development*, 1997. **124**(20): p. 4029-37.
252. Collier, S., et al., *The WD40 repeat protein fritz links cytoskeletal planar polarity to frizzled subcellular localization in the Drosophila epidermis*. *Genetics*, 2005. **169**(4): p. 2035-45.
253. Strutt, D. and S.J. Warrington, *Planar polarity genes in the Drosophila wing regulate the localisation of the FH3-domain protein Multiple Wing Hairs to control the site of hair production*. *Development*, 2008. **135**(18): p. 3103-11.
254. Lu, Q., J. Yan, and P.N. Adler, *The Drosophila planar polarity proteins inturned and multiple wing hairs interact physically and function together*. *Genetics*, 2010. **185**(2): p. 549-58.
255. Yan, J., et al., *The multiple-wing-hairs gene encodes a novel GBD-FH3 domain-containing protein that functions both prior to and after wing hair initiation*. *Genetics*, 2008. **180**(1): p. 219-28.
256. Strutt, D.I., U. Weber, and M. Mlodzik, *The role of RhoA in tissue polarity and Frizzled signalling*. *Nature*, 1997. **387**(6630): p. 292-5.

257. Winter, C.G., et al., *Drosophila Rho-associated kinase (Drok) links Frizzled-mediated planar cell polarity signaling to the actin cytoskeleton*. Cell, 2001. **105**(1): p. 81-91.
258. Das, G., J. Reynolds-Kenneally, and M. Mlodzik, *The atypical cadherin Flamingo links Frizzled and Notch signaling in planar polarity establishment in the Drosophila eye*. Dev Cell, 2002. **2**(5): p. 655-66.
259. Rawls, A.S. and T. Wolff, *Strabismus requires Flamingo and Prickle function to regulate tissue polarity in the Drosophila eye*. Development, 2003. **130**(9): p. 1877-87.
260. Strutt, D., et al., *Asymmetric localization of frizzled and the determination of notch-dependent cell fate in the Drosophila eye*. Curr Biol, 2002. **12**(10): p. 813-24.
261. Cooper, M.T. and S.J. Bray, *Frizzled regulation of Notch signalling polarizes cell fate in the Drosophila eye*. Nature, 1999. **397**(6719): p. 526-30.
262. Zheng, L., J. Zhang, and R.W. Carthew, *frizzled regulates mirror-symmetric pattern formation in the Drosophila eye*. Development, 1995. **121**(9): p. 3045-55.
263. Fanto, M. and M. Mlodzik, *Asymmetric Notch activation specifies photoreceptors R3 and R4 and planar polarity in the Drosophila eye*. Nature, 1999. **397**(6719): p. 523-6.
264. Axelrod, J.D., *Bad hair days for mouse PCP mutants*. Nat Cell Biol, 2008. **10**(11): p. 1251-3.
265. Bayly, R. and J.D. Axelrod, *Pointing in the right direction: new developments in the field of planar cell polarity*. Nat Rev Genet, 2011. **12**(6): p. 385-91.
266. Goodrich, L.V. and D. Strutt, *Principles of planar polarity in animal development*. Development, 2011. **138**(10): p. 1877-92.
267. Gray, R.S., I. Roszko, and L. Solnica-Krezel, *Planar cell polarity: coordinating morphogenetic cell behaviors with embryonic polarity*. Dev Cell, 2011. **21**(1): p. 120-33.
268. Kroiher, M., M.A. Miller, and R.E. Steele, *Deceiving appearances: signaling by "dead" and "fractured" receptor protein-tyrosine kinases*. Bioessays, 2001. **23**(1): p. 69-76.
269. Hayes, M., et al., *Ptk7 promotes non-canonical Wnt/PCP-mediated morphogenesis and inhibits Wnt/beta-catenin-dependent cell fate decisions during vertebrate development*. Development, 2013. **140**(8): p. 1807-18.
270. Lu, X., et al., *PTK7/CCK-4 is a novel regulator of planar cell polarity in vertebrates*. Nature, 2004. **430**(6995): p. 93-8.
271. Paudyal, A., et al., *The novel mouse mutant, chuzhoi, has disruption of Ptk7 protein and exhibits defects in neural tube, heart and lung development and abnormal planar cell polarity in the ear*. BMC Dev Biol, 2010. **10**: p. 87.
272. Ezan, J. and M. Montcouquiol, *Revisiting planar cell polarity in the inner ear*. Semin Cell Dev Biol, 2013. **24**(5): p. 499-506.
273. McNeill, H., *Planar cell polarity: keeping hairs straight is not so simple*. Cold Spring Harb Perspect Biol, 2010. **2**(2): p. a003376.
274. Curtin, J.A., et al., *Mutation of Celsr1 disrupts planar polarity of inner ear hair cells and causes severe neural tube defects in the mouse*. Curr Biol, 2003. **13**(13): p. 1129-33.
275. Etheridge, S.L., et al., *Murine dishevelled 3 functions in redundant pathways with dishevelled 1 and 2 in normal cardiac outflow tract, cochlea, and neural tube development*. PLoS Genet, 2008. **4**(11): p. e1000259.
276. Montcouquiol, M., et al., *Identification of Vangl2 and Scrb1 as planar polarity genes in mammals*. Nature, 2003. **423**(6936): p. 173-7.

277. Wang, J., et al., *Dishevelled genes mediate a conserved mammalian PCP pathway to regulate convergent extension during neurulation*. *Development*, 2006. **133**(9): p. 1767-78.
278. Wang, Y., N. Guo, and J. Nathans, *The role of Frizzled3 and Frizzled6 in neural tube closure and in the planar polarity of inner-ear sensory hair cells*. *J Neurosci*, 2006. **26**(8): p. 2147-56.
279. Eaton, S., *Planar polarization of Drosophila and vertebrate epithelia*. *Curr Opin Cell Biol*, 1997. **9**(6): p. 860-6.
280. Giese, A.P., et al., *Gipc1 has a dual role in Vangl2 trafficking and hair bundle integrity in the inner ear*. *Development*, 2012. **139**(20): p. 3775-85.
281. Montcouquiol, M., et al., *Asymmetric localization of Vangl2 and Fz3 indicate novel mechanisms for planar cell polarity in mammals*. *J Neurosci*, 2006. **26**(19): p. 5265-75.
282. Warchol, M.E. and M. Montcouquiol, *Maintained expression of the planar cell polarity molecule Vangl2 and reformation of hair cell orientation in the regenerating inner ear*. *J Assoc Res Otolaryngol*, 2010. **11**(3): p. 395-406.
283. Deans, M.R., et al., *Asymmetric distribution of prickle-like 2 reveals an early underlying polarization of vestibular sensory epithelia in the inner ear*. *J Neurosci*, 2007. **27**(12): p. 3139-47.
284. Wang, J., et al., *Regulation of polarized extension and planar cell polarity in the cochlea by the vertebrate PCP pathway*. *Nat Genet*, 2005. **37**(9): p. 980-5.
285. Lee, J., et al., *PTK7 regulates myosin II activity to orient planar polarity in the mammalian auditory epithelium*. *Curr Biol*, 2012. **22**(11): p. 956-66.
286. Andreeva, A., et al., *PTK7-Src signaling at epithelial cell contacts mediates spatial organization of actomyosin and planar cell polarity*. *Dev Cell*, 2014. **29**(1): p. 20-33.
287. Grimsley-Myers, C.M., et al., *The small GTPase Rac1 regulates auditory hair cell morphogenesis*. *J Neurosci*, 2009. **29**(50): p. 15859-69.
288. Sipe, C.W., et al., *Lis1 mediates planar polarity of auditory hair cells through regulation of microtubule organization*. *Development*, 2013. **140**(8): p. 1785-95.
289. Sipe, C.W. and X. Lu, *Kif3a regulates planar polarization of auditory hair cells through both ciliary and non-ciliary mechanisms*. *Development*, 2011. **138**(16): p. 3441-9.
290. Katsumi, A., et al., *Effects of cell tension on the small GTPase Rac*. *J Cell Biol*, 2002. **158**(1): p. 153-64.
291. Dearnorff, M.A., et al., *Frizzled-8 is expressed in the Spemann organizer and plays a role in early morphogenesis*. *Development*, 1998. **125**(14): p. 2687-700.
292. Sokol, S.Y., *Analysis of Dishevelled signalling pathways during Xenopus development*. *Curr Biol*, 1996. **6**(11): p. 1456-67.
293. Wallingford, J.B., et al., *Dishevelled controls cell polarity during Xenopus gastrulation*. *Nature*, 2000. **405**(6782): p. 81-5.
294. Goto, T. and R. Keller, *The planar cell polarity gene strabismus regulates convergence and extension and neural fold closure in Xenopus*. *Dev Biol*, 2002. **247**(1): p. 165-81.
295. Jessen, J.R., et al., *Zebrafish trilobite identifies new roles for Strabismus in gastrulation and neuronal movements*. *Nat Cell Biol*, 2002. **4**(8): p. 610-5.
296. Panousopoulou, E., et al., *The distribution of Dishevelled in convergently extending mesoderm*. *Dev Biol*, 2013. **382**(2): p. 496-503.
297. Park, T.J., et al., *Subcellular localization and signaling properties of dishevelled in developing vertebrate embryos*. *Curr Biol*, 2005. **15**(11): p. 1039-44.

298. Kim, H.Y. and L.A. Davidson, *Punctuated actin contractions during convergent extension and their permissive regulation by the non-canonical Wnt-signaling pathway*. J Cell Sci, 2011. **124**(Pt 4): p. 635-46.
299. Habas, R., Y. Kato, and X. He, *Wnt/Frizzled activation of Rho regulates vertebrate gastrulation and requires a novel Formin homology protein Daam1*. Cell, 2001. **107**(7): p. 843-54.
300. Liu, W., et al., *Mechanism of activation of the Formin protein Daam1*. Proc Natl Acad Sci U S A, 2008. **105**(1): p. 210-5.
301. Tanegashima, K., H. Zhao, and I.B. Dawid, *WGEF activates Rho in the Wnt-PCP pathway and controls convergent extension in Xenopus gastrulation*. EMBO J, 2008. **27**(4): p. 606-17.
302. Matussek, T., et al., *The Drosophila formin DAAM regulates the tracheal cuticle pattern through organizing the actin cytoskeleton*. Development, 2006. **133**(5): p. 957-66.
303. Musci, T.S. and R.J. Mullen, *All-or-none craniorachischisis in Loop-tail mutant mouse chimeras*. Development, 1990. **110**(1): p. 229-37.
304. Kibar, Z., et al., *Ltap, a mammalian homolog of Drosophila Strabismus/Van Gogh, is altered in the mouse neural tube mutant Loop-tail*. Nat Genet, 2001. **28**(3): p. 251-5.
305. Murdoch, J.N., et al., *Severe neural tube defects in the loop-tail mouse result from mutation of Lpp1, a novel gene involved in floor plate specification*. Hum Mol Genet, 2001. **10**(22): p. 2593-601.
306. Hamblet, N.S., et al., *Dishevelled 2 is essential for cardiac outflow tract development, somite segmentation and neural tube closure*. Development, 2002. **129**(24): p. 5827-38.
307. Wallingford, J.B. and R.M. Harland, *Neural tube closure requires Dishevelled-dependent convergent extension of the midline*. Development, 2002. **129**(24): p. 5815-25.
308. Ybot-Gonzalez, P., et al., *Convergent extension, planar-cell-polarity signalling and initiation of mouse neural tube closure*. Development, 2007. **134**(4): p. 789-99.
309. Ciruna, B., et al., *Planar cell polarity signalling couples cell division and morphogenesis during neurulation*. Nature, 2006. **439**(7073): p. 220-4.
310. Gong, Y., C. Mo, and S.E. Fraser, *Planar cell polarity signalling controls cell division orientation during zebrafish gastrulation*. Nature, 2004. **430**(7000): p. 689-93.
311. Bellaiche, Y., et al., *Frizzled regulates localization of cell-fate determinants and mitotic spindle rotation during asymmetric cell division*. Nat Cell Biol, 2001. **3**(1): p. 50-7.
312. Segalen, M., et al., *The Fz-Dsh planar cell polarity pathway induces oriented cell division via Mud/NuMA in Drosophila and zebrafish*. Dev Cell, 2010. **19**(5): p. 740-52.
313. Sausedo, R.A., J.L. Smith, and G.C. Schoenwolf, *Role of nonrandomly oriented cell division in shaping and bending of the neural plate*. J Comp Neurol, 1997. **381**(4): p. 473-88.
314. Chacon-Heszele, M.F., et al., *Regulation of cochlear convergent extension by the vertebrate planar cell polarity pathway is dependent on p120-catenin*. Development, 2012. **139**(5): p. 968-78.
315. Bartsch, O., et al., *Novel VANGL1 Gene Mutations in 144 Slovakian, Romanian and German Patients with Neural Tube Defects*. Mol Syndromol, 2012. **3**(2): p. 76-81.
316. Bosoi, C.M., et al., *Identification and characterization of novel rare mutations in the planar cell polarity gene PRICKLE1 in human neural tube defects*. Hum Mutat, 2011. **32**(12): p. 1371-5.

317. De Marco, P., et al., *Genetic analysis of disheveled 2 and disheveled 3 in human neural tube defects*. J Mol Neurosci, 2013. **49**(3): p. 582-8.
318. De Marco, P., et al., *FZD6 is a novel gene for human neural tube defects*. Hum Mutat, 2012. **33**(2): p. 384-90.
319. Kibar, Z., et al., *Novel mutations in VANGL1 in neural tube defects*. Hum Mutat, 2009. **30**(7): p. E706-15.
320. Kibar, Z., et al., *Contribution of VANGL2 mutations to isolated neural tube defects*. Clin Genet, 2011. **80**(1): p. 76-82.
321. Kibar, Z., et al., *Mutations in VANGL1 associated with neural-tube defects*. N Engl J Med, 2007. **356**(14): p. 1432-7.
322. Lei, Y.P., et al., *VANGL2 mutations in human cranial neural-tube defects*. N Engl J Med, 2010. **362**(23): p. 2232-5.
323. Reynolds, A., et al., *VANGL1 rare variants associated with neural tube defects affect convergent extension in zebrafish*. Mech Dev, 2010. **127**(7-8): p. 385-92.
324. Kibar, Z., et al., *Identification of a new chemically induced allele (Lp(m1Jus)) at the loop-tail locus: morphology, histology, and genetic mapping*. Genomics, 2001. **72**(3): p. 331-7.
325. Copp, A.J., I. Checiu, and J.N. Henson, *Developmental basis of severe neural tube defects in the loop-tail (Lp) mutant mouse: use of microsatellite DNA markers to identify embryonic genotype*. Dev Biol, 1994. **165**(1): p. 20-9.
326. Smith, L.J. and K.F. Stein, *Axial elongation in the mouse and its retardation in homozygous looptail mice*. J Embryol Exp Morphol, 1962. **10**: p. 73-87.
327. Torban, E., et al., *Independent mutations in mouse Vangl2 that cause neural tube defects in looptail mice impair interaction with members of the Dishevelled family*. J Biol Chem, 2004. **279**(50): p. 52703-13.
328. Merte, J., et al., *Sec24b selectively sorts Vangl2 to regulate planar cell polarity during neural tube closure*. Nat Cell Biol, 2010. **12**(1): p. 41-6; sup pp 1-8.
329. Wansleben, C., et al., *Planar cell polarity defects and defective Vangl2 trafficking in mutants for the COPII gene Sec24b*. Development, 2010. **137**(7): p. 1067-73.
330. Torban, E., et al., *Tissue, cellular and sub-cellular localization of the Vangl2 protein during embryonic development: effect of the Lp mutation*. Gene Expr Patterns, 2007. **7**(3): p. 346-54.
331. Gravel, M., et al., *Molecular and cellular mechanisms underlying neural tube defects in the loop-tail mutant mouse*. Biochemistry, 2010. **49**(16): p. 3445-55.
332. Torban, E., et al., *Genetic interaction between members of the Vangl family causes neural tube defects in mice*. Proc Natl Acad Sci U S A, 2008. **105**(9): p. 3449-54.
333. Jessen, J.R. and L. Solnica-Krezel, *Identification and developmental expression pattern of van gogh-like 1, a second zebrafish strabismus homologue*. Gene Expr Patterns, 2004. **4**(3): p. 339-44.
334. Lindqvist, M., et al., *Vang-like protein 2 and Rac1 interact to regulate adherens junctions*. J Cell Sci, 2010. **123**(Pt 3): p. 472-83.
335. Mahaffey, J.P., et al., *Cofilin and Vangl2 cooperate in the initiation of planar cell polarity in the mouse embryo*. Development, 2013. **140**(6): p. 1262-71.
336. Hardy, K.M., et al., *Non-canonical Wnt signaling through Wnt5a/b and a novel Wnt11 gene, Wnt11b, regulates cell migration during avian gastrulation*. Dev Biol, 2008. **320**(2): p. 391-401.

337. Qian, D., et al., *Wnt5a functions in planar cell polarity regulation in mice*. Dev Biol, 2007. **306**(1): p. 121-33.
338. Smith, J.C., et al., *Xwnt11 and the regulation of gastrulation in Xenopus*. Philos Trans R Soc Lond B Biol Sci, 2000. **355**(1399): p. 923-30.
339. Tada, M. and J.C. Smith, *Xwnt11 is a target of Xenopus Brachyury: regulation of gastrulation movements via Dishevelled, but not through the canonical Wnt pathway*. Development, 2000. **127**(10): p. 2227-38.
340. Yamaguchi, T.P., et al., *A Wnt5a pathway underlies outgrowth of multiple structures in the vertebrate embryo*. Development, 1999. **126**(6): p. 1211-23.
341. Kilander, M.B., J. Dahlstrom, and G. Schulte, *Assessment of Frizzled 6 membrane mobility by FRAP supports G protein coupling and reveals WNT-Frizzled selectivity*. Cell Signal, 2014. **26**(9): p. 1943-1949.
342. Takada, R., et al., *Analysis of combinatorial effects of Wnts and Frizzleds on beta-catenin/armadillo stabilization and Dishevelled phosphorylation*. Genes Cells, 2005. **10**(9): p. 919-28.
343. DeChiara, T.M., et al., *Ror2, encoding a receptor-like tyrosine kinase, is required for cartilage and growth plate development*. Nat Genet, 2000. **24**(3): p. 271-4.
344. Takeuchi, S., et al., *Mouse Ror2 receptor tyrosine kinase is required for the heart development and limb formation*. Genes Cells, 2000. **5**(1): p. 71-8.
345. Bai, Y., et al., *Ror2 Receptor Mediates Wnt11 Signaling and Affects Convergence and Extension Movements in Zebrafish*. J Biol Chem, 2014.
346. Hikasa, H., et al., *The Xenopus receptor tyrosine kinase Xror2 modulates morphogenetic movements of the axial mesoderm and neuroectoderm via Wnt signaling*. Development, 2002. **129**(22): p. 5227-39.
347. Gao, B., et al., *Wnt signaling gradients establish planar cell polarity by inducing Vangl2 phosphorylation through Ror2*. Dev Cell, 2011. **20**(2): p. 163-76.
348. Ho, H.Y., et al., *Wnt5a-Ror-Dishevelled signaling constitutes a core developmental pathway that controls tissue morphogenesis*. Proc Natl Acad Sci U S A, 2012. **109**(11): p. 4044-51.
349. Yang, Y., et al., *Wnt5a and Wnt5b exhibit distinct activities in coordinating chondrocyte proliferation and differentiation*. Development, 2003. **130**(5): p. 1003-15.
350. Kuss, P., et al., *Regulation of cell polarity in the cartilage growth plate and perichondrium of metacarpal elements by HOXD13 and WNT5A*. Dev Biol, 2014. **385**(1): p. 83-93.
351. Wallingford, J.B. and R. Habas, *The developmental biology of Dishevelled: an enigmatic protein governing cell fate and cell polarity*. Development, 2005. **132**(20): p. 4421-36.
352. Capelluto, D.G., et al., *The DIX domain targets dishevelled to actin stress fibres and vesicular membranes*. Nature, 2002. **419**(6908): p. 726-9.
353. Schwarz-Romond, T., et al., *The DIX domain of Dishevelled confers Wnt signaling by dynamic polymerization*. Nat Struct Mol Biol, 2007. **14**(6): p. 484-92.
354. Leonard, J.D. and C.A. Etensohn, *Analysis of dishevelled localization and function in the early sea urchin embryo*. Dev Biol, 2007. **306**(1): p. 50-65.
355. Torres, M.A. and W.J. Nelson, *Colocalization and redistribution of dishevelled and actin during Wnt-induced mesenchymal morphogenesis*. J Cell Biol, 2000. **149**(7): p. 1433-42.

356. Miller, J.R., et al., *Establishment of the dorsal-ventral axis in Xenopus embryos coincides with the dorsal enrichment of dishevelled that is dependent on cortical rotation*. J Cell Biol, 1999. **146**(2): p. 427-37.
357. Chang, W., C.E. Lloyd, and D. Zarkower, *DSH-2 regulates asymmetric cell division in the early C. elegans somatic gonad*. Mech Dev, 2005. **122**(6): p. 781-9.
358. Na, J., et al., *Dishevelled proteins regulate cell adhesion in mouse blastocyst and serve to monitor changes in Wnt signaling*. Dev Biol, 2007. **302**(1): p. 40-9.
359. Yu, A., et al., *Structural analysis of the interaction between Dishevelled2 and clathrin AP-2 adaptor, a critical step in noncanonical Wnt signaling*. Structure, 2010. **18**(10): p. 1311-20.
360. Matsumoto, S., et al., *Binding of APC and dishevelled mediates Wnt5a-regulated focal adhesion dynamics in migrating cells*. EMBO J, 2010. **29**(7): p. 1192-204.
361. Yanagawa, S., et al., *The dishevelled protein is modified by wingless signaling in Drosophila*. Genes Dev, 1995. **9**(9): p. 1087-97.
362. Hawkins, N.C., et al., *MOM-5 frizzled regulates the distribution of DSH-2 to control C. elegans asymmetric neuroblast divisions*. Dev Biol, 2005. **284**(1): p. 246-59.
363. Schwarz-Romond, T., C. Metcalfe, and M. Bienz, *Dynamic recruitment of axin by Dishevelled protein assemblies*. J Cell Sci, 2007. **120**(Pt 14): p. 2402-12.
364. Chen, W., et al., *Dishevelled 2 recruits beta-arrestin 2 to mediate Wnt5A-stimulated endocytosis of Frizzled 4*. Science, 2003. **301**(5638): p. 1391-4.
365. Schwarz-Romond, T., et al., *The Wnt signalling effector Dishevelled forms dynamic protein assemblies rather than stable associations with cytoplasmic vesicles*. J Cell Sci, 2005. **118**(Pt 22): p. 5269-77.
366. Tauriello, D.V., et al., *Wnt/beta-catenin signaling requires interaction of the Dishevelled DEP domain and C terminus with a discontinuous motif in Frizzled*. Proc Natl Acad Sci U S A, 2012. **109**(14): p. E812-20.
367. Simons, M., et al., *Electrochemical cues regulate assembly of the Frizzled/Dishevelled complex at the plasma membrane during planar epithelial polarization*. Nat Cell Biol, 2009. **11**(3): p. 286-94.
368. Consonni, S.V., M.M. Maurice, and J.L. Bos, *DEP domains: structurally similar but functionally different*. Nat Rev Mol Cell Biol, 2014. **15**(5): p. 357-62.
369. Wong, H.C., et al., *Structural basis of the recognition of the dishevelled DEP domain in the Wnt signaling pathway*. Nat Struct Biol, 2000. **7**(12): p. 1178-84.
370. Consonni, S.V., et al., *cAMP regulates DEP domain-mediated binding of the guanine nucleotide exchange factor Epac1 to phosphatidic acid at the plasma membrane*. Proc Natl Acad Sci U S A, 2012. **109**(10): p. 3814-9.
371. Yu, A., et al., *Association of Dishevelled with the clathrin AP-2 adaptor is required for Frizzled endocytosis and planar cell polarity signaling*. Dev Cell, 2007. **12**(1): p. 129-41.
372. Mashburn, D.N., et al., *Enabling user-guided segmentation and tracking of surface-labeled cells in time-lapse image sets of living tissues*. Cytometry A, 2012. **81**(5): p. 409-18.
373. Wiggan, O. and P.A. Hamel, *Pax3 regulates morphogenetic cell behavior in vitro coincident with activation of a PCP/non-canonical Wnt-signaling cascade*. J Cell Sci, 2002. **115**(Pt 3): p. 531-41.

374. Yates, L.L., et al., *The planar cell polarity gene Vangl2 is required for mammalian kidney-branching morphogenesis and glomerular maturation*. Hum Mol Genet, 2010. **19**(23): p. 4663-76.
375. Karner, C.M., et al., *Wnt9b signaling regulates planar cell polarity and kidney tubule morphogenesis*. Nat Genet, 2009. **41**(7): p. 793-9.
376. Neff, M.M., et al., *dCAPS, a simple technique for the genetic analysis of single nucleotide polymorphisms: experimental applications in Arabidopsis thaliana genetics*. Plant J, 1998. **14**(3): p. 387-92.
377. Nagy, A., et al., *Alcian blue staining of the mouse fetal cartilaginous skeleton*. Cold Spring Harb Protoc, 2009. **2009**(3): p. pdb prot5169.